On Code Design for Interference Channels

by

Shahrouz Sharifi

A Dissertation Presented in Partial Fulfillment
of the Requirements for the Degree
Doctor of Philosophy

Approved August 2015 by the
Graduate Supervisory Committee:

Tolga M. Duman, Chair
Junshan Zhang
Cihan Tepedelenlioglu
Martin Reisslein

ARIZONA STATE UNIVERSITY

December 2015

ABSTRACT

There has been a lot of work on the characterization of capacity and achievable rate regions, and rate region outer-bounds for various multi-user channels of interest. Parallel to the developed information theoretic results, practical codes have also been designed for some multi-user channels such as multiple access channels (MACs), broadcast channels (BCs) and relay channels (RCs); however, interference channels (ICs) have not received much attention and only a limited amount of work has been conducted on them. With this motivation, in this dissertation, design of practical and implementable channel codes is studied focusing on multi-user channels with special emphasis on ICs; in particular, irregular low-density-parity-check (LDPC) codes are exploited for a variety of cases and trellis based codes for short block length designs are performed.

Novel code design approaches are first studied for the two-user Gaussian multiple access (GMAC). Exploiting Gaussian mixture approximation, new methods are proposed wherein the optimized codes are shown to improve upon the available designs and off-the-shelf point-to-point (P2P) codes applied to the MAC scenario. The code design is then examined for the two-user Gaussian IC implementing the Han-Kobayashi encoding and decoding strategy. Compared with the P2P codes, the newly designed codes consistently offer better performance. Parallel to this work, code design is explored for the discrete memoryless interference channels (DMICs) wherein the channel inputs and outputs are taken from a finite alphabet and it is demonstrated that the designed codes are superior to the single user codes used with time sharing (TS). Finally, the code design principles are also investigated for the two-user GIC employing trellis-based codes with short block lengths for the case of strong and mixed interference levels.

To my dear family

ACKNOWLEDGEMENTS

I would like to express my sincere gratitude to my adviser and mentor, Prof. Tolga M. Duman for his appreciable patience and support. I am deeply indebted for his guidance and encouragement that helped me a great deal in the completion and success of this study. I would like also to thank my committee members, Prof. Junshan Zhang, Prof. Cihan Tepedelenlioglu and Prof. Martin Reisslein, for their invaluable comments. I also wish to thank Ahmad El Moslimany and Ahmad Salim, without them I would not have such colorful memories to cherish. Last but not least, I would like to thank my parents for their unconditional love and sustained support which was my main source of motivation in the face of challenges.

TABLE OF CONTENTS

CHAPTER Page

LIST OF TABLES

LIST OF FIGURES

Figure Page

LIST OF ACRONYMS

ARR achievable rate region

BC broadcast channel

BER bit error rate

BI-AWGN binary-input additive white Gaussian noise

BIBO binary-input binary-output

BP belief propagation

BPSK binary phase shift keying

CDMA code division multiple access

DE density evolution

DMIC discrete memoryless interference channel

DPC dirty paper coding

EXIT extrinsic information transfer

FDMA frequency division multiple access

GBC Gaussian broadcast channel

GIC Gaussian interference channel

GM Gaussian mixture

GMAC Gaussian multiple access channel

HK Han-Kobayashi

IC interference channel

JD joint decoding

LDPC low-density parity-check

LLR log likelihood ratio

MAC multiple access channel

MIMO multiple input multiple output

NLTC non-linear trellis code

P2P point-to-point

PDF probability density function

PMF probability mass function

QPSK quaternary phase shift keying

RC relay channel

SIC soft interference cancellation

SUD single user decoding

TDMA time division multiple access

TS time sharing

ZIC Z interference channel

Chapter 1

INTRODUCTION

Multi-user channels are general models for many communication scenarios. TV broadcast, communication of mobile users with a base station, exchange of information among multiple nodes in an adhoc network are all instances of multi-user communications. In order to share the common medium, conventional strategies such as time division multiple access (TDMA), frequency division multiple access (FDMA), and code division multiple access (CDMA) have been used for a long time to achieve reliable communication. However, these schemes are typically suboptimal and new coding schemes are needed in which all users can communicate and use the shared medium in a near optimal manner. Progress along these lines, both theoretical developments and in terms of practical designs, has shed light to different aspects of multi-user communications and has made this literature very rich particularly in recent years.

Basic multi-user channel models can be categorized as multiple access channels (MACs), broadcast channels (BCs), relay channels (RCs), and interference channels (ICs). In a MAC, multiple nodes communicate with a single receiver. As a dual, in a BC, a single transmitter transmits different messages to multiple receivers over the same medium. RCs are suitable models for configurations in which intermediate nodes assist the sender to communicate with its receiver, e.g., in adhoc networks. Treatment of interference is one of the most important issues in multi-user communication systems as apparent in modern wireless networks, such as mobile cellular communications where each receiver is interested in one signal among the received superposition of transmitted signals. This can be, as an example, the downlink of a cellular system, in which a mobile station tries to demodulate its own transmitted information stream in the presence of interfering signals from different base stations.

There has been a lot of work on characterization of the capacity and achievable rate regions, and rate region outer bounds of the aforementioned multi-user communication channels. Parallel to the information theoretic advancement, practical codes have been designed for some cases achieving points near the boundary of the known achievable rate or capacity regions. For instance, capacity region of the MAC has been characterized and specific low-density parity-check (LDPC) codes have been found achieving points near the boundary of the region for Gaussian channels. Degraded BCs which form a particular class of BCs have also been studied in terms of their capacity region [2], and very good practical channel codes have been designed [3]. However, there exists numerous problems which are still open. Among them is the capacity region of the interference channel which has been unknown for many decades even for the case of Gaussian case. Although there are rate region outer-bounds reported for the interference channel, only limited attempts have been made on designing practical codes in the existing literature. Motivated by this, in this dissertation, we study the code design for the ICs exploiting the irregular LDPC codes for a variety of cases.

1.1 Outline of the Dissertation

In Chapter 2, we describe the system model for MACs, BCs, RCs and ICs. We first present the models for the discrete memoryless channels and then provide the models for the Gaussian case. We also review the existing information theoretic bounds and comment on the performance of specific codes for the discussed channels.

In Chapter 3, we examine the code design principles for the two-user Gaussian multiple access channel (GMAC) for fixed and quasi-static fading suitable for modeling wireless links. Adopting joint decoding (JD) at the receiver, we derive the probability density functions (PDFs) of log likelihood ratios (LLRs) sent from the state

nodes to the variable nodes and illustrate that they can be closely approximated with a Gaussian mixture (GM) distribution, which is utilized in the two proposed methods of decoding analysis of LDPC codes employed for two-user GMACs. For fixed channel gains, we exploit the newly proposed method for code optimization and design specific LDPC codes for equal-power and unequal-power link scenarios. The performances of the optimized codes are compared against the existing designs in the literature. For quasi-static scenario, due to the amount of computations involved, we incorporate an existing (simple) approximate method and optimize codes for scenarios with real and complex channel gains. The performances of the optimized codes are compared against those of point-to-point (P2P) codes with time sharing (TS) both asymptotically and for finite code block lengths.

In Chapter 4, we turn our attention to the two-user Gaussian interference channel (GIC) when finite constellations are employed for transmission and the Han-Kobayashi (HK) coding/decoding scheme is implemented at the transmitter and receiver sides. We prove the symmetry property of the exchanged LLRs within the joint decoder and characterize the stability condition for different interference levels and modulations. Code optimization is carried out for a multitude of examples. Particularly, we consider examples of GICs experiencing strong and weak interference along with binary phase shift keying (BPSK) and quaternary phase shift keying (QPSK) modulation. Performances of the optimized codes are compared against naive and non-naive TS schemes. In addition, the performances of the P2P codes with TS are evaluated for the considered examples. Furthermore, as a different perspective, we perform algebraic code designs optimized for GIC and compare the results with those of random constructions for smaller block lengths.

In Chapter 5, we study LDPC code design for the two-user discrete memoryless

interference channel (DMIC) when the channel inputs and outputs are finite. As an example, we focus on the one-sided Z interference channel (ZIC) wherein one receiver is interference free and characterize a sub-region of the HK achievable rate region (ARR). Instead of the computing the complete achievable rate region, we consider a sub-region computed with no TS. We perform the code optimization exploiting simple non-linear trellis codes (NLTCs) combined with outer LDPC codes, which are employed to attain desired input distributions.

In Chapter 6, we focus on the code design for the two-user GIC when short block length codes are employed. In particular, we exploit trellis-based codes and perform code optimization for strong, weak and mixed interference levels. We derive performance bounds and utilize them for code optimization. We provide examples of the designed codes and compare their performance with that of LDPC codes.

Finally, we provide a summary of the results obtained in this dissertation and discuss possible directions for future research in Chapter 7.

Chapter 2

PRELIMINARIES

In this chapter, we present the system model for the MAC,the BC,the RC and the IC. Models are first described for the discrete memoryless case and then Gaussian cases are given. In addition, we review the existing information theoretic bounds and the practical code design approaches for these channels to set the steps for the rest of the thesis.

2.1 Multi-User Channels

2.1.1 Multiple Access Channel

Considering Figure 2.1, a two-user discrete memoryless MAC consists of $\mathcal{X}_1$, $\mathcal{X}_2$ as input alphabets, $\mathcal{Y}$ as its output alphabet and a probability transition matrix $p(y|x_1, x_2)$. A $\big((2^{nR_1}, 2^{nR_2}), n\big)$ code for the MAC consists of two sets of messages, $M_1 \in [1 : 2^{nR_1}]$ and $M_2 \in [1 : 2^{nR_2}]$, two encoding functions that map M_1 and M_2 to X_1^n and X_2^n, respectively, and a decoding function that maps the received signal Y^n to $\hat{M}_1 \in [1 : 2^{nR_1}]$ and $\hat{M}_2 \in [1 : 2^{nR_2}]$[1]. The average probability of error for the $\big((2^{nR_1}, 2^{nR_2}), n\big)$ code is defined as follows

$$P_e^{(n)} = \frac{1}{2^{n(R_1+R_2)}} \sum_{(M_1,M_2)} Pr(\hat{M}_1(Y_1^n) \neq M_1 \ \ or \ \ \hat{M}_2(Y_2^n) \neq M_2). \tag{2.1}$$

A rate pair (R_1, R_2) for the discrete memoryless MAC is said to be achievable if there exists a sequence of $\big((2^{nR_1}, 2^{nR_2}), n\big)$ codes with $P_e^{(n)} \to 0$ as $n \to \infty$. The capacity region of the MAC is the closure of the set of all rate pairs.

GMAC is a common model for a MAC in which signals of different users are added together and observed in Gaussian noise at the receiver. Figure 2.2 shows a simple configuration of this channel model. The channel output corresponding to the

[1]The notations in this chapter are in accordance with [4].

inputs X_1 and X_2 is given by

$$Y = h_1 X_1 + h_2 X_2 + Z, \tag{2.2}$$

where Z is a zero mean white Gaussian noise with unit variance. Power constraints for the users' signals are given by

$$\sum_{i=1}^{n} x_{ji}^2(m_j) \leq nP_j, \quad j = 1, 2, \tag{2.3}$$

where x_{ji} is the ith component of the user j's codeword.

2.1.2 Broadcast Channel

A two-user discrete BC is illustrated in Figure 2.3. It consists of three sets: $\mathcal{X}$ as the input alphabet, $\mathcal{Y}_1$, $\mathcal{Y}_2$ as output alphabets, and a channel transition probability function $p(y_1, y_2|x)$. A $\left((2^{nR_1}, 2^{nR_2}), n\right)$ code for a BC consists of two sets of messages, $M_1 \in [1 : 2^{nR_1}]$ and $M_2 \in [1 : 2^{nR_2}]$, an encoding function that maps M_1 and M_2 to the codeword X^n, and two decoders that map the received signals, i.e., Y_1^n and Y_2^n,

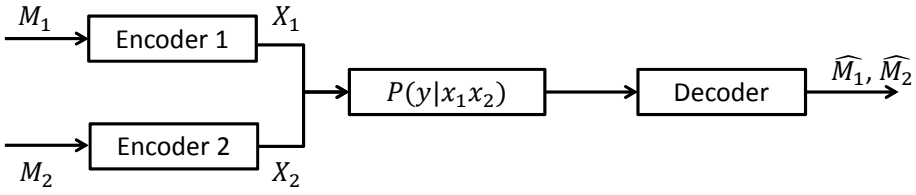

Figure 2.1: Multiple Access Channel

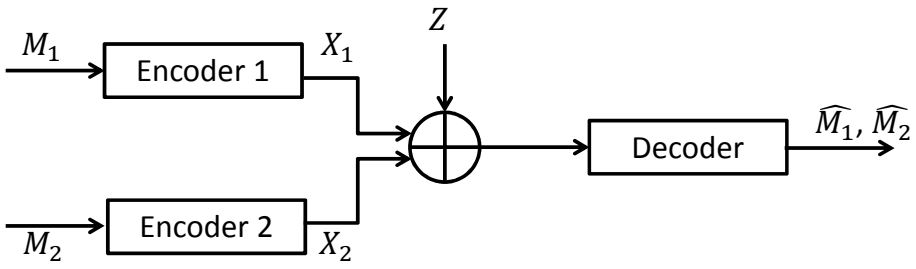

Figure 2.2: Gaussian Multiple Access Channel

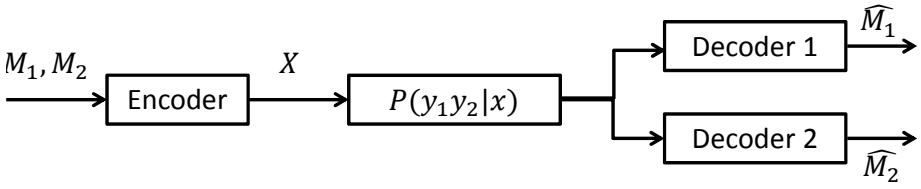

Figure 2.3: General Broadcast Channel

to $\hat{M}_1 \in [1 : 2^{nR_1}]$ and $\hat{M}_2 \in [1 : 2^{nR_2}]$. The probability of error $P_e^{(n)}$ is defined as

$$P_e^{(n)} = \frac{1}{2^{n(R_1+R_2)}} \sum_{(M_1,M_2)} P(\hat{M}_1(Y_1^n) \neq M_1 \ \ or \ \ \hat{M}_2(Y_2^n) \neq M_2). \tag{2.4}$$

The BC is said to be memoryless if

$$p(y_1^n, y_2^n|x^n) = \prod_{i=1}^{n} p(y_{1i}, y_{2i}|x_i). \tag{2.5}$$

A rate pair (R_1, R_2) is said to be *achievable* for the BC if there exists a sequence of $X^n(M_1, M_2)$ with $P_e^{(n)} \to 0$ as $n \to 0$. The capacity region of the BC is the convex hull of the set of all the achievable rates.

It is often the case that one of the receivers has a "better" version of the received signal, formally stated as the following Markov chain

$$X \to Y_1 \to Y_2 \tag{2.6}$$

being satisfied. In this case, the second receiver's signal is a degraded version of the first receiver's signal. Such a channel is called a *degraded* BC. A BC is said to be *physically degraded* if

$$p(y_1, y_2|x) = p(y_1|x)p(y_2|y_1) \tag{2.7}$$

and the channel is called *stochastically degraded* if there exists a distribution $p'(y_2|y_1)$ such that

$$p(y_2|x) = \sum_{y_1} p(y_1|x)p'(y_2|y_1). \tag{2.8}$$

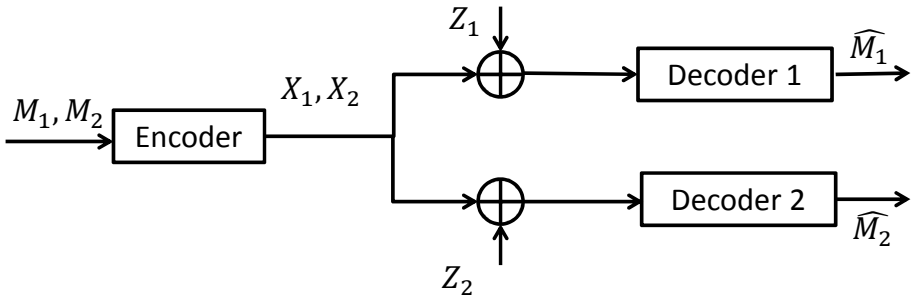

Figure 2.4: Gaussian Broadcast Channel

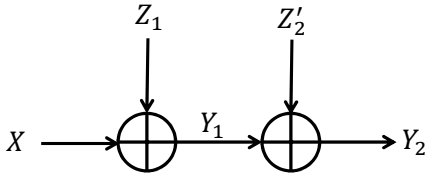

Figure 2.5: Physically Degraded Gaussian Broadcast Channel

Considering Figure 2.4, a two-user Gaussian BC can be modeled as

$$\begin{aligned} Y_1 &= X + Z_1, \\ Y_2 &= X + Z_2, \end{aligned} \tag{2.9}$$

where Z_1 and Z_2 are independent Gaussian random variables with zero mean and variances N_1 and N_2, respectively. Z_1 and Z_2 are also independent of the channel inputs X. Power constraint is given by

$$\sum_{i=1}^{n} x_i^2(M_1, M_2) \leq nP, \tag{2.10}$$

where P is the total power for the transmitted signal, and x_i is the ith bit of the codeword. The Gaussian BC is a particular example of a degraded BC because the channel can be modified as shown in Figure 2.5, where Z_2' is a zero mean Gaussian noise with variance $N_2 - N_1$ assuming that $N_1 \leq N_2$.

2.1.3 Relay Channel

The RC is a channel in which there is one sender and one receiver with a number of intermediate nodes which act as relays to help with the communication from the sender to the receiver. Here, we describe two models for the RC: discrete memoryless version referred as discrete relay channel and Gaussian RC. The simplest RC has only one intermediate or relay node. Consider the 3-node P2P communication system with a relay as depicted in Figure 2.6. The channel model $\big(\mathcal{X} \times \mathcal{X}_1, p(y, y_1|x, x_1), \mathcal{Y} \times \mathcal{Y}_1\big)$ consists of four finite sets of input and output alphabets and conditional probability mass functions (PMFs) $p(y, y_1|x, x_1)$. The interpretation is that x is the input to the channel and y is the output of the channel, y_1 is the relay's observation, and x_1 is the input symbol chosen by the relay. The RC combines a BC (X to Y and Y_1) and a MAC (X and X_1 to Y). A $(2^{nR}, n)$ code for a discrete RC consists of a message set $\big(M \in [1 : 2^{nR}]\big)$, an encoder that assigns a codeword $X^n(m)$ to each message, a relay encoder that assigns a symbol $X_{1i}(Y^{i-1})$ to each past received sequence $Y^{i-1} \in \mathcal{Y}^{i-1}$ for each $i \in [1 : n]$, and a decoder that assigns an estimate $\hat{m}$ to each received sequence $Y_1^n \in \mathcal{Y}_1^n$. The probability of error $P_e^{(n)}$ is defined as

$$P_e^{(n)} = \frac{1}{2^{nR}} \sum_{M} Pr\big(\hat{M}(Y^n) \neq M\big). \tag{2.11}$$

A rate R is said to be achievable for the RC if there exists a sequence of $\big(2^{nR}, n\big)$ codes with $P_e^{(n)} \to 0$ as $n \to \infty$. The capacity region of the RC is the convex hull

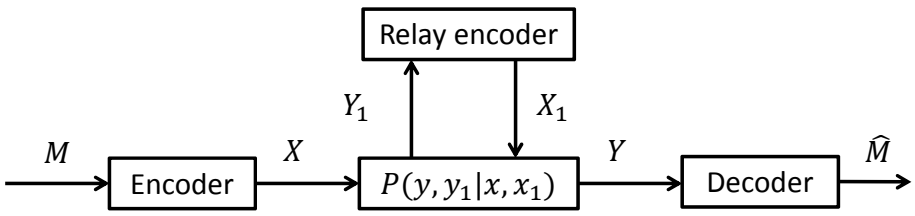

Figure 2.6: Discrete Relay Channel

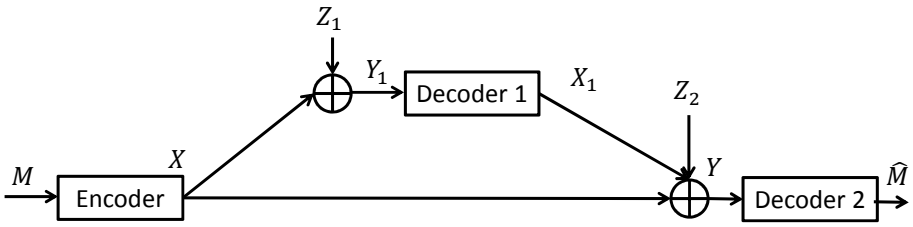

Figure 2.7: Gaussian Relay Channel

of the set of all achievable rate pairs. The RC is said to be *physically degraded* if $p(y, y_1|x, x_1)$ can be written in the form

$$p(y, y_1|x, x_1) = p(y_1|x, x_1)p(y|y_1, x_1). \tag{2.12}$$

Gaussian RC is a simple model for wireless cooperative communications with a relay. The channel outputs corresponding to the inputs X and X_1 with average power constraints P and P_1, are

$$\begin{aligned} Y_1 &= X + Z_1, \\ Y &= X + X_1 + Z_2, \end{aligned} \tag{2.13}$$

where Z_1 and Z_2 are independent zero mean Gaussian random variables with variances N_1 and N_2, respectively. Power constraints for the users' signals are given by

$$\sum_{i=1}^{n} x_i^2(m_1) \leq nP, \qquad \sum_{i=1}^{n} x_{1i}^2(m_2) \leq nP_1. \tag{2.14}$$

where $m_1 \in [1 : 2^{nR}]$ and $m_2 \in [1 : 2^{nR_1}]$. For the degraded model the channel output at the receiver Y is a corrupted version of that received at the relay Y_1 conditioned on X_1. As a result, the channel output at the receiver can be expressed as

$$Y = Y_1 + X_1 + Z_2. \tag{2.15}$$

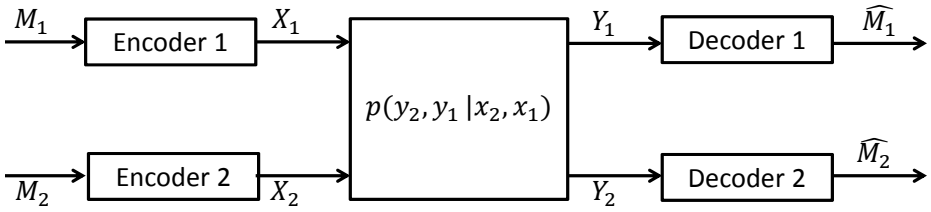

Figure 2.8: General Interference Channel

2.1.4 Interference Channel

Two-user DMIC model, in general, as depicted in Figure 2.8, consists of two input alphabets $\mathcal{X}_1$, $\mathcal{X}_2$, two output alphabets $\mathcal{Y}_1$, $\mathcal{Y}_2$, and channel transition probabilities $p(y_1, y_2|x_1, x_2)$. A sequence of $\left((2^{nR_1}, 2^{nR_2}), n\right)$ codes for a DMIC consists of $M_i \in [1 : 2^{nR_i}]$, $i = 1, 2$, as the message sets. $\widehat{M_1}$ and $\widehat{M_2}$ are the decoded messages at their respective receivers. Probability of error is defined as

$$P_{e_1}^{(n)} = \frac{1}{2^{n(R_1+R_2)}} \sum_{(M_1,M_2)} Pr\{\widehat{M_1}(Y_1^n) \neq M_1 | M_1 = m_1, M_2 = m_2\},$$
$$P_{e_2}^{(n)} = \frac{1}{2^{n(R_1+R_2)}} \sum_{(M_1,M_2)} Pr\{\widehat{M_2}(Y_2^n) \neq M_2 | M_1 = m_1, M_2 = m_2\}, \tag{2.16}$$

A rate pair (R_1, R_2) is said to be achievable for the DMIC if there exists a sequence of $\left((2^{nR_1}, 2^{nR_2}), n\right)$ codes with $P_{e_1}^{(n)}$, $P_{e_2}^{(n)} \to 0$ as $n \to \infty$. The capacity region of the DMIC is the convex hull of the set of all achievable rate pairs. A DMIC is said to have *very strong interference* if

$$I(X_1; Y_1|X_2) \leq I(X_1; Y_2),$$
$$I(X_2; Y_2|X_1) \leq I(X_2; Y_1), \tag{2.17}$$

for all product distributions on the inputs $p(x_1)p(x_2)$. A DMIC is said to have *strong*

interference if

$$I(X_1; Y_1|X_2) \leq I(X_1; Y_2|X_1),$$
$$I(X_2; Y_2|X_1) \leq I(X_2; Y_1|X_2), \tag{2.18}$$

for all product distributions on the inputs $p(x_1)p(x_2)$.

GIC as a simple model for wireless communication is depicted in Figure 2.9. Channel outputs for the system model can be written as

$$Y_1 = h_{11}X_1 + h_{21}X_2 + Z_1,$$
$$Y_2 = h_{12}X_1 + h_{22}X_2 + Z_2, \tag{2.19}$$

where X_1 and X_2 have power constraints of P_1 and P_2. Z_1 and Z_2 are zero mean Gaussian random variables with unit variances. Signal to noise ratios and interference to noise ratios are defined as follows

$$SNR_1 = |h_{11}|^2 P_1, \quad SNR_2 = |h_{22}|^2 P_2,$$
$$INR_1 = |h_{21}|^2 P_2, \quad INR_2 = |h_{12}|^2 P_1. \tag{2.20}$$

The interference conditions defined for the DMIC can be computed for the GIC. That

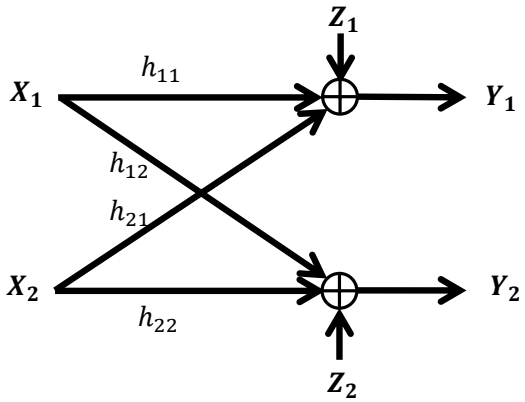

Figure 2.9: Gaussian Interference Channel

is, a GIC satisfies (2.17), thus, is said to have *very strong interference* if

$$\begin{aligned} INR_1 &\geq SNR_2^2 + SNR_2, \\ INR_2 &\geq SNR_1^2 + SNR_1. \end{aligned} \tag{2.21}$$

Similarly, a GIC satisfies (2.18), therefore, is said to have *strong interference* if

$$\begin{aligned} SNR_2 \leq INR_1 &< SNR_2^2 + SNR_2, \\ SNR_1 \leq INR_2 &< SNR_1^2 + SNR_1. \end{aligned} \tag{2.22}$$

A GIC is said to have *weak interference* [4] if for some $\rho_1, \rho_2 \in [0, 1]$,

$$\begin{aligned} \sqrt{\frac{INR_1}{SNR_2}}(1 + INR_2) &\leq \rho_2\sqrt{1-\rho_1^2}, \\ \sqrt{\frac{INR_2}{SNR_1}}(1 + INR_1) &\leq \rho_1\sqrt{1-\rho_2^2}. \end{aligned} \tag{2.23}$$

2.2 Review of Information Theoretic Results on Multi-User Channels

In this section, we review some existing results on the capacity and achievable rate regions, and rate region outer bounds for the basic multi-user channels provided in the previous section.

2.2.1 Multiple Access Channel

Considering the discrete memoryless MAC depicted in Figure 2.1, the capacity region can be shown to be the convex hull of rate pairs, (R_1, R_2) satisfying [5]

$$\begin{aligned} R_1 &\leq I(X_1; Y|X_2), \\ R_2 &\leq I(X_2; Y|X_1), \\ R_1 + R_2 &\leq I(X_1, X_2; Y). \end{aligned} \tag{2.24}$$

Similarly, the capacity region of the GMAC shown in Figure 2.2 is given by [5]

$$\begin{aligned} R_1 &\leq \log_2(1+P_1), \\ R_2 &\leq \log_2(1+P_2), \\ R_1+R_2 &\leq \log_2(1+P_1+P_2). \end{aligned} \tag{2.25}$$

For the two-user configuration, the corner points of the capacity region of the GMAC can be achieved by single user decoding also known as stripping, onion peeling, or step-by-step decoding [6]. In this scheme, the decoder starts by decoding one of the users data while treating the other as interference. Decoded data is then canceled out from the received signal prior to decoding the other users' signal. Using Gaussian codebooks, this decoding rule achieves rate pair (R_1, R_2) given by [6]

$$\begin{aligned} R_1 &= \log_2(1+P_1), \\ R_2 &= \log_2\left(1+\frac{P_2}{1+P_1}\right). \end{aligned} \tag{2.26}$$

Similarly $R_2 = \log_2(1+P_2)$ and $R_1 = \log_2(1+\frac{P_1}{1+P_2})$ can be achieved by using the reverse decoding order. The drawback of this scheme is that one should perform TS to achieve rate pairs on the dominant face of the rate region. As an alternative, there is a different strategy called rate-splitting through which one can achieve these points by single user decoding. The idea benefits from employing two codebooks at each transmitter with $C^{(ij)}$ denoting the codebook j adopted at transmitter i. The associated powers and rates for each codebook are [6]

$$\begin{aligned} R_1 = R_{11}+R_{12}, \quad P_1 = P_{11}+P_{12}, \\ R_2 = R_{21}+R_{22}, \quad P_2 = P_{21}+P_{22}. \end{aligned} \tag{2.27}$$

At the receiver, single user decoding is performed in three stages: first, the message corresponding to $C^{(21)}$ code is decoded, then the messages corresponding to the codes

$C^{(11)}$ and $C^{(12)}$ are decoded. Finally, the message corresponding to the $C^{(22)}$ code is decoded. Considering the decoding priorities, the following rate pair can be achieved,

$$\begin{aligned} R_1 &= \log_2\left(1+\frac{P_1}{1+P_{22}}\right), \\ R_2 &= R_{21}+R_{22} \\ &= \log_2\left(1+\frac{P_{21}}{1+P_1+P_{22}}\right)+\log_2(1+P_{22}). \end{aligned} \tag{2.28}$$

In special cases, assuming $P_{22}=0$ or $P_{22}=P_2$, one can achieve the corner points of the capacity region. Simultaneous decoding, also known as JD, also achieves rate pairs between the corner points without employing rate splitting or TS [7]. The optimal joint decoder is, however, much more complex than the optimal single user decoder due to considering all codeword pairs [6].

2.2.2 Broadcast Channel

The capacity region of the general BC has been an open problem for many years. However, capacities of some classes of BCs have been characterized. For instance, an achievable rate region for the degraded BC was first found by Cover [2] using "superposition coding", which is a layered coding scheme. Later, Bergman [8] showed that Cover's region is the actual capacity region given by the closure of all (R_1, R_2) satisfying

$$\begin{aligned} R_2 &< I(U;Y_2), \\ R_1 &< I(X;Y_1|U), \\ R_1+R_2 &< I(X;Y_1), \end{aligned} \tag{2.29}$$

over probability mass function of $p(u,x)$, where U is an auxiliary random variable with a cardinality bound $|\mathcal{U}| \leq \min\{|\mathcal{X}|, |\mathcal{Y}_1|, |\mathcal{Y}_2|\}$. Marton [9] and Pinsker [10] found the capacity region of the deterministic BC with $y_1 = f_1(x)$ and $y_2 = f_2(x)$

given by

$$\begin{aligned} R_1 &< H(Y_1), \\ R_2 &< H(Y_2), \\ R_1 + R_2 &< H(Y_1, Y_2). \end{aligned} \tag{2.30}$$

For a general DMIC, Marton in [11] showed that the following rate region is achievable

$$\begin{aligned} R_1 &< I(U; Y_1), \\ R_2 &< I(V; Y_2), \\ R_1 + R_2 &< I(U; Y_1) + I(V; Y_2) - I(U; V), \end{aligned} \tag{2.31}$$

for some $p(u, v, x)$ on $\mathcal{U} \times \mathcal{V} \times \mathcal{X}$, where U and V are auxiliary random variables. It is also indicated that this achievable region is the capacity region if the BC has one deterministic component. El Gamal in [12] discussed that feedback cannot increase the capacity of the physically degraded channel similar to the single user case. However, authors in [13, 14] show that feedback can indeed increase the capacity of general BCs. Korner and Marton [11] provided an outer bound for the capacity region by showing that $\mathcal{C}$ is the subset of the region characterized by

$$\begin{aligned} R_1 &< I(U; Y_1), \\ R_2 &< I(V; Y_2), \\ R_1 + R_2 &< I(U; Y_1) + I(V; Y_2|U), \\ R_1 + R_2 &< I(V; Y_2) + I(U; Y_1|V), \end{aligned} \tag{2.32}$$

for some $p(u, v, x)$ on $\mathcal{U} \times \mathcal{V} \times \mathcal{X}$.

The capacity region of the Gaussian broadcast channel (GBC) with power constraint P, as a degraded BC shown in Figure 2.5, is shown to be the convex hull

of the set of rate pairs (R_1, R_2) given by [5]

$$R_1 \leq \log_2\left(1+\frac{aP}{N_1}\right),$$
$$R_2 \leq \log_2\left(1+\frac{(1-a)P}{aP+N_2}\right), \tag{2.33}$$

where $a \in [0,1]$. There are also outer bounds reported in [15] and [16] for configuration where there is a common message sent to both receivers. Authors in [17] also have proposed a new outer bound called New-Jersey outer bound. Characterization of the full capacity region of the Gaussian multiple input multiple output (MIMO) channel was an open problem for a long time since it is non-degraded in general even when there is no fading. Authors in [18] characterized a rate region for Gaussian MIMO channels that achieve the sum rate capacity. It is proved later that the region is the actual capacity region [19] by matching an inner bound due to Marton [11] with an outer bound due to Sato [20].

2.2.3 Relay Channel

The capacity of the RC is not known in general, however, lower and upper bounds for the capacity have been found in the previous literature, see e.g., [21], [22]. It can be shown that the capacity of any RC is upper bounded as [4]

$$C \leq \max_{p(x,x_1)} \min\Big\{I(X,X_1;Y_1), I(X;Y,Y_1|X_1)\Big\}, \tag{2.34}$$

known as the *cutset bound* [4], which is tight for many classes of the discrete memoryless RC with known capacity such as the degraded RC and the class of *reversely degraded* RC in which $X \to Y_1 \to Y$ form a Markov chain conditioned on X_1. It can also be shown that the capacity of the RC is lower bounded by

$$C \geq \max_{p(x,x_1)} \min\Big\{I(X,X_1;Y_1), I(X;Y|X_1)\Big\}, \tag{2.35}$$

known as *decode and forward lower bound* [4]. A simple lower bound can be obtained by considering the P2P communication between sender and the receiver while the

relay transmission is fixed at the favorable symbol to the channel from the sender to the receiver, therefore the resulting capacity is lower bounded as [4]

$$C \geq \max_{p(x),x_1} I(X;Y_1|X_1 = x_1). \tag{2.36}$$

There are several coding schemes that are optimal in certain special cases. Among them, there are two extreme schemes named *direct transmission* and *decode-and-forward*. In the former scheme the relay is not actively involved in the communication process whereas in the latter one it plays a central role. It decodes the message and cooperates with the sender to communicate with the receiver. Direct transmission can beat decode and forward when the channel from the sender to the relay is weaker than that to the receiver. Considering the Gaussian RC depicted in Figure 2.7, the capacity region is given by

$$C = \max_{0\leq\alpha\leq 1} \min\left\{\log_2\left(1+\frac{P+P_1+2\sqrt{\alpha\bar{P}P_1}}{N_1+N_2}\right), \log_2\left(\frac{\alpha P}{N_1}\right)\right\}, \tag{2.37}$$

where $\bar{\alpha} = 1-\alpha$. It can be shown that if $\frac{P_1}{N_2} \geq \frac{P}{N_1}$, the capacity is given by

$$C = \log_2\left(1+\frac{P}{N_1}\right). \tag{2.38}$$

Although the capacity of the RC is still not known exactly even for the Gaussian case, much progress has been made recently in the characterization of its approximate capacity [23]. In [24], the capacity of a class of deterministic RCs with separate noiseless communication links from the relay to the receiver is provided. Authors in [25] provide an achievable rate for general Gaussian relay networks. They show that the achievable rate is within a constant from the cutset upper bound. Furthermore, it is shown that the constant does not depend on the values of the channel gains and it only depends on the topology of the network. In [26] the results are extended to include the case where the noises at the relay and at the destination are correlated.

2.2.4 Interference Channel

Characterization of capacity region for ICs has been pursued for more than three decades which have shed some light on various aspects of the problem. Carleial [27] and Sato [28] have shown that interference does not degrade the performance of the system if it is strong enough to be cancelled out from the received signal. For instance, the capacity region of the DMIC shown in Figure 2.8 with very strong interference is the set of rate pairs (R_1, R_2) such that

$$\begin{aligned} R_1 &\le I(X_1; Y_1|X_2, Q), \\ R_2 &\le I(X_2; Y_2|X_1, Q), \end{aligned} \tag{2.39}$$

for some PMF $p(q)p(x_1|q)p(x_2|q)$ with $|\mathcal{Q}| \le 2$. Similarly, the capacity region of the DMIC $p(y_1, y_2|x_1, x_2)$ with strong interference can be shown to be the set of rate pairs (R_1, R_2) such that

$$\begin{aligned} R_1 &\le I(X_1; Y_1|X_2, Q), \\ R_2 &\le I(X_2; Y_2|X_1, Q), \\ R_1 + R_2 &\le \min\{I(X_1, X_2; Y_1|Q), I(X_1, X_2; Y_2|Q)\}, \end{aligned} \tag{2.40}$$

for some PMF $p(q)p(x_1|q)p(x_2|q)$ with $|\mathcal{Q}| \le 4$. The capacity region of the GIC with very strong interference can be shown to be the set of rate pairs (R_1, R_2) such that

$$\begin{aligned} R_1 &\le \log_2(1 + SNR_1), \\ R_2 &\le \log_2(1 + SNR_2). \end{aligned} \tag{2.41}$$

Sato showed that the capacity region of GIC with strong interference is the intersection of the rate regions of two MAC channels [28], i.e.,

$$\begin{aligned} R_1 &\leq \log_2(1+SNR_1), \\ R_2 &\leq \log_2(1+SNR_2), \\ R_1+R_2 &\leq \min\{\log_2(1+SNR_1+INR_1), \log_2(1+SNR_2+INR_2)\}. \end{aligned} \tag{2.42}$$

Under weak interference, the capacity is unknown but a simple lower bound can be obtained by treating the interference as noise leading to

$$C_{sum} \geq \log_2\left(1+\frac{SNR_1}{1+INR_1}\right)+\log_2\left(1+\frac{SNR_2}{1+INR_2}\right). \tag{2.43}$$

It has been shown that if the interference is weak enough, the structure of the interference is not useful from an information theoretic perspective [29]. In other words, treating interference as noise can still achieve the maximum possible throughput, if it is below a certain level. It is proved that for the asymmetric IC satisfying

$$\left|\frac{h_{21}}{h_{11}}\left(1+\left(\frac{h_{12}}{h_{22}}\right)^2 SNR_1\right)\right|+\left|\frac{h_{12}}{h_{22}}\left(1+\left(\frac{h_{21}}{h_{11}}\right)^2 SNR_2\right)\right| \leq 1, \tag{2.44}$$

treating interference as noise achieves sum capacity as

$$C_{sum} = \log_2\left(1+\frac{SNR_1}{1+\left(\frac{h_{21}}{h_{11}}\right)^2 SNR_2}\right)+\log_2\left(1+\frac{SNR_2}{1+\left(\frac{h_{12}}{h_{22}}\right)^2 SNR_1}\right). \tag{2.45}$$

The HK achievable rate region is the best known rate region for IC in the general case [30]. In this scheme information of each user is divided into two parts, namely, private (U) and public (W). Public messages are intended to be decoded at both users while the private messages are only decodable at the intended receivers. At the receiver side, public messages are jointly decoded along with the intended

private message. A simplified version of the region is given by [30]

$$\begin{aligned} R_1 &\leq \rho_1, \\ R_2 &\leq \rho_2, \\ R_1 + R_2 &\leq \rho_{12}, \\ 2R_1 + R_2 &\leq \rho_{10}, \\ R_1 + 2R_2 &\leq \rho_{20}, \end{aligned} \tag{2.46}$$

where

$$\begin{aligned} \rho_1 &= \sigma_1^\star + I(Y_1; U_1|W_1W_2Q), \\ \rho_2 &= \sigma_2^\star + I(Y_2; U_2|W_1W_2Q), \\ \rho_{12} &= \sigma_{12} + I(Y_1; U_1|W_1W_2Q) + I(Y_2; U_2|W_1W_2Q), \\ \rho_{10} &= 2\sigma_1^\star + 2I(Y_1; U_1|W_1W_2Q) + I(Y_2; U_2|W_1W_2Q) - [\sigma_1^\star - I(Y_2; W_1|W_2Q)]^+ \\ &\quad + \min\big\{I(Y_2; W_2|W_1Q), I(Y_2; W_2|Q) + [I(Y_2; W_1|W_2Q) - \sigma_1^\star]^+, \\ &\qquad I(Y_1; W_2|W_1Q), I(Y_1; W_1W_2Q) - \sigma_1^\star\big\}, \\ \rho_{20} &= 2\sigma_2^\star + I(Y_1; U_1|W_1W_2Q) + 2I(Y_2; U_2|W_1W_2Q) - [\sigma_2^\star - I(Y_1; W_2|W_1Q)]^+ \\ &\quad + \min\big\{I(Y_1; W_1|W_2Q), I(Y_1; W_1|Q) + [I(Y_1; W_2|W_1Q) - \sigma_2^\star]^+, \\ &\qquad I(Y_2; W_1|W_2Q), I(Y_2; W_1W_2|Q) - \sigma_2^\star\big\}, \\ \sigma_1^\star &= \min\big\{I(Y_1; W_1|W_2Q), I(Y_2; W_1|U_2W_2Q)\big\}, \\ \sigma_2^\star &= \min\big\{I(Y_2; W_2|W_1Q), I(Y_1; W_2|U_1W_1Q)\big\}, \\ \sigma_{12} &= \min\big\{I(Y_1; W_1W_2|Q), I(Y_2; W_1W_2|Q), I(Y_1; W_1|W_2Q) + I(Y_2; W_2|W_1Q), \\ &\qquad I(Y_2; W_1|W_2Q) + I(Y_1; W_2|W_1Q)\big\}, \end{aligned}$$

with the following cardinality bounds

$$|\mathcal{U}_1| \leq |\mathcal{X}_1| + 2, \quad |\mathcal{W}_1| \leq |\mathcal{X}_1| + 7,$$

$$|\mathcal{U}_2| \leq |\mathcal{X}_2| + 2, \quad |\mathcal{W}_2| \leq |\mathcal{X}_2| + 7, \quad |\mathcal{Q}| \leq 11 \tag{2.47}$$

where Q is the TS random variable. For Gaussian signaling, mutual information functions are given by

$$\begin{aligned}
I(Y_1; U_1|W_1W_2) &= C(\lambda_1 P_1/(1 + h_{21}\lambda_2 P_2)), \\
I(Y_2; U_2|W_1W_2) &= C(\lambda_2 P_2/(1 + h_{21}\lambda_1 P_1)), \\
I(Y_1; W_1|W_2) &= C(\overline{\lambda_1} P_1/(1 + \lambda_1 P_1 + h_{21}\lambda_2 P_2)), \\
I(Y_1; W_2|W_1) &= C(h_{21}\overline{\lambda_2} P_2/(1 + \lambda_1 P_1 + h_{21}\lambda_2 P_2)), \\
I(Y_1; W_1W_2) &= C((\overline{\lambda_1} P_1 + h_{21}\overline{\lambda_2} P_2)/(1 + \lambda_1 P_1 + h_{21}\lambda_2 P_2)), \\
I(Y_2; W_2|W_1) &= C(\overline{\lambda_2} P_2/(1 + \lambda_2 P_2 + h_{12}\lambda_1 P_1)), \\
I(Y_2; W_1|W_2) &= C(h_{12}\overline{\lambda_1} P_1/(1 + \lambda_2 P_2 + h_{12}\lambda_1 P_1)), \\
I(Y_2; W_1W_2) &= C((\overline{\lambda_2} P_2 + h_{12}\overline{\lambda_1} P_1)/(1 + \lambda_2 P_2 + h_{12}\lambda_1 P_1)), \\
I(Y_1; W_1) &= C(\overline{\lambda_1} P_1/(1 + \lambda_1 P_1 + h_{21} P_2)), \\
I(Y_2; W_2) &= C(\overline{\lambda_2} P_2/(1 + \lambda_2 P_2 + h_{12} P_1)), \\
I(Y_1; W_2|U_1W_1) &= C(h_{21}\overline{\lambda_2} P_2/(1 + h_{21}\lambda_2 P_2), \\
I(Y_2; W_1|U_2W_2) &= C(h_{12}\overline{\lambda_1} P_1/(1 + h_{12}\lambda_1 P_1),
\end{aligned} \tag{2.48}$$

where C is a conventional P2P Gaussian capacity function in two dimensions defined as $C(x) = \log_2(1 + x)$ and λ_1 and λ_2 are private message power ratios of X_1 and X_2, respectively, i.e.,

$$\begin{aligned}
P_{u_1} &= \lambda_1 P_1, \\
P_{u_2} &= \lambda_2 P_2, \\
\lambda_1 + \overline{\lambda_1} &= 1.
\end{aligned} \tag{2.49}$$

Although the general rate region is formulated, computation of the entire region is very difficult since one should perform optimization over PMFs of many random

variables with large cardinalities. A simplified version of the general rate region is proposed in [31] named Chong-Motani-Garg rate region and it is proved to be identical to the HK rate region.

There are four main outer bounds for the GIC in the literature. The first bound is obtained in [32] for the degraded GIC based on the capacity region of a specific degraded BC. The second is due to Kramer for a GIC with weak interference where the bound is attained by discarding one of the interfering links in the channel [33]. The third is proposed by Etkin *et al.* for a general GIC exploiting a genie-aided technique [34]. The fourth, which is the most recent one, is reported by Motahari and Khandani based on the concept of *admissible channels* [35]. The outer bounds are revisited in [29] and tighter bounds are derived. A common feature of all these given bounds is that they are all based on a genie providing side information to the receivers.

Despite many information theoretic advances, practical solutions of interference managements are either sub-optimal and do not leverage the spectrum fully. Treating the interference as noise is a common approach from engineering point of view, however, this strategy is optimal when interference is considerably weak [4]. Another practical solution is to avoid interference through orthogonalizing techniques, such as TDMA, FDMA, CDMA, for which different users' signals are transmitted via channels separated in time, frequency, and code domains, respectively. Neither of these approaches fully exploit the available degrees of freedom defined as the linear growth factor of the logarithm of the capacity of the channel.

Another important line of work for transmission over ICs is interference alignment introduced in [36] by proposing an impressive coding scheme for MIMO X channel using dirty paper coding (DPC) and successive interference cancellation. The main

idea is to obtain asymptotic results on the possible transmission rates called degrees of freedom defined as

$$d = \lim_{SNR \to \infty} \frac{C}{\log(SNR)}, \tag{2.50}$$

where C denotes the capacity of the channel. In essence, interference alignment technique at each receiver aims at concatenating the interference roughly into one half of the signal space, leaving the other half available to the desired signal and free of interference, thus achieving more degrees of freedom [37]. Cadambe and Jafar in [37] exploit the idea for k-user ICs demonstrating that suitably designed precoders can result in achieving $\frac{K}{2}$ degrees of freedom. Wu et. al [38] explored the design of linear precoders for K-user MIMO ICs employing finite alphabet inputs. They demonstrate that the common interference alignment method for Gaussian inputs results in a constant rate loss when applied haphazardly to finite alphabet inputs.

Despite the superiority of the interference alignment, the scheme requires global channel knowledge so that users at the transmitter side can compute and use appropriate beamforming vectors to make the interference signals aligned at the receivers. Also, the results on this scheme are only asymptotic in terms of the SNRs which may not be the regime of operation for practical wireless systems.

2.3 Review of Practical Coding Schemes for Multi-User Channels

Initial work on designing practical codes for the MAC has appeared in [39, 40] where optimized codes were shown to achieve points close to the corner points of the capacity region. Exploiting LDPC codes, authors in [7] showed that any rate pair in the capacity region can be achieved without requiring TS or rate splitting. The codes were designed employing the density evolution (DE) technique [41] which is a powerful tool in tracking the probability density function of the LLRs exchanged among the nodes of the Tanner [42] graph representation. Authors in [43] proposed an efficient

coding scheme for MIMO MAC and showed that single user codes are not suitable for the MIMO case highlighting that new codes should be optimized for such channel. Authors in [1] explored the code design principles for the GMAC with equal-power for the transmitted signals. In particular, they utilized an extrinsic information transfer (EXIT) chart method, which visualizes the exchange of the information between the constituent decoders of the LDPC decoder first introduced by ten Brink [44]. They proposed a simple optimization approach based on Gaussian approximation of the exchanged messages, and they have shown that the designed codes operate close to the capacity boundary.

Practical codes using superposition coding, first introduced by Cover [2], appeared in [3] for the degraded Gaussian BC which combines superposition coding with trellis coded modulation. The designed codes have shown to achieve points within 1dB of the capacity region. DPC [45], which uses side information at the transmitter for encoding has been used in [18] for non-degraded Gaussian MIMO BCs. DPC has a performance gain over conventional schemes, e.g., TDMA, FDMA, especially when the SNR is high and the number of transmit antennas is large. Authors in [46], [47] designed practical and implementable capacity achieving codes utilizing DPC, which involve joint source channel coding. However, the proposed schemes based on DPC seem to be difficult to implement practically. As a result, authors in [48] analyzed the performance of different coding techniques as sub-optimal approaches for the fading MIMO Gaussian BC and they derived practical coding schemes that achieve points very close to the theoretical bounds. Better codes for MIMO BC are reported in [49]. These codes are designed by using nested turbo codes and DPC. One should note that superposition coding also achieves the capacity of simple Gaussian BC and practical codes exploiting superposition technique preform well [3]. However, superposition coding approach cannot be extended to include the MIMO Gaussian BC, where the

channels are not necessarily degraded. On the other hand, DPC achieves the capacity of both degraded and non degraded BCs. In [50] LDPC codes are used for single antenna fading BCs and suitable EXIT chart analysis is utilized to determine the degree distributions.

Thanks to their excellent performance, LDPC codes are also exploited for RCs. Khojastepour et. al. [51] discussed a novel method in designing LDPC codes for full duplex Gaussian RC. Having used partial graph factor to avoid cycles, they designed powerful codes that achieve points within 1dB of the theoretical outer bounds. Authors in [52, 53] designed turbo-based coding/decoding schemes for MIMO RCs where the relay forwards simultaneously its estimate for the previous coded block to the destination after decoding and re-encoding and the destination uses an iterative decoding algorithm to estimate the transmitted messages. They showed that the performances of codes are within the 1.5 dB of the theoretical limits. They also proposed a coding scheme in [54–56] for the half-duplex RCs and designed codes for the source and relay nodes. Specifically, they compute the period of time during which the relay node should listen and exploit it in their code design. The designed codes are shown to operate about 1.2 dB away from the theoretical bounds.

Authors in [57] introduced a new type of codes called bi-layer LDPC codes that operate simultaneously at two different SNRs to accommodate the different levels of SNRs at the relay and the destination. The proposed scheme is shown to have a close to optimal performance for the RC at high SNRs. Authors in [58] proposed practical coding schemes and developed receiver structures for the half duplex RCs. In particular, they utilized LDPC codes and designed codes operating within 1.1 dB of the information theoretic limits. Authors in [59, 60] studied the code design for the full duplex RCs with fading. EXIT charts analysis is exploited to optimize the codes

which are shown to operate very close to the information theoretic limits. They also examined the coded cooperation strategies for frequency selective fading RCs where they develop a distributed turbo-coding strategy demonstrating that with the proposed coding and iterative decoding method, one can approach existing approximate information rates closely [61, 62]. LDPC codes are optimized in [63] for two-way relay systems with physical-layer network coding wherein optimized codes shown to outperform the off-the-shelf codes designed for the P2P channel considerably.

Unlike the rich literature for designing practical codes for aforementioned channels, there is very limited work for the IC in terms of practical code designs to achieve points close to the boundaries of the known rate regions. Wu et. al [38] derive the optimal linear precoder for K-user MIMO ICs utilizing finite alphabet inputs. They employ LDPC codes and show that the bit error rate (BER) performance of the optimal precoders significantly outperform the ones utilized based upon the common Gaussian signalling. Authors in [64] carry on a comparative study of the few existing interference alignment schemes when combined with turbo coding. The results demonstrate the performance of the practical interference alignment techniques in LTE-compliant systems. Recently, authors in [65] explored the problem of code design for the two-user GIC optimizing codes for an example of symmetric GICs experiencing weak interference. They utilized a soft information cancellation method where the interfering signals at the receivers are partially decoded aiming at improving the decoding of the desired messages. The proposed implementation is, however, limited to the symmetric scenarios where identical degree distributions are utilized for both users' messages, therefore it is not directly applicable for the general case.

2.4 Chapter Summary

In this chapter, we have described the system models for MAC, BC, RC, and IC. We have reviewed the existing literature on the discussed channels from information theoretic point of view. In addition, we have summarized the existing results on practical and implementable channel codes designed for the studied multi-user channels. It is noted that information theoretic limit approaching codes are reported for MAC, BC and RC; however, a very limited work has been performed on optimizing codes for the IC motivating us to study this problem further, which is precisely the main contribution of this dissertation.

Chapter 3

LDPC CODE DESIGN FOR TWO-USER MULTIPLE ACCESS CHANNELS

In this chapter, We study code design for two-user GMACs under fixed channel gains and under quasi-static fading. We employ LDPC codes with BPSK modulation and utilize an iterative joint decoder consisting of two component decoder interacting through so-called state nodes. Adopting a belief propagation (BP) algorithm, we characterize the PDF of the outgoing LLRs from the state nodes. Via examples, we illustrate that the characterized PDF does not match a Gaussian density, and instead, it resembles a GM distribution. We then exploit the GM assumption in predicting the decoding performance of LDPC codes over GMACs and propose variants of existing analysis methods, named modified DE and modified EXIT. We derive a stability condition on the degree distributions of the LDPC code ensembles and utilize it in the code optimization. Through our extensive results, we demonstrate that for the case of fixed channel gains, the newly optimized codes perform close to the capacity region boundary outperforming the existing designs and the off-the-shelf P2P codes. Under quasi-static fading, optimized codes exhibit consistent improvements upon the P2P codes as well. Finite block length simulations of specific codes picked from the designed ensembles are also carried out where the performances of the optimized codes are shown to be close to the outage limits of the channel.

The rest of the chapter is organized as follows. In Section 3.2, the system model is described and coding/decoding schemes are elaborated. In Section 3.3, the PDF of the outgoing LLRs from the state nodes is computed and a stability condition is derived for the LDPC codes employed for two-user GMACs. In Section 3.4, we explain the proposed variants of the DE and the EXIT analysis based on GM

Full version of this work has been submitted to IEEE Transactions on Wireless Communications [66].

assumption. In Section 3.5, we elaborate on the code optimization procedure. In Section 3.6, numerical examples and simulation results are provided. Finally, Section 3.7 concludes the chapter.

3.1 Introduction

A Gaussian multiple access channel (GMAC) in its simplest form consists of two users communicating with one receiver in the presence of additive white Gaussian noise (AWGN). The capacity region of the two-user GMAC has been completely characterized. The corner points of the capacity region can be achieved via single user decoding (SUD), hence via time sharing one can achieve the points in between. It is also shown that any rate pair in the capacity region can be attained utilizing rate splitting or joint decoding without the need for time sharing [7]. From a practical channel coding prospective, authors in [1, 7] utilize LDPC codes and implement a joint decoding algorithm through iterative decoding achieving rate pairs close to the boundary for a two-user GMAC with equal channel gains.

LDPC codes are powerful linear block codes introduced by Gallager in [67]. While they were forgotten for a long time (except for some sporadic works) presumably due to the complexity of the encoding and decoding schemes, they were reintroduced in the work of MacKay [68] who rediscovered the potential of the linear block codes with sparse parity-check matrices. These codes have been successfully employed for various channels achieving promising rates close to the information theoretic limits. Motivated by their superior performance for different channels and their premise in [1] and [7], in this chapter, we explore the problem of LDPC code design for the more general two-user GMAC with BPSK modulation. We consider two scenarios for channel gains: fixed and quasi-static fading. The former scenario suits time-invariant models, while the latter models the scenarios for which the fading is

so slow that no matter how long the codeword is, the (random) channel gain remains constant. We do not consider the fast fading scenario, since a similar model is already investigated in [50] for the two-user degraded broadcast channel whose results can be readily applied to the MAC scenario.

LDPC codes exhibit a threshold effect which determines, in terms of the channel parameters, when the decoding error probability can be made arbitrary small. DE [41] is the primary technique in computing the decoding thresholds. Full implementation of the DE requires extensive calculations, therefore quantized DE [41] is commonly employed in the literature. A similar approach is followed in [69] where the authors employ DE for the two-user GMAC for a joint decoder wherein look-up tables are exploited to update the PDFs of the log-likelihood-ratios (LLRs) fed to the component LDPC decoders through the so-called state nodes [1].

EXIT analysis [70] is an alternative to the DE method tracking the evolution of the mutual information between the transmitted bits and the corresponding LLRs exchanged within the decoder. The common assumption in the EXIT analysis, which greatly simplifies the computations, is to consider Gaussian densities for the LLRs. Authors in [50] employ an EXIT analysis to optimize LDPC codes for the two-user degraded broadcast channel utilizing a joint decoder at the better receiver where they adopt a simple linear approximation to update the evolution of the mutual information at the state nodes. The authors in [1] also utilize an EXIT analysis to optimize irregular LDPC codes for the two-user GMAC with equal channel gains. Unlike [50], they compute the evolution of the mutual information as the average of the values obtained for two types of state nodes based on the transmitted (coded) bits. Authors in [71] study a similar channel model and adopt an EXIT analysis to design distributed joint source-channel codes. They show for some (simulation) examples

that the PDFs of the outgoing LLRs from the state nodes resemble a Gaussian mixture (GM) distribution, however, for simplification, they opt for using the Gaussian assumption.

Motivated by the results of [71], we analytically characterize the PDF of the outgoing LLRs from the state nodes for fixed channel gains and illustrate via examples that the PDF of the outgoing LLRs from the state nodes resembles a GM distribution. Based on this observation, we utilize the GM assumption and modify the existing DE [69] and EXIT analysis [50] methods. We refer to the new algorithms as the modified DE and the modified EXIT analysis throughout the chapter. For the modified DE, the PDFs of the outgoing LLRs from the state nodes are fitted with GM distributions. The parameters of the GM distributions are estimated by employing the expectation maximization (EM) method run over the samples generated via Monte Carlo simulations [72]. The obtained PDFs are then fed to the component LDPC decoders where common method of [73] is adopted to track the evolution of the PDFs exchanged between the check nodes and the variable nodes. For the modified EXIT analysis, the evolution of the mutual information associated with the exchanged LLRs are computed analytically exploiting the GM assumption. Unlike [74], the computations are performed with no limitation on the ratio of the variance to the mean of the PDFs. Considering the fixed channel gains scenario, we incorporate the proposed methods of modified DE and modified EXIT analysis into the LDPC code optimization, which is based on a random perturbation technique also exploited in [75] for a different problem.

We provide many code design examples in the chapter. We demonstrate that the optimized LDPC codes for the case of equal channel gains are shown to improve upon the ones designed in [1]. For the case of unequal channel gains, we show

that our optimized codes offer better performance compared to the ones attained via the method of [50]. In addition, we highlight that the optimized codes outperform the point-to-point (P2P) codes designed for binary-input AWGN (BI-AWGN) channels. For the quasi-static fading scenario, we consider the common outage probability [76] as the performance measure. Despite the superiority of our proposed methods, the amount of computations prohibits their use in quasi-static fading, hence to simplify the analysis and reduce the amount of computations, we incorporate the simple method of [50] in the code optimization process. We carry out the code design for examples of real and complex channel gains and demonstrate that the newly designed codes consistently improve upon the existing P2P designs. We also perform finite code block length simulations for the optimized codes and the P2P codes confirming the superiority of the new designs.

3.2 System Model and Preliminaries

Consider a two-user GMAC where the received signal Y is expressed as

$$Y = H_1 X_1 + H_2 X_2 + Z,$$

where X_i represents the signal of the user i with the average power $E\{|X_i|^2\} = 1$ $(i = 1, 2)$, and Z denotes the circularly symmetric complex AWGN with variance $\frac{1}{2}$ per dimension. The average received power of the user i is defined as $P_i = |H_i|^2$ with H_i denoting the channel gain between the user i and the receiver. We consider two scenarios: fixed channel gains and quasi-static fading. For the former case, the channel gains are unchanged throughout the entire transmissions, while in the latter, they are drawn randomly but kept fixed during the transmission of each codeword.

3.2.1 Shannon Capacity vs Outage Capacity

For the case with fixed channel gains, the Shannon capacity of the two-user GMAC is the convex hull of the rate pairs (R_1, R_2) characterized as [4]

$$\begin{aligned} R_1 &< I(X_1; Y|X_2), \\ R_2 &< I(X_2; Y|X_1), \\ R_1 + R_2 &< I(X_1, X_2; Y), \end{aligned}$$

over all product distributions $p_{X_1}(x_1) \cdot p_{X_2}(x_2)$. Under quasi-static fading, reliable transmission is not guaranteed for all the channel realizations, therefore the Shannon capacity is zero. Authors in [76] introduced the common outage capacity region (COCR) computed as

$$\begin{aligned} Pr\{R_1 < I(Y; X_1|X_2)\} &\geq 1 - P_o, \\ Pr\{R_2 < I(Y; X_2|X_1)\} &\geq 1 - P_o, \\ Pr\{R_1 + R_2 < I(Y; X_1, X_2)\} &\geq 1 - P_o, \end{aligned} \tag{3.1}$$

over all PDFs $p_{X_1}(x_1) \cdot p_{X_2}(x_2)$ where P_o is called common outage probability.

The rate region in (3.1) can be calculated analytically for Gaussian signaling [77]. For BPSK signaling, however, numerical calculations are needed. Here, we adopt a grid search method to characterize COCR for BPSK signaling considering real channel gains. The boundary of the COCR can be characterized by solving

$$\begin{aligned} \min_{R_1, R_2} \quad & |\tilde{P}_o(R_1, R_2) - P_o| \\ s.t. \quad & 0 \leq R_1 \leq R_{1_{max}}, \\ & 0 \leq R_2 \leq R_{2_{max}}, \end{aligned}$$

where $\tilde{P}_o(R_1, R_2)$ is computed as

$$\tilde{P}_o(R_1, R_2) = \int_0^\infty \int_0^\infty \mathbb{1}_{COCR}(R_1, R_2, h_1, h_2) f_{H_1}(h_1) f_{H_2}(h_2) dh_1 dh_2.$$

The function $\mathbb{1}_{COCR}$ equals 1 if, for a given (R_1, R_2, h_1, h_2), the rate pairs are inside the conditional rate region (3.1), otherwise is set to 0. $R_{i_{max}}$ denotes the capacity of the P2P channel between the user i and the receiver.

3.2.2 Coding and Decoding Schemes

At the transmitter sides, the information bits of each user are encoded with an LDPC code. The ith encoded bits of message u_j, denoted with $c_j(i)$, is modulated using BPSK constellation and sent over the channel as $X_j(i) = \big(1 - 2c_j(i)\big)$. At the receiver side, we can employ JD [1] or the successive cancellation method ([78, 79]). In successive cancellation, decoding is done sequentially adopting component LDPC decoders where the decoded messages at each stage are subtracted from the original signal until all the messages are estimated (Fig. 3.1a). It is possible to improve the overall performance by iterating between the component LDPC decoders.

Under JD, in contrast to successive cancellation, decoding of the messages are performed concurrently and in rounds. Each round starts with computing the LLRs to be fed to the component LDPC decoders, where each decoder runs for some iterations utilizing the BP algorithm. The round is completed by passing the updated LLRs from the variable nodes to the so-called state nodes [1], denoted with the black circle in Fig. 3.1a. The exchange of LLRs between the component LDPC decoders and the state nodes can be performed serially or in parallel. In parallel scheduling both component LDPC decoders run simultaneously whereas in serial scheduling only one component LDPC decoder is active at each iteration [1]. As in [1], we adopt parallel scheduling in the rest of the chapter.

3.3 Analysis of Joint Decoding

In this chapter we utilize irregular LDPC codes which have been successfully employed over various channels [1], [50], [60]. Following the notation in [41], an ensemble

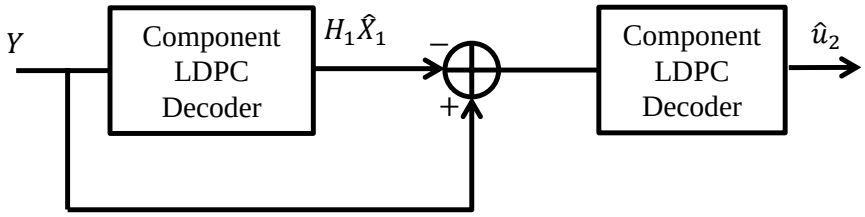

(a) Successive Canceler Block Diagram

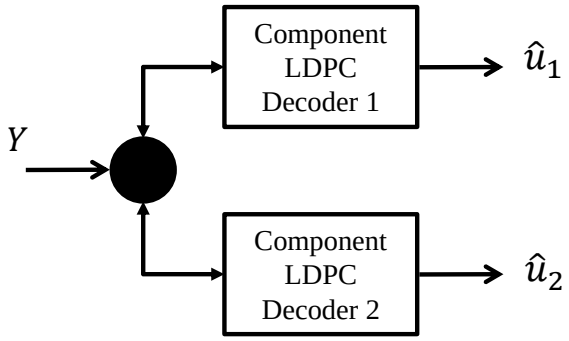

(b) Joint Decoder Block Diagram

Figure 3.1: Block Diagram of the Decoder Structures ($\hat{X}$ Denotes the Decoded Message for the Transmitted Message X.)

of irregular LDPC codes (λ, ρ) is described with $\lambda(x) = \sum_{i=2}^{d_v} \lambda_i x^{i-1}$ and $\rho(x) = \sum_{i=2}^{d_c} \rho_i x^{i-1}$, where d_v and d_c are maximum degrees of variable nodes and check nodes, respectively, and the *design rate* of the code is computed as

$$r = 1 - \frac{\sum_{i=2}^{d_c} \rho_i / i}{\sum_{i=2}^{d_v} \lambda_i / i}. \tag{3.2}$$

In the following, we review i.i.d. channel adapters and study the stability conditions for the degree distributions of the LDPC employed for the two-user GMAC. In addition, we elaborate on the computation of the outgoing LLRs from the state nodes and derive the associated PDF.

3.3.1 I.I.D. Channel Adapters

The decoding analysis of the LDPC codes can be greatly simplified for a symmetric channel by analyzing the behavior of the decoder for the all-zero codeword [41]. A

channel is called symmetric if $f_{Y_i}(y|C_i = 0) = f_{Y_i}(-y|C_i = 1)$, where C_i and Y_i refer to the ith coded bit and the ith channel output, respectively, and f_{Y_i} denotes the PDF of Y_i conditioned on C_i. Unlike the case of BI-AWGN channels, the channel symmetry does not hold for multi-user channels in general. To address this issue in our setting, we employ the independent and identically distributed (i.i.d.) channel adapters [80] applied at the transmitter and receiver sides. The idea is to combine each codeword with a random sequence prior to transmission and utilize the same set of sequences at the receiver for decoding of each codeword in order to enforce symmetry. It should be noted that the i.i.d. channel adapters are employed to simplify the analysis and are not implemented during the actual encoding and decoding processes.

3.3.2 Stability Condition

Authors in [41] introduced a stability condition analyzing the asymptotic decoding behavior of an LDPC code ensemble used over a BI-AWGN channel. The stability condition is further studied for multi-user scenarios [1, 50, 75], for instance, authors in [1] compute the stability condition for two-user GMACs when channel gains are identical and real. Here, we derive the stability condition conditioned on the channel gains for the general scenario of complex channel gains[1]. For simplicity of the analysis, we follow the approach taken in [75] and assume that the joint decoder is operating at steady state and close to successful decoding. We derive the stability condition for the component LDPC decoder j assuming the other component LDPC decoder has *almost* decoded its own message, therefore the *modified* channel output Y' [75] is obtained as $Y' = H_j X_j + Z$, which resembles a P2P channel. As a consequence, the LLR received at the ith variable node of component LDPC decoder j is simplified to $L\big(c_j(i)\big) = 4\,\mathrm{Re}\{H_j Y^*\}$. Considering the symmetry condition [75], it is easy to show that after applying the channel adapters, $L\big(c_j(i)\big)$ is distributed as $\mathcal{N}\Big(4|H_j|^2, 8|H_j|^2\Big)$.

[1]The case of real channel gains can be handled similarly.

Hence, results of [41] can be utilized to derive the stability condition, given by

$$\lambda_j'(0)\rho_j'(1) < \exp\Big(|H_j|^2\Big), \tag{3.3}$$

where $\lambda_j'(0)$ denotes the derivative of polynomial λ of user j computed at zero. For the quasi-static scenario, H_j changes from one codeword to another.

3.3.3 Characterization of Outgoing LLRs from State Nodes

Considering the BP rule at the state nodes, the LLR corresponding to the ith coded bit of the message of user j is computed as

$$L\big(c_j(i)\big) = \log\left(\frac{f_{Y_i}(y|c_j(i)=0)}{f_{Y_i}(y|c_j(i)=1)}\right). \tag{3.4}$$

The update rule (3.4) is a non-linear operation, therefore existing performance analysis techniques employ look-up tables or numerical methods to evaluate the PDF of the outgoing LLRs from the state nodes. In the following, we derive the PDF of the LLRs analytically. To simplify the analysis, we consider the case of real channel gains. Also, we discard the bit index in the expressions for the ease of the exposition. Without loss of generality, we consider the LLR sent from the state node to the variable node of component LDPC decoder 1 computed as

$$\begin{aligned} L &= 4Y(H_1 - H_2) + \log\left(\frac{\exp\Big(4H_2(Y-H_1)\Big)\exp(X)+1}{\exp(X)+\exp\Big(-4H_2(Y+H_1)\Big)}\right) \\ &= BY' + \log\left(\frac{1+A\exp(Y'+X)}{\exp(X)\Big(1+A\exp(-Y'-X)\Big)}\right), \end{aligned} \tag{3.5}$$

where $A = \exp(-4H_2H_1), Y' = 4H_2Y$, $B = \frac{(H_1-H_2)}{H_2}$, and X denotes the LLR received at the state node from the other component LDPC decoder. Considering i.i.d. channel adapters, X can be written as $t \cdot X'$ where t is a random sequence consisting of 1 and -1 with equal probability for the user 2 [80] and X' denotes the LLR prior to applying the channel adapters. Therefore, the PDF of the random variable X can be

obtained as

$$f_X(x) = \frac{1}{2}\Big(f_{X'}(x) + f_{X'}(-x)\Big).$$

Similarly, Y can be considered as the channel output corresponding to the transmission of all-ones sequence for user 1 and a sequence with symbols 1 and -1 drawn with equal probability [1] for user 2. Hence, the PDF of Y' is computed as

$$f_{Y'}(y') = \frac{1}{8H_2\sqrt{\pi}}\left(e^{-\left(\frac{y'}{4H_2}-H_1-H_2\right)^2} + e^{-\left(\frac{y'}{4H_2}-H_1+H_2\right)^2}\right).$$

We derive the PDF of L for the equal channel gains and the unequal channel gains, separately.

3.3.3.1 Equal channel gains

Consider the transformation

$$\begin{aligned} Z_1 =& \log\left(\frac{1 + A\exp(Y' + X)}{\exp(X)\big(1 + A\exp(-Y' - X)\big)}\right), \\ Z_2 =& Y', \end{aligned}$$

implying

$$\begin{aligned} X =& -Z_1 + \log\left(\frac{1 - A\exp(Z_1 - Z_2)}{1 - A\exp(Z_2 - Z_1)}\right) \quad -|\log(A)| + Z_2 \le Z_1 \le |\log(A)| + Z_2, \\ Y' =& Z_2. \end{aligned}$$

Since $L = Z_1$, $f_L(l)$ is obtained by marginalizing f_{Z_1,Z_2} over Z_2, which is given by

$$\begin{aligned} f_L(l) &= \int_{\mathbb{F}} |J(l, z_2)| f_{Z_1,Z_2}(l, z_2) dz_2, \\ &\overset{(a)}{=} \int_{-|\log(A)|}^{|\log(A)|} \left|\frac{A^2 - 1}{(A^2 - 2A\cosh(z_2') + 1)}\right| f_X\left(-l + \log\left(\frac{1 - A\exp(-z_2')}{1 - A\exp(z_2')}\right)\right) \\ &\qquad \times f_{Y'}(z_2' + l) dz_2' \end{aligned} \tag{3.6}$$

where (a) follows from the transformation $z_2' = z_2 - l$ and $J(.,.)$ is the Jacobian function defined as

$$|J(z_1, z_2)| = \begin{vmatrix} \frac{\partial x}{\partial z_1} & \frac{\partial y'}{\partial z_1} \\ \frac{\partial x}{\partial z_2} & \frac{\partial y'}{\partial z_2} \end{vmatrix}.$$

3.3.3.2 Unequal Channel Gains

Similar to the previous case, we adopt the random variable transformation

$$\begin{aligned} Z_1 =& \log\left(\frac{1 + A\exp(X + Y')}{\exp(X)\big(1 + A\exp(-X - Y')\big)}\right), \\ Z_2 =& BY', \end{aligned}$$

where

$$X = -Z_1 + \log\left(\frac{1 - A\exp\left(Z_1 - \frac{Z_2}{B}\right)}{1 - A\exp\left(-Z_1 + \frac{Z_2}{B}\right)}\right) \quad -|\log(A)| + \frac{Z_2}{B} < Z_1 < |\log(A)| + \frac{Z_2}{B},$$

$$Y' = \frac{Z_2}{B}.$$

Since $L = Z_2 + Z_1$, it follows that

$$\begin{aligned} f_L(l) &= \int f_{Z_1 Z_2}(l - z_2, z_2) dz_2 \\ &= \int_{-|\frac{B\log(A)}{1+B}|}^{|\frac{B\log(A)}{1+B}|} f_X\left(z_2 - \frac{l}{B+1} + \log\left(\frac{1 - A\exp\left(-z_2(\frac{B+1}{B})\right)}{1 - A\exp\left(z_2(\frac{B+1}{B})\right)}\right)\right) f_Y\left(\frac{z_2 + \frac{Bl}{B+1}}{B}\right) \\ &\qquad \times \left|J\Big(\frac{l}{B+1} - z_2, z_2\Big)\right| dz_2 \end{aligned} \tag{3.7}$$

for $B \neq -1$ and

$$f_L(l) = \int_{-\infty}^{\infty} |J(l - z_2, z_2)| f_X\left(z_2 - l + \log\left(\frac{1 - A\exp(l)}{1 - A\exp(-l)}\right)\right) f_Y\left(\frac{z_2}{B}\right) dz_2 \tag{3.8}$$

for $B = -1$. Note that at the zeroth iteration, $X = 0$, therefore $f_L(l)$ for both cases of equal channel gains and unequal channel gains can be computed via the one-to-one transformation from Y' to L. The computations of (3.6), (3.7), and (3.8), are

costly for practical implementations. Therefore, we propose approximating the PDF by a simpler form. In the following, we show that the GM distributions are good candidates for approximating the PDFs.

3.3.4 GM Approximation

GM distributions are parametric PDFs represented as a weighted sum of Gaussian component densities given by

$$f_L(l) = \sum_{i=1}^{N} w_i \exp\left(- \frac{(l-\mu_i)^2}{2\sigma_i^2} \right),$$

where μ_i, σ_i^2, and w_i denote the mean, the variance, and the mixing proportion of the Gaussian component i, respectively, and N denotes the number of Gaussian components involved. The GM distribution's parameters are commonly estimated via the EM [72] method run on the samples of the random variable.

GM distributions are commonly exploited to characterize a large class of sample distributions, primarily due to their ability to form smooth approximations for various densities. In this chapter, we study their use in approximating the PDF of the outgoing LLRs from the state nodes under joint decoding. To simplify the calculations, similar to [1, 50], we assume that the LLRs sent from the variable nodes to the state nodes have a Gaussian density. Fig. 3.2 illustrates the PDF of the outgoing LLRs sent from the state nodes to the variable nodes of component LDPC decoder 1 computed with different methods. I_{vs} denotes the mutual information between the transmitted bits and the LLRs sent from the variable nodes of component LDPC decoder 2 to the state nodes. According to the figure, the PDFs computed via the Monte Carlo simulations match closely with the ones calculated through the analytical derivations. Furthermore, it is clear that the PDFs do not resemble Gaussian densities, instead they are well-approximated with a GM distribution with two Gaussian components. Motivated by these observations, we propose two methods of

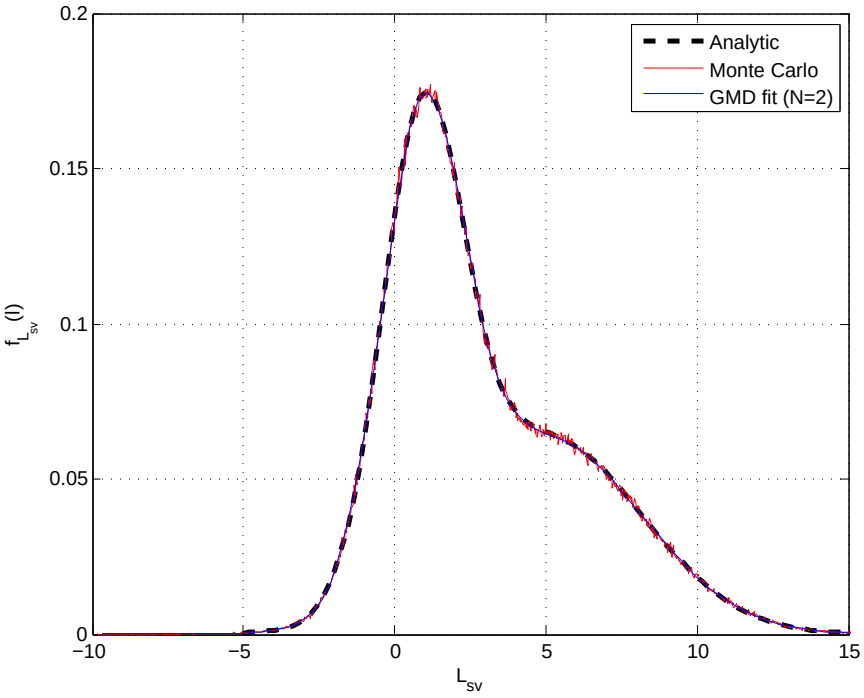

(a) $P_1 = 4$ dB, $P_2 = 4$ dB, $I_{vs} = 0.3$.

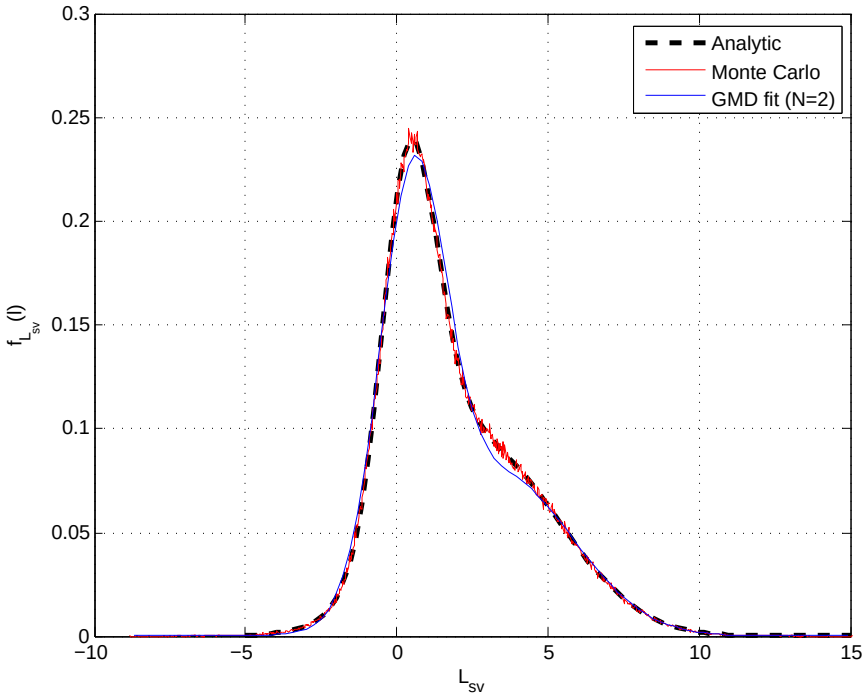

(b) $P_1 = 2$ dB, $P_2 = 1$ dB, $I_{vs} = 0.1$.

Figure 3.2: Illustration of the PDFs of the Outgoing LLRs from the State Nodes to the Variable Nodes of the Component LDPC Decoder of User 1 for Different Values I_{vs}

performance analysis exploiting GM approximation for the LLRs exchanged within the joint decoder. For simplicity of the exposition, the methods are outlined for GM distributions with two components. We note that extensions to higher number of Gaussian components would follow similar steps.

3.4 Proposed Performance Evaluation Methods

3.4.1 Modified DE

For the proposed method, we utilize the GM approximation and track the PDF of the LLRs exchanged among the nodes of the Tanner graph of the joint decoder. In the following we elaborate on the computations performed for each phase of the decoding iteration separately.

State Node to Variable Node: We exploit the GM assumption to characterize the PDF of the outgoing LLRs from the state nodes. To estimate the parameters of the GM distributions, we utilize the EM method on the samples of the actual PDF computed through (3.4) based on the samples of the received LLRs from the variable nodes of the other LDPC component decoder. These samples are generated by applying the inverse transform sampling technique [81] on the corresponding PDF obtained in the previous iteration. It is worth mentioning that the burden of the computations is primarily due to the EM method. To reduce the amount of EM computations, the initial estimates of the each parameter of the GM distribution at each iteration can be chosen as the value for the corresponding parameter estimated in the previous iteration.

Variable Node to Check Node: At the variable node with degree k, the LLR $L_{vc_j}^{(k)}$ sent on the jth edge is computed as $L_{vc_j}^{(k)} = L_{sv} + \sum_{\substack{i=1 \\ i \neq j}}^{k} L_{cv_i}$, where L_{sv} and L_{cv_i} are the LLRs received from the connected stated node and the ith connected check node, respectively. For a cycle free Tanner graph, the incoming messages at each node are

i.i.d, hence the PDF of $L_{vc}^{(k)}$ is obtained as $f_{L_{vc}^{(k)}} = f_{L_{sv}} \otimes \left(\bigotimes_{i=1}^{d_v-1} f_{L_{cv}} \right)$ where $\bigotimes$ denotes the convolution operation. Considering all the variable nodes, the PDF of the L_{vc} is computed as $f_{L_{vc}} = \sum_{i=2}^{d_v} \lambda_i \cdot f_{L_{vc}^{(k)}}$.

Check Node to Variable Node: At the check node with degree k, the LLR $L_{cv_j}^{(k)}$ sent on the jth edge is computed as $L_{cv_j}^{(k)} = 2\tanh^{-1}\left(\prod_{\substack{i=1 \\ i\neq j}}^{k} \tanh\left(\frac{L_{vc_i}}{2}\right) \right)$. Due to the non-linearity of the update rule, the PDF of $L_{cv}^{(k)}$ is typically computed via a look-up table [73]. In this chapter, we follow a similar approach where the PDF is calculated by applying a two-input operator R, that is, $f_{L_{cv}^{(k)}} = R^{k-1} f_{L_{vc}}$, where $R(a,b) = \mathcal{Q}\left(2\tanh^{-1}\left(\tanh\left(\frac{a}{2}\right)\tanh\left(\frac{b}{2}\right)\right)\right)$ with $\mathcal{Q}(.)$ representing the quantization operator. Considering all the check nodes, the PDF of L_{cv} is obtained as $f_{L_{cv}} = \sum_{i=2}^{d_c} \rho_i \cdot f_{L_{cv}^{(k)}}$.

Variable Node to State Node: The outgoing LLR from the variable node with degree k to the connected state node is computed as $L_{sv} = \sum_{i=1}^{k} L_{cv_i}$, therefore $f_{L_{vs}^k} = \bigotimes_{i=1}^{k} f_{L_{cv}}$ and $f_{L_{vs}} = \sum_{i=2}^{d_v} \bar{\lambda}_i \cdot f_{L_{vs}^{(k)}}$ where $\bar{\lambda}_i$ represents the node degree distribution computed as $\bar{\lambda}_i = \frac{\lambda_i}{\sum_{j=2}^{d_v} \frac{\lambda_j}{j}}$.

Yedla et. al. in [69] also utilize the DE method to analyze the performance of the joint decoder employed for the two-user GMAC. They exploit look-up tables to characterize the PDFs of the outgoing LLRs from the state nodes. Despite the accuracy of the method, considerable amount of memory is required to construct the look-up tables. We need to highlight that the proposed method here is inherently different from [69] as in the modified DE the PDF of the outgoing LLRs from the state nodes are approximated with a GM distribution rather than being exactly characterized. Moreover, compared to [69], the complexity of the modified DE does not grow with the number of involved component LDPC decoders hence it is more amenable for extension to higher number of users.

We observe through examples that the proposed method provides accurate threshold estimates for a large range of user powers; however, we also notice that for large values of powers, when the channel gains are equal, the PDFs of the outgoing LLRs from the state nodes contain spikes around zero which cannot be well approximated with GM distributions, hence leading to poor decoding threshold estimates.

3.4.2 Modified EXIT Analysis

We exploit the GM approximation in tracking the evolution of the mutual information between the transmitted BPSK symbol X and the exchanged LLR L. It is shown in [75] that under joint decoding the symmetry property of the exchanged LLRs is preserved, therefore the associated mutual information can be obtained as [82]

$$I(X;L) = 1 - E\Big\{ \log_2 \Big(1 + \exp(-L)\Big)\Big\}, \tag{3.9}$$

where the expectation is taken over L. For L with a GM distribution with N Gaussian components, (3.9) can be computed as

$$\begin{aligned} I(X;L) =& 1 - \int_{-\infty}^{\infty} \left(\sum_{i=1}^{N} \frac{w_i}{\sqrt{2\pi\sigma_i^2}} \exp\left(- \frac{(l-\mu_i)^2}{2\sigma_i^2} \right) \log_2 \Big(1 + \exp(-l)\Big) \right) dl \\ =& \sum_{i=1}^{N} w_i J'(\mu_i, \sigma_i), \end{aligned} \tag{3.10}$$

where $N = 2$ for the proposed method and $J'(\mu, \sigma)$ is defined as

$$J'(\mu,\sigma) = 1 - \frac{1}{\sqrt{2\pi\sigma^2}} \int_{-\infty}^{\infty} \exp\left(- \frac{(l-\mu)^2}{2\sigma^2} \right) \log_2 \Big(1 + \exp(-l)\Big) dl. \tag{3.11}$$

The J' function is analytically calculated in Appendix A. The introduced function can be considered as an extension to the J function in [74]; however, no specific relation is assumed between the mean and the variance in the computation. In the following, we detail the approach taken to compute the mutual information associated with the exchanged LLRs between the different nodes of the Tanner graph, separately.

State Node to Variable Node: We consider a GM distribution for the PDF of L_{sv}. To characterize the associated GM distribution, we generate samples of the outgoing LLRs through (3.5) based on the samples of the received LLRs from the other component LDPC decoder whose PDF is approximated with $\mathcal{N}(\mu_{vs}, 2\mu_{vs})$ where $\mu_{vs} = \frac{J^{-1}(I_{vs})}{2}$. The EM method is then utilized to calculate the parameters of the GM distribution. The mutual information associated with L_{sv} is computed via (3.10). Note that at the zeroth iteration $\mu_{vs} = I_{vs} = 0$.

Variable Node to Check Node: Considering the factor graph, the outgoing LLR sent on an edge from each variable node is computed by adding the received LLRs from the connected check nodes and the neighboring state node. Assuming the factor graph of the joint decoder is cycle free, the Central Limit Theorem (CLT) can be invoked to approximate the PDF of the added LLRs received from the check nodes with a Gaussian density. As a consequence, the PDF of the outgoing LLRs can be computed as the convolution of a Gaussian density with a GM distribution, which results in a GM distribution. The parameters of the GM distribution corresponding to the variable nodes with degree k are computed as

$$\begin{aligned} \mu_{vc_m}^{(k)} &= (k-1)\mu_{cv} + \mu_{sv_l}, \\ \sigma_{vc_m}^{(k)} &= \sqrt{(k-1)\sigma_{cv}^2 + \sigma_{sv_l}^2}, \\ w_{vc_m}^{(k)} &= w_{sv_m}, \end{aligned} \tag{3.12}$$

where μ_{sv_m} and σ_{sv_m} denote the mean value and the standard deviation of the mth ($m = 1, 2$) Gaussian component of the GM distribution associated with L_{sv}, respectively. The subscripts cv and vc in (3.12) correspond to the LLRs sent from the check nodes to the variable nodes and from the variable nodes to the check nodes, respectively. The computed GM distribution parameters in (3.12) can then be used

towards computation of the associated mutual information I_{vc} calculated as

$$I_{vc}(X; L_{vc}) = \sum_{i=2}^{dv} \lambda_i \cdot \Big(w_{vc_1}^{(i)} J'(\mu_{vc_1}^{(i)}, \sigma_{vc_1}^{(i)}) + w_{vc_2}^{(i)} J'(\mu_{vc_2}^{(i)}, \sigma_{vc_2}^{(i)}) \Big). \tag{3.13}$$

Check Node to Variable Node: L_{cv} is a non-linear function of L_{vc}, therefore we approximate the PDF of L_{cv} with a GM distribution computed based on the samples of L_{vc}. For ease of computation, the samples are drawn from $\mathcal{N}(\mu_{vc}, 2\mu_{vc})$ where $\mu_{vc} = \frac{\left(J^{-1}(I_{vc})\right)^2}{2}$ with J^{-1} introduced in [74]. The mutual information associated with L_{cv} is obtained similar to (3.13).

Variable Node to State Node: The computation of L_{vs} is performed by simply adding the received LLRs from the connected check nodes. Assuming the factor graph of the joint decoder is cycle-free, the CLT can be involved approximating the PDF of $L_{vs}^{(k)}$ with a Gaussian density with $\mu_{vs}^{(k)} = k.\bar{\mu}_{cv}$ and $\sigma_{vs}^{(k)} = \sqrt{k}.\bar{\sigma}_{cv}$ where $\bar{\mu}_{cv}$ and $\bar{\sigma}_{cv}$ denote the mean and variance of the LLRs received from the check nodes, respectively. We have

$$\begin{aligned}
\bar{\mu}_{cv} =& w_{cv_1}\mu_{cv_1} + w_{cv_2}\mu_{cv_2}, \\
\bar{\sigma}_{cv} =& \sqrt{w_{cv_1}(\mu_{cv_1}^2 + \sigma_{cv_1}^2) + w_{cv_2}(\mu_{cv_2}^2 + \sigma_{cv_2}^2) - (\bar{\mu}_{cv})^2}.
\end{aligned}$$

The average mutual information associated with L_{vs} is computed as

$$I_{vs}(X; L_{vs}) = \sum_{i=2}^{d_v} \bar{\lambda}_i \cdot J'(\mu_{vs}^{(i)}, \sigma_{vs}^{(i)}).$$

To asses the performance, we compute the decoding thresholds for the optimized degree distributions in [1] utilizing the proposed and the existing methods of EXIT analysis. Table 3.1 shows the decoding thresholds computed in terms of the average received power measured in dB. We refer to the methods of [1], [50], and the modified EXIT analysis as method (1), method (2), and method (3), respectively. P^* denotes the true decoding threshold estimates obtained with the Monte

Carlo simulations. $P^*_{(1)}$, $P^*_{(2)}$, and $P^*_{(3)}$ represent the values of the decoding thresholds computed via the methods (1), (2), and (3), respectively. According to the table, our proposed method provides better estimates of the decoding thresholds compared to the two other methods. This superiority is especially prominent for the case of $R = 0.6$. Fig. 3.3 demonstrates the PDF of the LLRs corresponding to the optimized degree distributions in [1] for a two-user GMAC with equal channel gains computed via different methods. It can be observed that our proposed method provides more accurate PDF estimates compared to the methods adopted in [1] and [50]. According to Fig. 3.3, the GM approximation matches with the PDF of the outgoing LLRs from the state nodes; however, such accuracy is not achieved for the PDF associated with the check nodes.

Table 3.1: Decoding Thresholds of the Optimized LDPC Codes in [1] Computed with Different Methods of EXIT Analysis

R	P^*	$P^*_{(1)}$	$P^*_{(2)}$	$P^*_{(3)}$
0.3	-1.61	-1.75	-1.73	-1.64
0.4	0.32	0.35	0.32	0.32
0.5	2.19	2.11	2.11	2.19
0.6	4.4	4.16	4.01	4.31

3.5 LDPC Code Optimization

In order to design ensemble of good LDPC codes for GMACs, we utilize an instance of differential evolution [83]. The optimization process is initialized with two LDPC code ensembles selected from the P2P codes optimized for the BI-AWGN channel utilizing the method of EXIT analysis in [74]. The adopted codes for a GMAC with fixed channel gains are referred to as admissible if they lead to asymptotically error free decoding. For the case of quasi-static fading scenario, the employed degree distribution are called admissible if they asymptotically lead to error-free decoding for $1 - P_o$ of the considered channel realizations computed through Monte Carlo

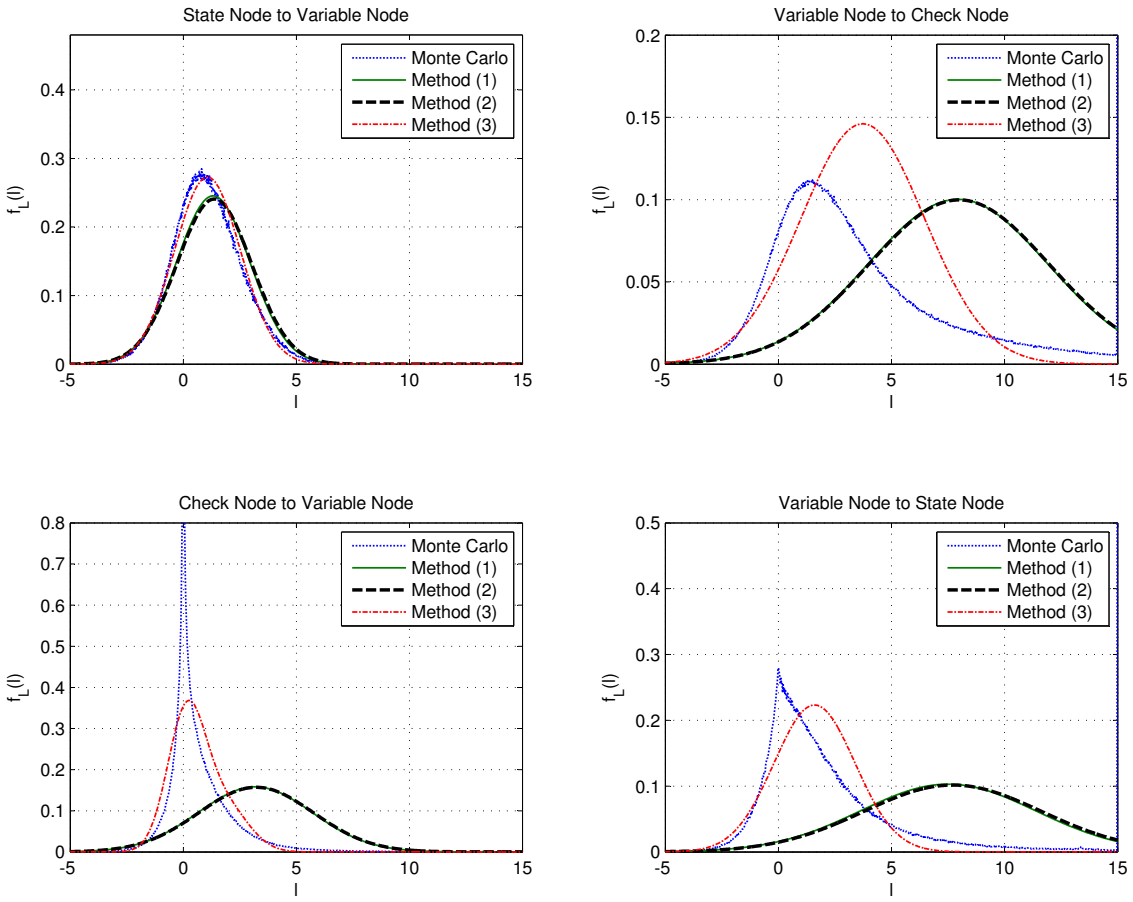

Figure 3.3: Comparison of the Different Methods in Characterizing the PDFs of the LLRs Exchanged in the Joint Decoder at Iteration 100 for the Optimized Code in [1] Corresponding to the Code Rate $R = 0.3$

simulations.

The admissibility of the employed degree distributions can be verified through tracking the evolution of the PDF or the mutual information associated with the LLRs exchanged within the joint decoder. For the next step of the code optimization, the obtained admissible degree distributions are modified via the perturbing vectors. For the general case, both variable node and check node degree distributions are perturbed, however, to simplify the optimization, we consider a singleton distribution for the check node degrees, therefore only the variable node degree distribution is perturbed.

The ith polynomial coefficient of variable node degree distribution is perturbed as $\tilde{\lambda}_i = \lambda_i + e_i$, where e_i is the ith element of the perturbing vector $\mathbf{e}$. For simplification, we only perturb the non-zero values of the polynomial coefficient of the initial degree distributions, i.e., $e_i = 0$ if $\lambda_i = 0$. The perturbed degree distribution should satisfy $\tilde{\lambda}(1) = 1,\ 0 \leq \tilde{\lambda}_i \leq 1$ implying

$$\sum_{i=2}^{d_v} e_i = 0, \qquad 0 \leq \lambda_i + e_i \leq 1. \tag{3.14}$$

To control the variations at each iteration, it is beneficial to limit the variance of the elements of the perturbing vector σ_e^2 computed as

$$\sigma_e^2 = \sum_{i=2}^{d_v} e_i^2. \tag{3.15}$$

LDPC codes can be optimized with different objectives such as rate maximization or SNRs minimization. For rate maximization the decoding threshold is fixed, and at each iteration of the perturbation, the code rates of the employed degree distributions are incremented, therefore the perturbing vector should satisfy $1 - \frac{1}{d_c}\frac{1}{\sum_{i=2}^{d_v}\frac{\tilde{\lambda}_i}{i}} = r_0 + \Delta$, where Δ denotes the rate increment. This constraint can be written as $\sum_{i=2}^{d_v}\frac{\tilde{\lambda}_i}{i} = \frac{1}{d_c}\frac{1}{1-(r_0+\Delta)}$, which is equivalent to

$$\sum_{i=2}^{d_v}\frac{e_i}{i} = \frac{\Delta/d_c}{(1-r_0)^2 - \Delta(1-r_0)}. \tag{3.16}$$

For minimization of required SNRs, the code rates are kept fixed, hence (3.16) is simplified to $\sum_{i=2}^{d_v}\frac{e_i}{i} = 0$. At each iteration of the code optimization, the admissibility of the degree distributions are checked for a decrease in the received powers.

To generate the perturbing vector, we can draw all the elements except three from a normal distribution, i.e., $\mathcal{N}(0,1)$, and compute the remaining elements by solving (3.14), (3.15) and (3.16). The perturbing vector is adopted if it satisfies the inequality constraint (3.14) and the stability condition (3.3), otherwise a new

perturbing vector is generated. The perturbed degree distributions will replace the initial degree distributions if they are admissible, otherwise they are dismissed and a new iteration is performed. The code optimization is concluded if new admissible degree distributions cannot be found after a predetermined number of iterations. Therefore, the last pair of admissible degree distributions is the optimum.

3.6 Simulation Results

In this section, we perform the LDPC code optimization for the two-user GMAC considering two scenarios of fixed channel gains and quasi-static fading.

3.6.1 Fixed Channel Gains

For this scenario, we incorporate the proposed modified methods of EXIT analysis and DE into the LDPC code optimization with the objective of minimization of required SNRs. For equal channel gains, we compare our designed codes with those corresponding to the code rates 0.3 and 0.6 in [1]. We employ the designed degree distributions in [1] to initialize the code optimization. We utilize the modified DE to design codes for the code rate 0.3. For the code rate 0.6, we perform the code optimization employing the modified EXIT analysis.

Table 3.2 presents the resulting optimized degree distributions whose decoding thresholds are denoted by P^* computed via Monte Carlo simulation. The decoding thresholds of the optimized degree distributions [1] associated with code rates 0.3 and 0.6 are -1.61 dB and 4.4 dB which are inferior to our optimized codes by 0.12 dB and 0.15 dB, respectively.

We also compute the performance of the P2P codes optimized for the BI-AWGN channel when employed over the two-user GMAC. The degree distributions are optimized for the code rates associated with those designed in [1]. The decoding thresholds of the degree distributions corresponding to code rates 0.3, 0.4, 0.5 are

-0.81 dB, 1.96 dB, and 5.06 dB. For the case of code rate 0.6, the P2P codes are not supported over the two-user GMAC even if there is no noise. These findings suggest that optimized codes achieve considerable improvement over P2P when employed for the two-user GMAC with equal channel gains.

Table 3.2: Optimized Degree Distributions for Equal Channel Gains Scenario

R	d_c	P^* (dB)	λ_2	λ_3	λ_4	λ_5	λ_6	λ_7	λ_8	λ_{13}	λ_{20}	λ_{21}	λ_{100}
0.3	6	-1.73	0.2741	0.2113	0.0078	0.0178	0.0206	0.0063	0.0239	0.1992	0	0	0.2389
0.6	9	4.25	0.4771	0.0744	0	0	0	0	0	0	0.1322	0.1231	0.1931

For unequal channel gains, there are no specific designs in the literature. So, we consider a degree profile with maximum degree 50 and choose the non-zero variable node degrees as $2, 3, 4, 9, 10, 19, 20, 49, 50$. Although there is no guarantee that this is the best choice, the selected degree profile is motivated by the pattern suggested in [41] for the optimized codes over the BI-AWGN channel for which the non-zero variable node degrees are distributed around the minimum and maximum degrees and a few values in between. Similar pattern is also followed by codes designed in [1, 50].

We consider $P_1 = 0$ dB and $P_2 = -8$ dB and select the rate pair $(0.486, 0.059)$, which corresponds to a corner point of the dominant face of the capacity region, as the rates of the employed LDPC codes. For code optimization, we select a pair of admissible off-the-shelf P2P codes with similar code rates as the initial degree distributions. During the code optimization process, we start with higher values for the received powers and decrease the values at each iteration keeping the power ratio unchanged, i.e., $\frac{P_1}{P_2} = 6.31$ throughout the code optimization. We perform separate code designs utilizing the proposed modified EXIT analysis and DE method. The decoding thresholds of the optimized codes are compared against the ones obtained via the method (2). Furthermore, we calculate the decoding threshold of the off-the-shelf P2P codes optimized over BI-AWGN channels when they are employed for the

GMAC with the constraint $\frac{P_1}{P_2} = 6.31$. Table 3.3 demonstrates the degree distributions for the optimized codes. The decoding thresholds are computed via Monte Carlo simulations and are provided in terms of P_1^* with $P_2^* = \frac{P_1^*}{6.31}$. It is clear from the table that the codes designed via the proposed methods outperform the ones optimized with method (2) and the P2P codes.

Similar code optimization is performed for the two-user GMAC considering $P_1 = 1$ dB and $P_2 = -7$ dB for the rate pair $(0.502, 0.131)$. Table 3.4 shows the optimized degree distributions obtained via the modified EXIT, the modified DE, and method (2) along with the best P2P codes with decoding thresholds 0.36 dB, 0.4 dB, 0.46 dB, and 0.55 dB away from the capacity boundary, respectively. As another instance, we consider $P_1 = 3$ dB and $P_2 = -5$ dB and select the rate pair $(0.627, 0.197)$ for which the optimized degree distributions along with the best P2P codes are shown in Table 3.5. The decoding thresholds corresponding to the degree distributions, with the order presented in the table, are 0.22 dB, 0.18 dB, 0.28 dB, and 0.42 dB away from the capacity boundary demonstrating the superiority of the proposed methods in code design over the existing ones.

Table 3.3: Optimized Degree Distributions for Unequal Channel Gains Scenario ($R_1 = 0.486, R_2 = 0.059$)

	P_1^*	Msg.	d_c	λ_2	λ_3	λ_4	λ_9	λ_{10}	λ_{19}	λ_{20}	λ_{49}	λ_{50}
Modified EXIT	0.22	X_1	8	0.2023	0.2635	0.0770	0.1730	0.0654	0.0948	0.0557	0.0547	0.0134
		X_2	3	0.5358	0.1017	0.1398	0.0362	0.1012	0.0052	0.0479	0.0254	0.0067
Modified DE	0.18	X_1	8	0.2262	0.2251	0.0718	0.2688	0.0044	0.0115	0.0772	0.0250	0.0899
		X_2	3	0.5066	0.2330	0.0187	0.0711	0.0790	0.0248	0.0042	0.0380	0.0246
Method (2)	0.24	X_1	8	0.2107	0.1903	0.1790	0.0768	0.1195	0.0665	0.0839	0.0103	0.0630
		X_2	3	0.4847	0.2578	0.0286	0.1214	0.0250	0.0179	0.0175	0.0426	0.0044
P2P	0.34	X_1	8	0.2145	0.2397	0.0725	0.1293	0.1391	0.1383	0.0345	0.0171	0.0151
		X_2	3	0.4770	0.2569	0.0597	0.0579	0.0402	0.0392	0.0433	0.0210	0.0049

3.6.2 Quasi-Static Fading

To illustrate the code design principles for the fading case, we provide several examples. Two scenarios of real and complex channel gains are considered. We declare a pair of degree distributions admissible if the computed decoding behavior, measured

Table 3.4: Optimized Degree Distributions for Unequal Channel Gains Scenario ($R_1 = 0.502, R_2 = 0.131$)

		d_c	λ_2	λ_3	λ_4	λ_9	λ_{10}	λ_{19}	λ_{20}	λ_{49}	λ_{50}
Modified EXIT	X_1	9	0.1866	0.2731	0.0408	0.0761	0.0328	0.1925	0.0909	0.0909	0.0163
	X_2	4	0.3410	0.2352	0.0574	0.0206	0.1453	0.0454	0.0699	0.0161	0.0691
Modified DE	X_1	9	0.1476	0.2703	0.1116	0.1770	0.0050	0.0781	0.0928	0.0552	0.0623
	X_2	4	0.3612	0.0804	0.2563	0.0566	0.0045	0.1146	0.0303	0.0181	0.0781
Method (2)	X_1	9	0.2105	0.1359	0.1604	0.0593	0.1744	0.0483	0.0526	0.1049	0.0536
	X_2	4	0.3655	0.0860	0.2342	0.0300	0.0956	0.0098	0.0230	0.1180	0.0380
P2P	X_1	9	0.1882	0.1987	0.1231	0.0477	0.1505	0.0910	0.0947	0.0445	0.0617
	X_2	4	0.3554	0.0929	0.2469	0.0368	0.0740	0.0311	0.0304	0.0166	0.1160

Table 3.5: Optimized Degree Distributions for Unequal Channel Gains Scenario ($R_1 = 0.627, R_2 = 0.197$)

		d_c	λ_2	λ_3	λ_4	λ_9	λ_{10}	λ_{19}	λ_{20}	λ_{49}	λ_{50}
Modified EXIT	X_1	11	0.2293	0.1212	0.2266	0.1347	0.1208	0.0068	0.0454	0.0837	0.0315
	X_2	4	0.3933	0.2023	0.0748	0.1143	0.1268	0.0214	0.0243	0.0178	0.0250
Modified DE	X_1	11	0.1558	0.2643	0.1760	0.1550	0.0979	0.0749	0.0411	0.0236	0.0113
	X_2	4	0.3853	0.1697	0.1552	0.0793	0.0931	0.0797	0.0086	0.0178	0.0113
Method (2)	X_1	11	0.2368	0.0361	0.3609	0.0104	0.0856	0.2368	0.0065	0.0124	0.0144
	X_2	4	0.3815	0.1499	0.1938	0.0615	0.1281	0.0186	0.0064	0.0422	0.0180
P2P	X_1	11	0.1775	0.2965	0.0657	0.2346	0.0571	0.1263	0.0151	0.0069	0.0204
	X_2	4	0.3673	0.1742	0.2002	0.0677	0.0500	0.0836	0.0503	0.0040	0.0027

in frame error rate (FER), meets the given outage probability asymptotically. The accuracy of the computations relies on the number of channel realizations taken into account. In our designs, we consider the outage probability of 0.1 and perform the computations for 10^4 channel realizations. It is easy to check that for the considered number of channel realizations the associated outage probability is bounded as $0.0941 < P_o < 0.1059$ for a 95% confidence level.

Due to extensive computations, for the case of quasi-static fading the proposed methods of decoding threshold estimation (the modified DE and the modified EXIT analysis) is not efficient in the current form to be incorporated into the code optimization. Hence, we employ the EXIT chart analysis in [50] wherein the evolution of the mutual information is computed through a simple linear approximation and LLRs are assumed to have Gaussian distribution. Note that the linear approximation used in [50] does not result in accurate decoding thresholds for some ranges of the power values; however, the simplicity of the method renders it very efficient for the

involved computations under the quasi-static fading scenario.

Fig. 3.4 illustrates the COCRs for Gaussian and BPSK signaling computed for real channel gains. Code optimization is performed for four instances of rate pairs with the goal of rate maximization. The initial degree distributions are picked from the P2P codes designed for the BI-AWGN channel. For each instance, the trajectory of the rate increments is a straight line passing through the origin. Table 3.6 shows the degree distributions of the optimized codes and those of the available P2P codes. Fig. 3.4 presents the achieved rate pairs employing the optimized codes and the best P2P ones clearly demonstrating the superiority of the newly optimized codes. Finally, Fig. 3.5 shows the FERs for finite block lengths of the specific codes selected from the optimized degree distributions corresponding to the code rate pair $(0.139, 0.208)$ where the FERs associated with 1k and 10k are 1.75 and 1.1 dB away from the outage limit, respectively at an FER of 0.1. The newly designed codes provide better performance than the P2P codes for the rate pair $(0.133, 0.199)$ (at an FER of 0.1) as well.

Table 3.6: Optimized Degree Distributions (Real Channel Gains), $P_1 = 5$ dB, $P_2 = 4$ dB, $P_o = 0.1$

		R	d_c	λ_2	λ_3	λ_4	λ_9	λ_{10}	λ_{19}	λ_{20}	λ_{49}	λ_{50}
P2P Opt.	X_1	0.064	3	0.4867	0.2377	0.0838	0.0498	0.0226	0.0065	0.0715	0.0030	0.0383
	X_2	0.256	5	0.3061	0.1309	0.2011	0.0734	0.0309	0.0968	0.0765	0.0554	0.0289
P2P Opt.	X_1	0.058	3	0.4879	0.2134	0.0967	0.0676	0.0214	0.0822	0.0009	0.0044	0.0256
	X_2	0.232	5	0.2679	0.2237	0.1087	0.0408	0.0937	0.1633	0.0066	0.0331	0.0623
P2P Opt.	X_1	0.139	4	0.3301	0.2451	0.0917	0.0680	0.0291	0.0486	0.1259	0.0372	0.0242
	X_2	0.208	4	0.3853	0.1183	0.2652	0.1004	0.0166	0.0642	0.0027	0.0032	0.0442
P2P Opt.	X_1	0.133	4	0.3385	0.1884	0.1455	0.0157	0.1059	0.0497	0.0614	0.0222	0.0729
	X_2	0.199	4	0.3851	0.1155	0.2426	0.0444	0.1067	0.0063	0.0843	0.0077	0.0076
P2P Opt.	X_1	0.216	4	0.3470	0.3315	0.0422	0.1338	0.0479	0.0811	0.0015	0.0040	0.0110
	X_2	0.144	4	0.3505	0.1134	0.2524	0.0110	0.0880	0.0199	0.0503	0.0872	0.0274
P2P Opt.	X_1	0.207	5	0.2602	0.2339	0.0646	0.1279	0.0756	0.0373	0.0074	0.0908	0.1024
	X_2	0.138	4	0.3515	0.1390	0.1923	0.1162	0.0077	0.0701	0.0000	0.0806	0.0426
P2P Opt.	X_1	0.285	5	0.2935	0.1809	0.2107	0.0824	0.0151	0.1143	0.0363	0.0231	0.0437
	X_2	0.071	3	0.4668	0.2551	0.1187	0.0156	0.0461	0.0613	0.0120	0.0136	0.0108
P2P Opt.	X_1	0.272	5	0.2875	0.2117	0.1342	0.0930	0.0707	0.0610	0.1129	0.0267	0.0023
	X_2	0.068	3	0.4950	0.1890	0.1403	0.0025	0.0739	0.0565	0.0201	0.0110	0.0117

As the second example, we consider a quasi-static fading channel with complex

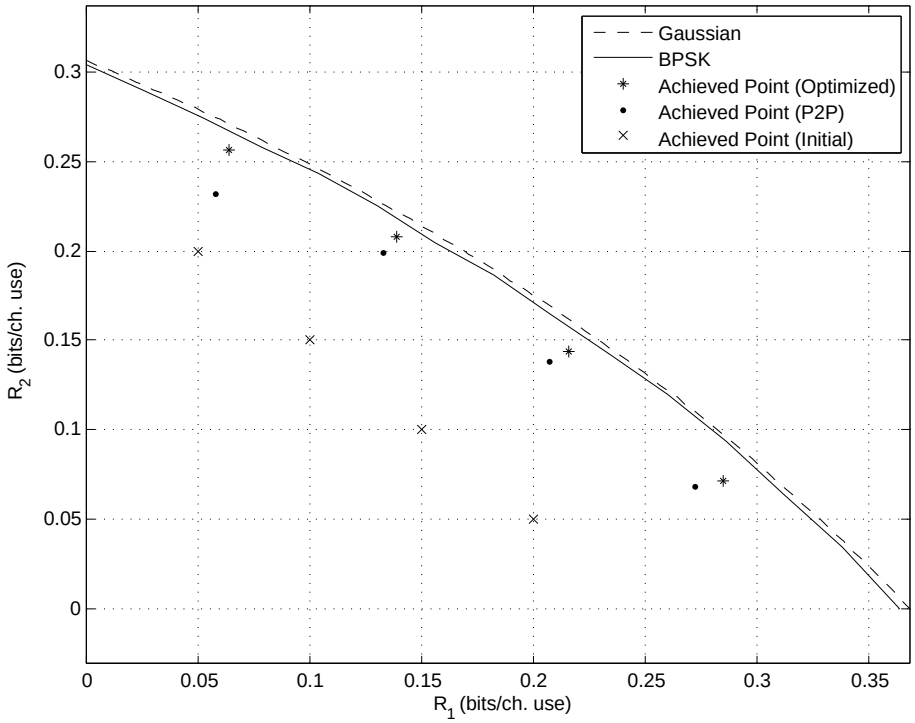

Figure 3.4: COCRs of Gaussian and BPSK Signaling Along with the Optimized and the P2P Codes. $P_1 = 5$ dB, $P_2 = 4$ dB, and $P_{\mathrm{o}} = 0.1$

channel gains. Since characterization of the COCR for the BPSK signaling is difficult, we calculate the Gaussian signaling COCR as an outer bound. Similar to the previous example, we perform the code optimization for four instances and compare them with the P2P codes optimized for the BI-AWGN channel. Degree distributions are shown in Table 3.7 for the optimized codes and the reference P2P ones. Achieved rate pairs are shown in Fig. 3.6. Fig. 3.7 demonstrates the decoding results for finite block length codes picked from the optimized degree distributions corresponding to the code rate pair $(0.289, 0.072)$. At an FER of 0.1, the code block lengths with 1k and 10k operate 1.6 dB and 1.25 dB away from the outage limit computed for Gaussian signaling, respectively. Furthermore, the optimized codes offer better performance than the P2P codes corresponding to the rate pair $(0.268, 0.067)$ as well.

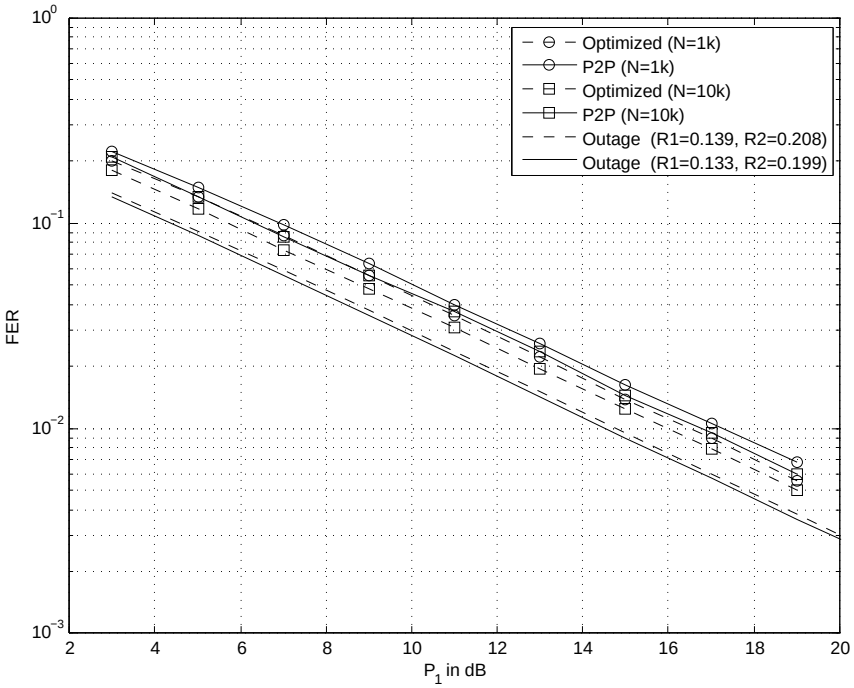

Figure 3.5: FER of the Optimized Codes and the P2P Codes Employing Real Channel Gains

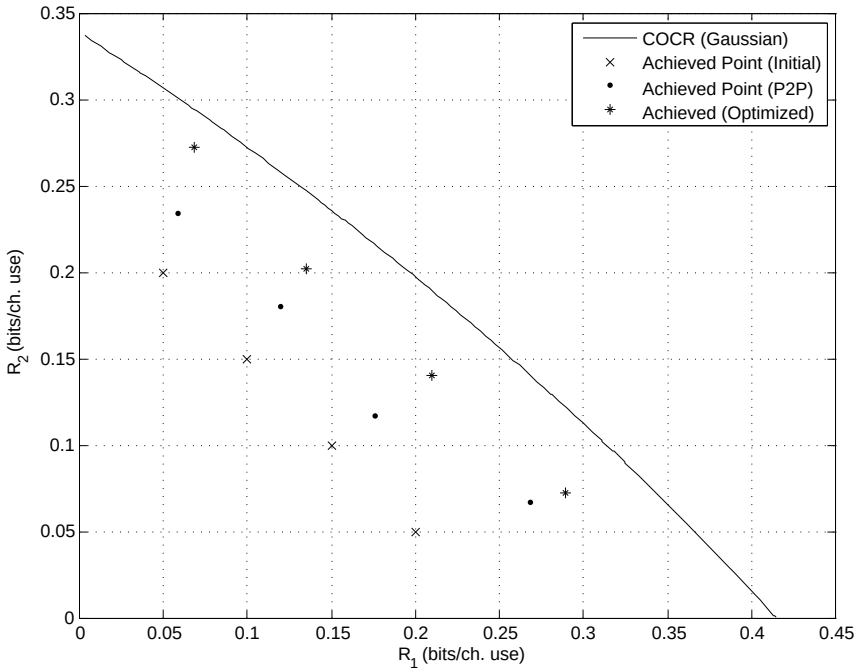

Figure 3.6: COCR for the Gaussian Signaling and the Achieved Rate Pairs. $P_1 = 5$ dB, $P_2 = 4$ dB, $P_o = 0.1$

Table 3.7: Optimized Degree Distributions (Complex Channel Gains), $P_1 = 5$ dB, $P_2 = 4$ dB, $P_o = 0.1$

		R	d_c	λ_2	λ_3	λ_4	λ_9	λ_{10}	λ_{19}	λ_{20}	λ_{49}	λ_{50}
Opt.	X_1	0.068	3	0.4906	0.3029	0.0021	0.0125	0.0254	0.0963	0.0117	0.0243	0.0340
	X_2	0.272	5	0.2593	0.2876	0.1044	0.0948	0.0445	0.0599	0.0673	0.0252	0.0570
P2P Opt.	X_1	0.059	3	0.4770	0.2569	0.0597	0.0579	0.0402	0.0392	0.0433	0.0210	0.0049
	X_2	0.234	5	0.2790	0.1898	0.1271	0.0680	0.1133	0.0895	0.0093	0.0838	0.0403
P2P Opt. P2P Opt.	X_1	0.135	4	0.3344	0.2055	0.1097	0.1235	0.0597	0.0461	0.0409	0.0415	0.0387
	X_2	0.202	4	0.3732	0.2722	0.0354	0.1051	0.1222	0.0199	0.0250	0.0167	0.0304
P2P Opt. P2P Opt. P2P Opt.	X_1	0.12	4	0.3243	0.2267	0.0965	0.0850	0.0743	0.0233	0.0248	0.0704	0.0748
	X_2	0.18	4	0.3587	0.2273	0.0973	0.1078	0.0848	0.0193	0.0613	0.0228	0.0206
P2P Opt. P2P Opt. P2P Opt. P2P Opt.	X_1	0.21	4	0.3958	0.2366	0.0903	0.0747	0.0121	0.0117	0.1122	0.0576	0.0090
	X_2	0.14	4	0.3254	0.1985	0.1763	0.0740	0.0072	0.0255	0.1201	0.0429	0.0300
P2P Opt. P2P Opt. P2P Opt. P2P Opt. P2P Opt.	X_1	0.176	4	0.3554	0.2131	0.1220	0.1638	0.0028	0.0787	0.0078	0.0363	0.0200
	X_2	0.117	4	0.3438	0.1145	0.2342	0.0087	0.0426	0.0474	0.0859	0.0345	0.0883
P2P Opt. P2P Opt. P2P Opt. P2P Opt. P2P Opt. P2P Opt.	X_1	0.289	5	0.2634	0.3123	0.0900	0.0887	0.0448	0.0697	0.0779	0.0326	0.0205
	X_2	0.072	3	0.5259	0.1626	0.0962	0.0643	0.0823	0.0133	0.0258	0.0012	0.0283
P2P Opt. P2P Opt. P2P Opt. P2P Opt. P2P Opt. P2P Opt.	X_1	0.268	5	0.2948	0.2026	0.1153	0.1107	0.0959	0.0188	0.1104	0.0399	0.0116
	X_2	0.067	3	0.4910	0.2239	0.0849	0.1004	0.0002	0.0320	0.0578	0.0059	0.0040

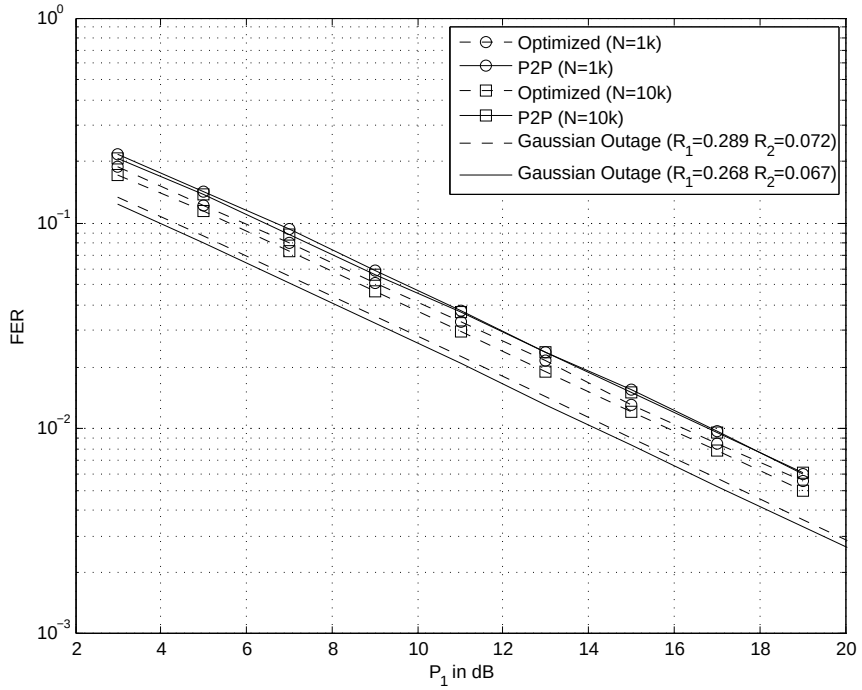

Figure 3.7: FER of the Optimized Codes and the P2P Codes Employing Complex Channel Gains

3.7 Chapter Summary

In this chapter, we studied the problem of LDPC code design for the two-user GMAC exploring two scenarios of fixed and quasi-static fading channel gains. Considering joint decoding of the two users coded bits, we characterized the PDF of the outgoing LLRs from the state nodes and observed that it can be well approximated with GM distributions. We then exploited the GM approximation to develop variants of existing DE and EXIT analysis methods. We utilized the newly proposed methods to design codes for fixed channel gain scenarios and showed that the optimized codes obtained via the proposed methods offer better performance than the P2P codes and those achieved from the already existing. For the quasi-static fading case, we adopted an existing (simple) implementation of EXIT analysis and performed code optimization for real and complex channel gains. The optimized codes improve upon the P2P codes in this case too. Finally, finite code block lengths simulations of codes from the designed ensembles demonstrate that the performance of the optimized codes is close to the outage limits.

Chapter 4

LDPC CODE DESIGN FOR GAUSSIAN INTERFERENCE CHANNELS

In this chapter, we focus on GICs and study the HK coding strategy for the two-user case with the objective of designing implementable (explicit) channel codes. Specifically, irregular LDPC codes are adopted for use over the channel. Iterative JD is utilized at the receivers, where it is proved that LLRs exchanged among the nodes of the Tanner graph enjoy symmetry when BPSK or QPSK with Gray coding is employed. We derive the stability condition for the admissible degree distributions under strong and weak interference levels. Degree distribution optimization and convergence threshold computations are carried out for different GICs employing finite constellations by tracking the average mutual information. Via examples, it is observed that optimized codes using BPSK or QPSK Gray coding operate close to capacity boundary for strong interference. For the case of weak interference, it is shown that nontrivial rate pairs are achievable via the newly designed codes, previously not possible by single user codes with TS. Performance of the designed codes is also studied for finite block lengths through simulations of specific codes picked from the designed code ensembles.

The rest of the chapter is organized as follows. In Section 4.1, we first give an introduction on interference channels and state the contributions of this chapter. In Section 4.2, the system model is described, i.i.d. channel adapters are introduced, and the computation of the HK sub-region is summarized. In Section 4.3, we explain the implementation of HK coding strategies and the operations at the transmitter and receiver sides. In Section 4.4, symmetry property of the exchanged LLRs under JD is proved, stability condition of the degree distribution profiles of public and private

Part of this work was presented at IEEE ISIT 2014 [84] and a full version is published in IEEE Transactions on Communications in February 2015 [75].

messages are derived and the proposed code optimization approach is detailed. In Section 4.5, performance of the P2P and the optimized LDPC codes are investigated via a multitude of examples. In Section 4.6, finite block length code simulation results are provided, and finally, in Section VII the conclusions and future work are given.

4.1 Introduction

There is a large body of work on two-user GICs, in which two independent transmitters communicate with their intended receivers through a shared medium. In spite of this intense research, full characterization of the capacity region is still an open problem, and only inner and outer bounds on achievable rates are available in the literature. The best reported inner bound to date is due to Han and Kobayashi referred as the HK coding scheme [30]. Despite the superiority of the HK strategy, there is no work on exploring explicit and implementable channel codes adopting this technique in the current literature. With this motivation, in this chapter, we study the design and performance of LDPC codes over GICs implementing the HK strategy.

LDPC codes have been shown to achieve a performance extremely close to the Shannon limit for P2P channels [41]. They have also been successfully applied to multi-user channels, where promising results have been obtained. For instance, capacity (or capacity bound) approaching codes are designed for two-user MACs, GBCs, and RCs [1, 50, 51, 57, 60, 69]. There is also a recent work on the use of LDPC codes on symmetric GICs under weak interference [65]. However, there is no work in the existing literature on explicit code designs for GICs implementing the HK strategy in a practical manner.

In this chapter, we investigate the performance of irregular LDPC codes over two-user GICs with fixed channel gains. We adopt finite constellations for transmission as Gaussian codebooks cannot be used due to practical transmission constraints

such as synchronization, encoding, and decoding limitations. In the proposed scheme, the message of each transmitter is split into private and public parts encoded by separate LDPC codes. The encoded bits are modulated and superimposed to generate the transmitted signal. At each receiver, the public messages and the intended private message are jointly decoded in an iterative fashion.

Symmetry of the channel outputs considerably simplifies the analysis of the decoder for LDPC codes over P2P channels. In order to simplify the analysis for our multi-user setting in a similar manner, we exploit the i.i.d. channel adapters introduced in [80]. We propose a code optimization based on a specific instance of differential evolution [85] where, at each iteration, perturbing vectors are utilized to generate admissible degree distributions. To simplify the code optimization, we prove a symmetry property of the exchanged LLRs within the joint decoder for BPSK and QPSK with Gray coding using the assumption that the Tanner graph of the joint decoder is cycle-free and the exchanged LLRs within the decoder are independent. The symmetry property of the exchanged LLRs plays a key role in simplifying the mutual information calculations exploited to verify the admissibility of the perturbed degree distributions. Stability conditions are also derived for strong and weak interference levels employing BPSK and QPSK with Gray coding to ensure that the optimized codes do not suffer from elevated error floors.

Throughout the chapter, for comparison purposes we will use naive and non-naive TS strategies. Under naive TS, we have individual power constraints for each users' transmitted symbols. This is motivated by the practical limitations in the transmission process, e.g., due to restrictions on the power amplifiers. Under non-naive TS the users can increase their individual power levels for a certain fraction of the total transmission time while keeping the average power over the entire codeword

under a certain value.

Having implemented the HK strategy, we carry out the code optimization for symmetric and asymmetric GICs for various scenarios with different levels of interference. In all the investigated examples, it is observed that the optimized codes for the two-user GIC outperform P2P codes optimized for the binary-input additive white Gaussian noise (BI-AWGN) channel, and for most cases significant improvements are possible. Promising results are obtained under strong interference and rate pairs very close to the capacity boundaries are achieved. Under weak interference, the message of each transmitter is composed of private and public parts, therefore a power allocation optimization is performed prior to the code optimization. It is observed in this case that non-trivial rate pairs, which are not achievable with P2P codes used with TS, are attainable. We also provide simulation results with specific finite-length codes picked from the optimized code ensembles utilizing random constructions. Furthermore, the performance of the random constructions is compared to that of structured constructions utilizing an algebraic design approach.

4.2 System Model and Preliminaries

The input-output relationship for the two-user GIC (as illustrated in Fig. 4.1) is expressed as

$$\begin{aligned} Y_1 &= h_{11}X_1 + h_{21}X_2 + Z_1, \\ Y_2 &= h_{12}X_1 + h_{22}X_2 + Z_2, \end{aligned} \tag{4.1}$$

where h_{ij} is the fixed complex channel gain from the user i to the receiver j. Z_1 and Z_2 are i.i.d. circularly symmetric complex Gaussian noise samples with zero mean and $\frac{N_0}{2}$ variance per dimension. X_1 and X_2 are the transmitted complex signals with individual power constraints of P_1 and P_2, respectively, that is, $E\{|X_i|^2\} \leq P_i$ $(i = 1, 2)$. Signal-to-noise-ratio (SNR) and interference-to-noise-ratio (INR) at

receiver i are defined as $SNR_i = \frac{|h_{ii}|^2 P_i}{N_0}$ and $INR_i = \frac{|h_{ji}|^2 P_j}{N_0}$, respectively, where $i, j = 1, 2$ and $i \neq j$. Based on the interference and signal levels, the interference can be categorized as strong (if $INR_i > SNR_j$), weak (if $SNR_i > INR_j$), or mixed (if $INR_i > SNR_j,\ INR_j < SNR_i$) with $i \neq j$. For the case of a symmetric GIC, $h_{11} = h_{22},\ h_{12} = h_{21},\ SNR_1 = SNR_2 = SNR$, and $INR_1 = INR_2 = INR$.

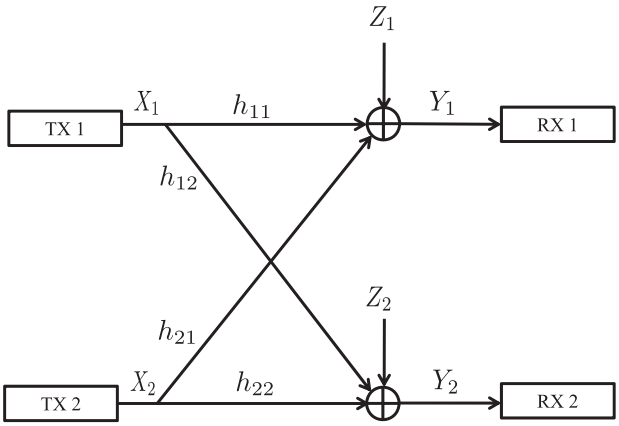

Figure 4.1: Two-User GIC Block Diagram

HK ARR Computation

The HK ARR is the best known inner bound on the capacity of interference channels. Under strong interference, this inner bound treats all messages as public [4] and characterizes the capacity region. Despite the superiority of the HK coding scheme, the computation of the entire rate region is prohibitively difficult since one should perform an optimization over the joint probability distribution of many random variables with large cardinalities. Authors in [31] provide a simplified expression of the rate region which is still difficult to compute. In this chapter, the focus is on GICs, and instead of the entire region, a sub-region is obtained with a lower complexity by considering the superposition of independent uniformly distributed inputs from specific constellations as transmitted signals with no TS [30]. Denoting the code rates at the transmitters 1 and 2 by R_1 and R_2, respectively, the rate vector $\mathbf{R} = [R_1, R_2]^t$

is in the sub-region $\mathcal{R}_0$ if

$$\mathcal{R}_0 = \{\mathbf{R} | A\mathbf{R} \leq \Psi(P_1, P_2, \alpha_1, \alpha_2)\}, \tag{4.2}$$

where

$$\begin{aligned} \Psi &= [\rho_1, \rho_2, \rho_{12}, \rho_{10}, \rho_{20}]^t, \\ A^t &= \begin{bmatrix} 1 & 0 & 1 & 2 & 1 \\ 0 & 1 & 1 & 1 & 2 \end{bmatrix}, \end{aligned} \tag{4.3}$$

and α_i denotes the fraction of the power allocated to the private message of user i. In (4.2), the inequality sign is applied element-wise and Ψ is defined in [30, pp. 54–55]. As (4.2) suggests, different power allocations to the public and private messages give rise to different sub-regions. Thus, the above sub-region can be enlarged to

$$\mathcal{R}_1 = \bigcup_{(\alpha_1,\alpha_2)\in[0,1]\times[0,1]} \mathcal{R}_0(P_1, P_2, \alpha_1, \alpha_2). \tag{4.4}$$

Since $\mathcal{R}_1$ is not necessarily convex, it can be further enlarged by a convex hull operation. We denote the resulting sub-region by $\mathcal{R}$, which is an inner bound for the actual ARR. We note that, as mentioned in [30], the introduced inner bound may not cover the entire rate region obtained by non-naive TS. For instance, Fig. 4.9 demonstrates the inner bounds (HK ARR) $\mathcal{R}_1$ for a finite constellation and for Gaussian signaling where it is clear that the non-naive TS rate region is not contained within the inner bound $\mathcal{R}_1$. To compute the outer bound on the capacity, we use the results of [34] since the bounds require only simple calculations and are shown to be within one bit of the capacity region.

4.3 Implementation of the HK Encoding and Decoding Scheme

Considering the HK coding scheme, the message of each user is divided into two parts, namely, the private message (U) and the public message (W). The public messages

are decodable at both receivers while the private messages are only decodable at the intended receivers. Although in the general scheme messages are split into public and private parts, there are special cases where there may be no need to allocate the power to both; for instance, under strong interference, both users' messages are public (and no private message is transmitted) since all the messages are decodable at both receivers.

Fig. 4.2 shows the block diagram of the transmitter incorporating the HK coding scheme wherein the messages of each transmitter (U and W) are encoded with separate LDPC codes (resulting in C_u and C_w). The resulting bits are then modulated (denoted by X_u and X_w) and superimposed to form the overall transmitted signal (X). Here, we superimpose the two signals with standard addition; however, it is also possible to consider other alternatives. For instance, superimposing of two signals can be done in the "code" domain through modulo-2 addition (which may be the proper choice in the case of binary input channels), however, this scheme would require a different code optimization which is out of the scope of this chapter. As another example, it is also possible to consider higher order signal constellations, and perform mappings of the public and private coded bits to the constellation points jointly. It should further be emphasized that our focus is on practical modulation techniques such as PSK signaling since Gaussian signaling (as usually assumed in information theoretic studies) cannot be used in practical systems.

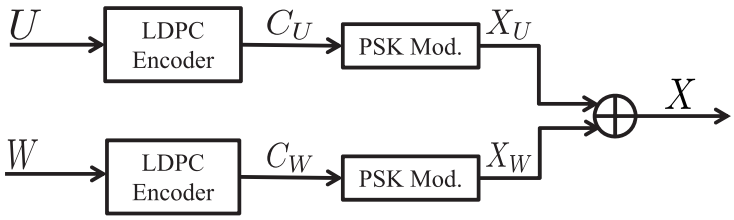

Figure 4.2: Construction of the Transmitted Signal for the Proposed Implementation of the HK Coding Scheme

At the receiver side, the public messages and the private message of the desired user are decoded by utilizing a BP algorithm wherein the soft-information about the messages are exchanged within the decoder in an iterative fashion [86]. Similar to the case of the GMAC, messages can be decoded successively and jointly, as illustrated in Figs. 4.3a and 4.3b, respectively. We exploit a joint decoder at each receiver run through the parallel scheduling.

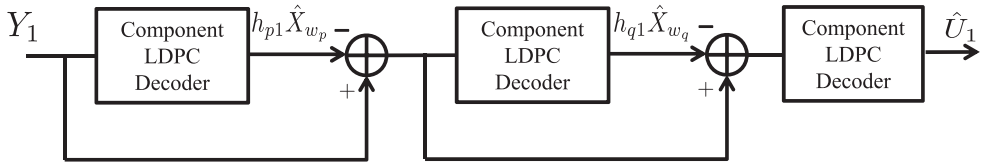

(a) Successive Interference Canceler Block Diagram

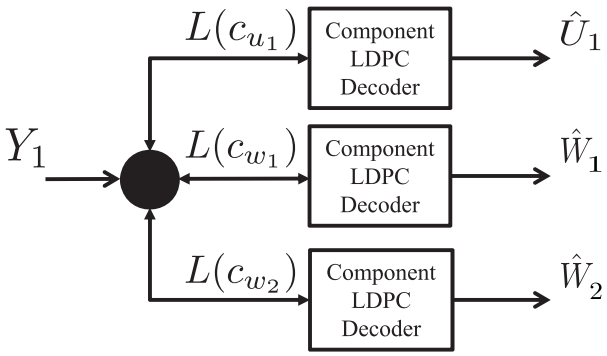

(b) Joint Decoder Block Diagram

Figure 4.3: Block Diagram of the Decoder Structures at Receiver 1 ($p, q = 1, 2,\ p \neq q$) ($\hat{X}$ Denotes the Decoded Message for the Transmitted Message X.)

4.4 Analytic Properties and Optimization of LDPC Codes over GICs

The objective in this section is to develop an optimization method for LDPC code ensembles over GICs. Irregular LDPC codes have previously been employed for communication over different multi-user channels due to their excellent performance [1], [50], [60]. In this chapter, we follow similar ideas, and consider their use over GICs.

DE is the most reliable method to compute the threshold of an LDPC code ensemble, however, under JD, due to the non-linearity of the update rule at the state nodes, it is very difficult to characterize the PDF of the outgoing LLRs from the state nodes. Furthermore, the computation becomes cumbersome for multiuser scenarios where the PDFs of multiple users' LLRs are involved. An EXIT chart analysis is an alternate method based on the Gaussian assumption on the LLRs exchanged within the decoder, however, as highlighted in Chapter 3, the Gaussian assumption is not accurate under JD. In fact, we notice that for certain ranges of the channel parameters, the thresholds obtained with Gaussian assumption significantly differ from the ones obtained through finite block length code simulations. Therefore, in this chapter, we propose to track the evolution of the mutual information with no Gaussianity assumption on the exchanged LLRs.

4.4.1 LLR Computation at the State Nodes

The LLR of the ith coded bit of message j at receiver k is computed as

$$L\big(c_j(i), Y_k(i)\big) = \log\left(\frac{f_{Y_k(i)}\big(Y_k(i)|c_j(i)=0\big)}{f_{Y_k(i)}\big(Y_k(i)|c_j(i)=1\big)}\right), \tag{4.5}$$

where $c_j(i)$ is the ith coded bit of message j, which can be a public message or the intended private message, and $f_{Y_k(i)}$ represents the PDF of $Y_k(i)$ conditioned on $C_j(i)$. Considering parallel scheduling, upon the start of each iteration, the LLR corresponding to $c_j(i)$ provided to the component LDPC decoder of message j is computed at the state nodes by marginalization, that is,

$$L\big(c_j(i), Y_k(i)\big) = \log\left(\frac{\sum_{C_i \in S_i^{j+}} f_{Y_k(i)}\big(Y_k(i)|C_i\big)P\big(C_i\big)}{\sum_{C_i \in S_i^{j-}} f_{Y_k(i)}\big(Y_k(i)|C_i\big)P\big(C_i\big)}\right), \tag{4.6}$$

where C_i is the vector comprising the ith coded bits of all public and private codewords, i.e., $C_i = \{c_{u_1}(i), c_{w_1}(i), c_{u_2}(i), c_{w_2}(i)\}$ and $P(C_i)$ denotes the probability of C_i which is determined by the outputs of component LDPC decoders and gets updated

at each iteration. S_i^{j+} and S_i^{j-} denote the subsets of the codewords with $c_j(i) = 0$ and $c_j(i) = 1$, respectively. Note that at the receiver r, U_k $(k \neq r)$ is not decoded, hence, the corresponding component in C_i does not get updated and remains constant throughout the iterations. The computation of the extrinsic LLRs at the state nodes for BPSK differs from that for higher order modulations such as QPSK. For BPSK, the extrinsic LLRs sent to each component LDPC decoder are updated based on the received LLRs from other component LDPC decoders. In contrast, for higher order modulations, the LLR sent from each variable node to the connected state node contributes to the updated extrinsic LLR sent to its neighbor node(s) from that state node. For instance, Fig. 4.4 illustrates a portion of the joint decoder for QPSK, where each state node is connected to two variable nodes, hence, the LLR sent from each variable node to the state node contributes to the updated extrinsic LLR sent to its neighbor.

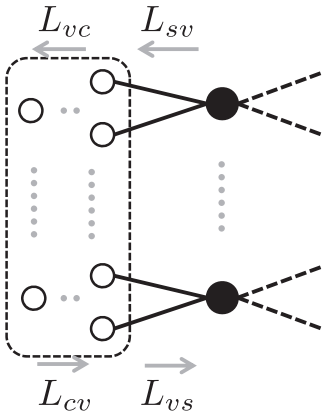

Figure 4.4: The Tanner Graph Representation of LDPC Codes with QPSK Mapping

In the following, we prove a symmetry property of the exchanged LLRs within the joint decoder. Furthermore, we study the stability conditions for the degree distributions of the public and private messages for different interference levels.

4.4.2 LLR Symmetry Property

The PDF of the LLRs sent from the state nodes to the component LDPC decoder of message j is symmetric if

$$l = \log\left(\frac{f_L(l|c_j(i)=0)}{f_L(-l|c_j(i)=0)}\right), \quad l \in \mathbb{R}. \tag{4.7}$$

It is shown in [73] that for a BI-AWGN channel the symmetry property holds for the PDF of the channel LLRs delivered to the iterative decoder and the property is preserved for the exchanged LLRs in the decoder throughout the decoding iterations. In contrast to BI-AWGN channels, for multi-user channels, wherein a joint decoder is employed at the receiver, the LLRs sent from the state nodes to each component LDPC decoder depend on both the channel LLRs and the extrinsic LLRs received from the other component LDPC decoders. In the following, we prove the symmetry property for the LLRs exchanged within the joint decoder for the considered GICs adopting BPSK or QPSK with Gray coding.

Theorem 1. *Consider a receiver in a two-user output-symmetric GIC for which the private and public messages are obtained by BPSK or QPSK with Gray coding*[1]*. For a joint decoder with a cycle free Tanner graph, the extrinsic LLR sent from the state node to the variable node of the component LDPC decoder of message j is inverted if the signs of the channel outputs and the a-priori LLRs received from the other component LDPC decoders are inverted.*

Proof. We denote the LLR sent from the state node to the variable node of the component LDPC decoder of message j obtained by inverting the signs of the channel

[1]The result also holds for higher order modulations if the corresponding constellation is symmetric with respect to origin and the sequences of bits assigned to two symmetric points in the constellation are flipped versions of one another.

outputs and the a-priori LLRs received from the other component LDPC decoders by L'_{sv} and show that

$$L_{sv} = -L'_{sv}. \tag{4.8}$$

We show the property for QPSK with Gray coding, and simply note that the case of BPSK can be handled similarly. Considering Gray coding, the real and imaginary parts of the ith transmitted symbol $X_m(i)$ (m can be a public message or the intended private message) are $\sqrt{\frac{P_m}{2}}\Big(1 - 2c_m(2i)\Big)$ and $\sqrt{\frac{P_m}{2}}\Big(1 - 2c_m(2i+1)\Big)$, respectively. It can easily be shown that

$$\begin{aligned} P\bigg(Re\big(X_m(i)\big) = \pm\sqrt{\frac{P_m}{2}}\bigg) &= \frac{\exp\big(\pm L_{vs}(c_m(2i))\big)}{1+\exp\big(\pm L_{vs}(c_m(2i))\big)}, \\ P\bigg(Im\big(X_m(i)\big) = \pm\sqrt{\frac{P_m}{2}}\bigg) &= \frac{\exp\big(\pm L_{vs}(c_m(2i+1))\big)}{1+\exp\big(\pm L_{vs}(c_m(2i+1))\big)}. \end{aligned} \tag{4.9}$$

Using (4.6), (4.9), and the fact that LLRs sent along all the edges in a cycle free Tanner graph are independent, (4.8) follows completing the proof. □

Considering (4.5) and Theorem 1, it is easy to show that the symmetry property of the LLRs sent from the state nodes to the variable nodes holds, and since the property is preserved under BP [41], the property holds for all the LLRs exchanged within the joint decoder. The symmetry property of the LLRs can be exploited to show that [82]

$$I(L;c) = 1 - E\Big\{\log_2(1+e^{-L})\Big\}, \tag{4.10}$$

where $I(L;c)$ denotes the mutual information between the exchanged LLR L and the corresponding coded bit c assuming that the all zero-codeword is transmitted. The expectation in (4.10) can be computed by invoking the ergodicity assumption for the exchanged LLRs. As a result, the mutual information calculations can be performed without requiring the analytical PDFs of the exchanged LLRs, which plays a key role in the proposed code optimization approach.

4.4.3 Stability Condition

We analyze the stability conditions for the joint decoder adopted for the two-user GIC when the HK strategy is implemented for different cases. For the sake of analysis, we assume that the joint decoder has run for a sufficient number of iterations so that the performance of each component LDPC decoder has reached to steady state. To analyze the stability condition, similar to [50], the PDFs of the LLRs corresponding to the ith coded bit of message m (m can be a public message or the intended private message), sent from the check nodes to the ith variable node of the corresponding component LDPC decoder, conditioned on having transmitted all-zero codeword for message m, is expressed as

$$f_L(l) = (1 - \epsilon_m)\Delta_\infty + \epsilon_m \Delta_0, \tag{4.11}$$

where Δ_a denotes the Dirac delta function at a and $\epsilon_m \approx 0$ is the probability of the error for message m. Note that the assumption of transmitting the all-zero codeword is valid for all the messages when channel adapters are employed. For a cycle free Tanner graph, the PDF of the LLRs sent from the variable nodes to the state nodes evolves from (4.11) to

$$f_L(l) = (1 - \epsilon_m^2)\Delta_\infty + \mathcal{O}(\epsilon_m^2), \tag{4.12}$$

which implies that $P\big(c_m(i) = 0\big) = 1 - \epsilon_m^2$. Considering (4.6), at the receiver k, the update rule at the state nodes for $L\big(c_j(i), Y_k(i)\big)$, can be written as

$$L\big(c_j(i), Y_k(i)\big) = L\big(c_j(i), Y'_k(i)\big) + \mathcal{O}(\epsilon^2), \tag{4.13}$$

where j can be a public message or the intended private message and $\epsilon = \max\{\epsilon_{m_1}, \epsilon_{m_2}\}$. $Y'_k(i)$ is the ith modified channel output symbol with respect to the message j at the receiver k, which is obtained by removing the effect of the messages m_1 and m_2.

To simplify the analysis, we neglect the effect of $\mathcal{O}(\epsilon^2)$ and work with the modified channel output Y'_k.

Following the approach taken in [50], we derive the stability conditions for the degree distributions of public and private messages under strong and weak interference levels. Note that both receivers should be analyzed in deriving the stability condition for the degree distributions of public messages while for the degree distribution of each private message only the intended receiver needs to be considered. Since the computations of the LLRs at the state nodes for real and complex signaling are not the same (refer to Fig. 3 and Fig. 4), we separately derive the conditions for BPSK with real channel gains and QPSK with Gray coding with complex channel gains.

4.4.3.1 Strong Interference

Under strong interference the messages are transmitted as public, therefore the stability condition is only derived for the degree distributions of public messages.

BPSK with Real Channel Gains: For this case, the channel gains and the transmitted symbols are real, hence the imaginary part of the received signal can be discarded. At receiver k, the modified channel output with respect to W_i is obtained as

$$Y'_k = h_{ik}X_{w_i} + \mathrm{Re}(Z_k), \tag{4.14}$$

which resembles a P2P channel and the existing results in [2] can be utilized. Considering both receivers, since $INR_j > SNR_i$, $i \neq j$, the stability condition for $(\lambda_{w_i}, \rho_{w_i})$ is expressed as

$$\lambda'_{w_i}(0)\rho'_{w_i}(1) < e^{SNR_i}, \quad i = 1, 2. \tag{4.15}$$

QPSK with Gray Coding and Complex Channel Gains: For QPSK with Gray coding, each state node in the Tanner graph of the joint decoder is connected to two successive variable nodes corresponding to the real part and the imaginary part of

the transmitted symbol. Without loss of generality, we consider the variable node corresponding to the real part of the transmitted symbol X_{w_i} in the joint decoder at the receiver k. The modified channel output with respect to $\mathrm{Re}(X_{w_i})$ is obtained as

$$Y'_k = h_{ik}\,\mathrm{Re}(X_{w_i}) + Z_k. \tag{4.16}$$

Therefore, similar to the previous case, the stability condition for $(\lambda_{w_i}, \rho_{w_i})$ is

$$\lambda'_{w_i}(0)\rho'_{w_i}(1) < e^{\frac{SNR_i}{2}}, \quad i = 1, 2. \tag{4.17}$$

4.4.3.2 Weak Interference

Under weak interference, the two public messages and the intended private message are decoded at each receiver, i.e., the private message of the interfering signal is not decoded, and the corresponding part is present in the modified channel output.

BPSK with Real Channel Gains: For this scenario, the modified channel output at the receiver k with respect to the message U_k is

$$Y'_k = h_{kk}X_{u_k} + h_{rk}X_{u_r} + \mathrm{Re}(Z_k) \quad k \neq r, \tag{4.18}$$

which is similar to the channel studied in [50], hence the stability condition for $(\lambda_{u_k}, \rho_{u_k})$ is given by

$$\lambda'_{u_k}(0)\rho'_{u_k}(1) < \left(e^{-\alpha_k SNR_k - \alpha_r INR_k} E_{N_1}\left\{ \sqrt{\frac{\cosh(2N_1\sqrt{2\alpha_r INR_k}) + \cosh(4\sqrt{\alpha_r \alpha_k SNR_k INR_k})}{2}} \right\} \right)^{-1}, \tag{4.19}$$

where E_{N_1} denotes the expectation taken with respect to a standard Gaussian random variable $N_1 \sim \mathcal{N}(0, 1)$. Similarly, the modified channel outputs with respect to W_k at the receiver k and r $(k \neq r)$ are obtained as

$$\begin{aligned} Y'_k =& h_{kk}X_{w_k} + h_{rk}X_{u_r} + \mathrm{Re}(Z_k), \\ Y'_r =& h_{kr}(X_{w_k} + X_{u_k}) + \mathrm{Re}(Z_r). \end{aligned} \tag{4.20}$$

Considering both receivers, the stability condition for $(\lambda_{w_k}, \rho_{w_k})$ is obtained as

$$\lambda'_{w_k}(0)\rho'_{w_k}(1) < \min\left\{\left(e^{-(1-\alpha_k)SNR_k-\alpha_r INR_k} \times E_{N_1}\left\{\sqrt{\frac{\cosh(2N_1\sqrt{2\alpha_r INR_k})+\cosh(4\sqrt{(1-\alpha_k)\alpha_r SNR_k INR_k})}{2}}\right\}\right)^{-1}, \left(e^{-INR_r} \times E_{N_1}\left\{\sqrt{\frac{\cosh(2N_1\sqrt{2\alpha_k INR_r})+\cosh(4INR_r\sqrt{(1-\alpha_k)(\alpha_k)})}{2}}\right\}\right)^{-1}\right\}. \tag{4.21}$$

QPSK with Gray Coding and Complex Channel Gains: Similar to the strong interference case, we consider the LLR sent from the state node to the variable node corresponding to the real part of the message of interest. Therefore, the modified channel output with respect to U_k is obtained as

$$Y'_k = h_{kk}\,\mathrm{Re}(X_{u_k}) + h_{rk}X_{u_r} + Z_k, \tag{4.22}$$

where $k \neq r$. The stability condition for $(\lambda_{u_k}, \rho_{u_k})$ can be obtained by computing the Bhattacharyya constant [50] for the modified channel output resulting in

$$\lambda'_{u_k}(0)\rho'_{u_k}(1) < \left(e^{-\frac{\alpha_k SNR_k}{2}-\alpha_r INR_k} E_{N_1N_2}\left\{\sqrt{g(N_1, N_2, h_{kk}\sqrt{\frac{\alpha_k P_k}{2}}, h_{rk}\sqrt{\frac{\alpha_r P_r}{2}})}\right\}\right)^{-1}, \tag{4.23}$$

for $r \neq k$, where N_1 and N_2 are Gaussian random variables with zero mean and variance $\frac{1}{2}$, and

$$\begin{aligned} g(N_1, N_2, A_1, A_2) =& \frac{1}{16}\sum_{a=0}^{1}\sum_{b=0}^{1}\sum_{c=0}^{1}\sum_{d=0}^{1}\exp\left(\frac{1}{N_0}\Big(2N_1\Big(A_{2_i}(-1)^a \right. \\ & - A_{2_q}(-1)^b + A_{2_i}(-1)^c - A_{2_q}(-1)^d\Big) - 2A_{1_i}\Big(A_{2_i}(-1)^a \\ & - A_{2_q}(-1)^b - A_{2_i}(-1)^c + A_{2_q}(-1)^d\Big) + 2N_2\Big(A_{2_i}(-1)^b \\ & + A_{2_q}(-1)^a + A_{2_i}(-1)^d + A_{2_q}(-1)^c\Big) - 2A_{1_q}\Big(A_{2_i}(-1)^b \\ & \left. + A_{2_q}(-1)^a - A_{2_i}(-1)^d - A_{2_q}(-1)^c\Big)\Big)\right), \end{aligned} \tag{4.24}$$

where A_{j_i} and A_{j_q} in (4.4.3.2) denote the real and imaginary parts of A_j, respectively, with $j = 1, 2$. Similar analysis can be performed for $(\lambda_{w_k}, \rho_{w_k})$ considering both receivers, where the stability condition is expressed as

$$\lambda'_{w_k}(0)\rho'_{w_k}(1) < \min\left\{\left(e^{-\frac{(1-\alpha_k)SNR_k}{2}-\alpha_r INR_k}\right.\right.$$
$$\left.\times E_{N_1N_2}\left\{\sqrt{g(N_1, N_2, h_{kk}\sqrt{\frac{(1-\alpha_k)P_k}{2}}, h_{rk}\sqrt{\frac{\alpha_r P_r}{2}})}\right\}\right)^{-1},$$
$$\left(e^{-\frac{(1+\alpha_k)INR_r}{2}}\right.$$
$$\left.\left.\times E_{N_1N_2}\left\{\sqrt{g(N_1, N_2, h_{kr}\sqrt{\frac{(1-\alpha_r)P_r}{2}}, h_{kr}\sqrt{\frac{\alpha_r P_r}{2}})}\right\}\right)^{-1}\right\}. \quad (4.25)$$

4.4.4 Proposed Code Optimization Method

To initialize the code optimization procedure, for each of the involved messages, we select the degree distributions of the LDPC codes among the optimized P2P codes for BI-AWGN channels (obtained via the EXIT chart method in [74]). The selected degree distributions are then employed for the two-user GIC and checked whether they are admissible for the given channel parameters, meaning that the probability of decoding error for the corresponding code goes to zero asymptotically. To verify this, we assume that the joint decoder is cycle free and run the decoder with a sufficient number of state nodes (taken as 10^6 in our examples) fed with realizations of the channel outputs. The employed degree distributions are declared admissible if, for each component LDPC decoder, the mutual information between the transmitted bits and the exchanged LLRs within the component LDPC decoder evolves to 0.995. Note that we do not simulate any specific code realization, hence the adopted method captures the average behavior of the code ensembles by tracking the evolution of the

mutual information without using any Gaussianity assumption for the PDFs of the exchanged LLRs within the joint decoder.

Having obtained the admissible degree distributions, perturbing vectors are utilized to generate a new instance of degree distributions with increased rates following the approach utilized in [83] in an iterative fashion. To simplify the code optimization, we assume that the check node degree distribution is a singleton and it does not change throughout the iterations; therefore, only the variable node degree distribution is perturbed as $\tilde{\lambda}_i = \lambda_i + e_i$, where e_i denotes the ith element of the perturbing vector and $\tilde{\lambda}_i$ represents the ith coefficient of $\tilde{\lambda}$. For the variable node degree distribution to be valid, $\sum_{i=2}^{d_v} \tilde{\lambda}_i = 1$, which enforces

$$\sum_{i=2}^{d_v} e_i = 0 \quad \text{and} \quad 0 \leq \lambda_i + e_i \leq 1. \tag{4.26}$$

At each iteration, the current rate (r_0) is increased with the rate increment K, that is

$$1 - \frac{1}{d_c} \frac{1}{\sum_i \frac{\tilde{\lambda}_i}{i}} = r_0 + K, \tag{4.27}$$

which implies that

$$\sum_i \frac{\tilde{\lambda}_i}{i} = \frac{1}{d_c\big(1 - r_0 - K\big)}, \tag{4.28}$$

resulting in

$$\sum_i \frac{e_i}{i} = \frac{K}{d_c\big((1-r_0)^2 - K(1-r_0)\big)}. \tag{4.29}$$

The perturbing vector is generated by drawing all the elements except two from a standard normal distribution, i.e., $\mathcal{N}(0,1)$. The remaining two elements are obtained by solving the set of linear equations (4.26) and (4.29). The perturbing vector is adopted if it meets the inequality constraints in (4.26) and the resulting variable node degree distribution satisfies the stability condition, otherwise a new perturbing vector is generated. The perturbed variable node degree distribution will replace the current

one if the resulting degree distributions are admissible, otherwise it is dismissed and a new perturbation is performed. The process is stopped if new admissible degree distributions cannot be found after a predetermined number of perturbations.

Remark: Although we have assumed a singleton distribution for the check nodes, this constraint can be relaxed by adding a separate perturbing vector. In this case, both the check node and the variable node degree distributions are perturbed jointly where the constraints on the perturbing vectors should be changed accordingly. Note that the proposed optimization is not limited to a specific modulation, however, in order to exploit the symmetry property of the LLRs in the computation of (4.10), the employed constellation should be symmetric with respect to origin and the sequences of bits assigned to two symmetric points in the constellation should be flipped versions of one another.

4.5 Examples of LDPC Codes Over GICs

In this section, we investigate the performance of irregular LDPC codes adopted for transmission over two-user GICs implementing the HK coding/decoding strategy. We restrict our attention to the case of fixed channel gains and finite signal constellations. A range of examples for different interference levels employing BPSK and QPSK with Gray coding are studied. In all the instances, code optimization is performed for symmetric and asymmetric rate pairs with the goal of sum rate maximization where the rate increments are along a straight line in the rate region. Similar to Chapter 3, we employ degree distributions with nonzero variable node degrees as $\{2, 3, 4, 9, 10, 19, 20, 49, 50\}$, and singleton check nodes, i.e., $\rho(x) = x^{d_c-1}$. The degree of the check nodes (d_c) is determined by optimizing the initial degree distribution for a BI-AWGN channel utilizing the EXIT chart analysis [74]. The performance of the optimized codes for the two-user GIC is compared with that of the P2P codes

optimized for a BI-AWGN achieving the highest sum-rate, which does not necessarily correspond to the initial degree distributions. Note that for symmetric channels, the degree distributions corresponding to the rate pair (R_1, R_2) can also be used to achieve (R_2, R_1) by interchanging the employed degree distributions. Moreover, for symmetric rate pairs (i.e., when $R_1 = R_2$) achieved for symmetric channels, identical degree distributions (with distinct code realizations) are adopted for the messages of both users.

4.5.1 GIC with Strong Interference

Under strong interference, all the messages are public and the capacity region is known. Although the capacity region is determined by those of two MACs, the code design method in [1] is not directly applicable since the channel gains are not equal in general, and each message should be decodable at each of the receivers. In the following, we study several different scenarios.

Scenario I – Symmetric GIC with BPSK

For this instance, a symmetric GIC is considered, whose capacity regions with different inputs and achieved rate pairs are shown in Fig. 4.5. The best achievable rate pairs obtained with P2P codes are also depicted in Fig. 4.5. It can be observed that, for the optimized codes, the achieved rate pairs are close to the boundary of the capacity region and they outperform the P2P codes. Moreover, the P2P codes and the optimized codes perform better than the single user codes with non-naive TS.

Scenario II – Asymmetric GIC with BPSK

In this example, an asymmetric GIC with channel parameters shown in Fig. 4.6 is considered. Unlike the previous example, for both symmetric and asymmetric rate pairs, two degree distributions are optimized separately since the channels observed by each receiver are different. It can be observed that, similar to the previous example,

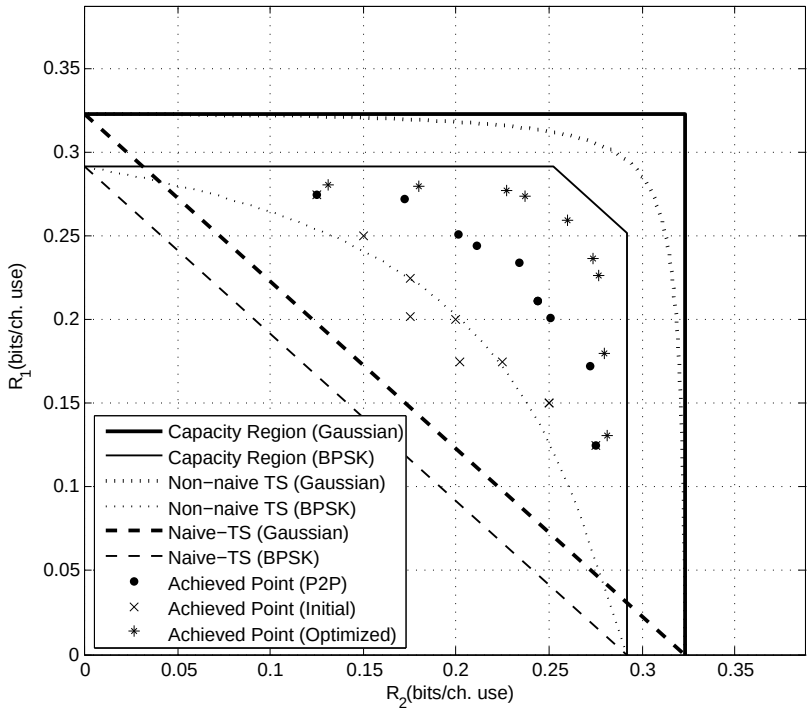

Figure 4.5: Scenario I: Capacity Regions and Achieved Rate Pairs for a Symmetric GIC with Strong Interference $SNR = -6$ dB, $INR = -5$ dB

Table 4.1: Degree Distributions for Scenario I.

	Msg.	R	d_c	λ_2	λ_3	λ_4	λ_9	λ_{10}	λ_{19}	λ_{20}	λ_{49}	λ_{50}
P2P	$W_{1,2}$	0.234	5	0.2790	0.1898	0.1271	0.0679	0.1133	0.0895	0.0093	0.0838	0.0403
Opt.	$W_{1,2}$	0.26	5	0.2695	0.3292	0.0050	0.1281	0.0246	0.0780	0.0136	0.1428	0.0092
Opt. P2P	W_1	0.211	5	0.2845	0.1207	0.1863	0.0539	0.1322	0.0146	0.0091	0.0417	0.1570
	W_2	0.244	5	0.2691	0.2724	0.0219	0.2258	0.0320	0.0432	0.0141	0.0676	0.0539
Opt. P2P	W_1	0.237	5	0.3198	0.0985	0.2097	0.0400	0.0698	0.0037	0.0057	0.0683	0.1845
	W_2	0.274	5	0.2884	0.2563	0.0703	0.0890	0.1329	0.0467	0.0060	0.0394	0.0710
Opt. P2P	W_1	0.201	5	0.2717	0.1798	0.1179	0.1454	0.0063	0.0557	0.0273	0.0807	0.1152
	W_2	0.251	5	0.2897	0.1963	0.1024	0.2137	0.0066	0.0388	0.0549	0.0232	0.0744
Opt. P2P	W_1	0.227	5	0.2988	0.1951	0.0890	0.0962	0.0415	0.0420	0.0077	0.1049	0.1248
	W_2	0.277	5	0.2935	0.2555	0.0486	0.1187	0.1137	0.1090	0.0336	0.0124	0.0150
Opt. P2P	W_1	0.172	4	0.3494	0.2303	0.1019	0.1463	0.0380	0.0642	0.0043	0.0482	0.0174
	W_2	0.272	5	0.2875	0.2117	0.1342	0.0930	0.0707	0.0610	0.1129	0.0267	0.0023
Opt. P2P	W_1	0.18	4	0.2936	0.3264	0.1352	0.0012	0.1076	0.0332	0.0257	0.0596	0.0175
	W_2	0.28	5	0.2957	0.2261	0.1041	0.0809	0.1319	0.0199	0.0840	0.0393	0.0181
Opt. P2P	W_1	0.125	4	0.3321	0.2067	0.1087	0.1679	0.0120	0.0014	0.0059	0.0801	0.0852
	W_2	0.275	5	0.2864	0.2289	0.1014	0.1580	0.0746	0.0155	0.0823	0.0041	0.0488
Opt. P2P	W_1	0.131	4	0.3715	0.1972	0.0594	0.1000	0.0147	0.0320	0.0840	0.0716	0.0696
	W_2	0.281	5	0.3088	0.2130	0.0785	0.1950	0.0657	0.0249	0.0440	0.0296	0.0405

the achieved rate pairs for the optimized degree distributions outperform the ones obtained with the P2P codes. Furthermore, all the achieved rate pairs with the P2P and optimized codes are superior to the ones obtained via the single user codes

utilizing non-naive TS.

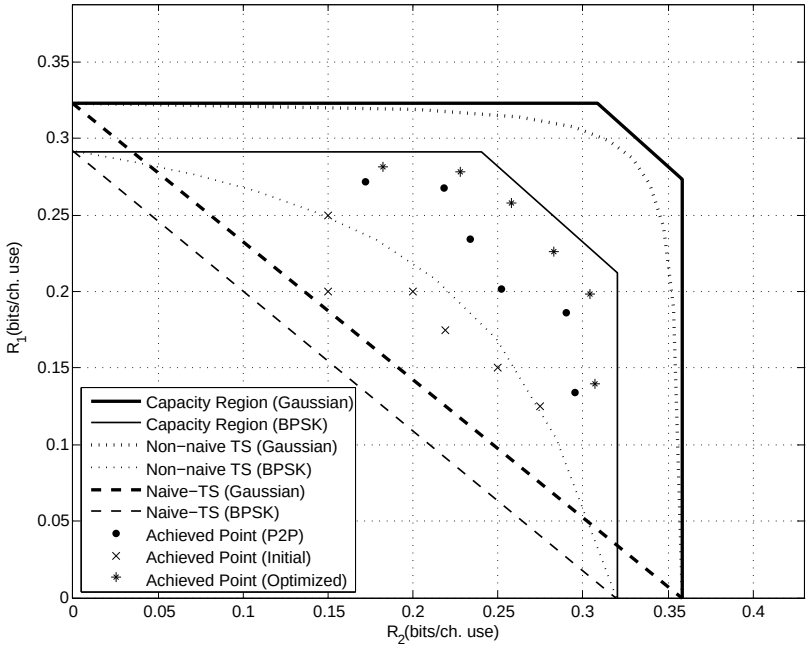

Figure 4.6: Scenario II: Capacity Regions and Achieved Rate Pairs for an Asymmetric GIC with Strong Interference $SNR_1 = -6\ dB,\ INR_1 = -5.25\ \ dB,\ SNR_2 = -5.5\ dB,\ INR_2 = -4.75\ dB$

Table 4.2: Degree Distributions for Scenario II

	Msg.	R	d_c	λ_2	λ_3	λ_4	λ_9	λ_{10}	λ_{19}	λ_{20}	λ_{49}	λ_{50}
Opt. P2P	W_1	0.272	5	0.2875	0.2117	0.1342	0.0930	0.0707	0.0610	0.1129	0.0267	0.0023
	W_2	0.172	4	0.3494	0.2303	0.1019	0.1463	0.0380	0.0642	0.0043	0.0482	0.0174
Opt. P2P Opt.	W_1	0.282	5	0.3188	0.1587	0.1549	0.0567	0.1369	0.0424	0.0903	0.0274	0.0139
	W_2	0.182	4	0.3708	0.1025	0.2918	0.0147	0.0645	0.0167	0.0445	0.0453	0.0492
Opt. P2P Opt.	W_1	0.268	5	0.2948	0.2026	0.1153	0.1107	0.0959	0.0188	0.1104	0.0399	0.0116
	W_2	0.218	5	0.2823	0.1020	0.2457	0.0393	0.0500	0.0870	0.0457	0.0234	0.1246
Opt. P2P Opt.	W_1	0.278	5	0.3106	0.1901	0.1065	0.1691	0.0809	0.0337	0.0297	0.0033	0.0761
	W_2	0.228	4	0.3815	0.2999	0.0280	0.1453	0.0719	0.0340	0.0074	0.0093	0.0227
P2P	$W_{1,2}$	0.234	5	0.2790	0.1898	0.1271	0.0679	0.1133	0.0895	0.0093	0.0838	0.0403
Opt. P2P Opt.	W_1	0.258	5	0.3007	0.1981	0.1377	0.0228	0.0607	0.0291	0.1192	0.0963	0.0354
	W_2	0.258	5	0.3282	0.1432	0.1499	0.0567	0.0132	0.1182	0.0856	0.0902	0.0148
Opt. P2P Opt.	W_1	0.202	5	0.2680	0.1786	0.1434	0.0359	0.0667	0.1314	0.0040	0.0141	0.1579
	W_2	0.252	5	0.2799	0.2054	0.1315	0.0421	0.1286	0.1237	0.0078	0.0733	0.0077
Opt. P2P Opt.	W_1	0.226	4	0.4126	0.2658	0.0247	0.0933	0.0754	0.0303	0.0176	0.0170	0.0633
	W_2	0.283	5	0.3066	0.2792	0.0384	0.0047	0.0777	0.2256	0.0485	0.0103	0.0090
Opt. P2P Opt.	W_1	0.186	4	0.3501	0.2414	0.1135	0.0614	0.1191	0.0078	0.0648	0.0089	0.0330
	W_2	0.290	5	0.2954	0.2212	0.1310	0.1526	0.0311	0.0702	0.0592	0.0376	0.0017
Opt. P2P Opt.	W_1	0.198	4	0.4218	0.1239	0.1579	0.1236	0.0169	0.0314	0.0191	0.0671	0.0383
	W_2	0.304	5	0.3269	0.1697	0.1583	0.1164	0.1081	0.0261	0.0264	0.0335	0.0346
Opt. P2P Opt.	W_1	0.134	4	0.3308	0.1876	0.1603	0.1012	0.0377	0.0450	0.0179	0.0292	0.0903
	W_2	0.295	5	0.2816	0.2614	0.1105	0.1229	0.0776	0.0622	0.0598	0.0064	0.0176
Opt. P2P Opt.	W_1	0.14	4	0.3283	0.1667	0.2039	0.0596	0.0285	0.0612	0.1450	0.0048	0.0020
	W_2	0.307	5	0.3146	0.2326	0.0770	0.2500	0.0139	0.0701	0.0289	0.0031	0.0098

Scenario III – Symmetric GIC with QPSK

The details for this example are given in Fig. 4.7. The code optimization is performed for both symmetric and asymmetric rate pairs. Similar to the BPSK example, only one code is optimized for both messages when symmetric rate pairs are considered. We observe that the achieved rate pairs with optimized codes outperform the ones obtained with P2P codes, and that both optimized and P2P codes beat the non-naive TS results with QPSK inputs. Furthermore, the optimized codes even outperform the non-naive TS results with Gaussian signaling.

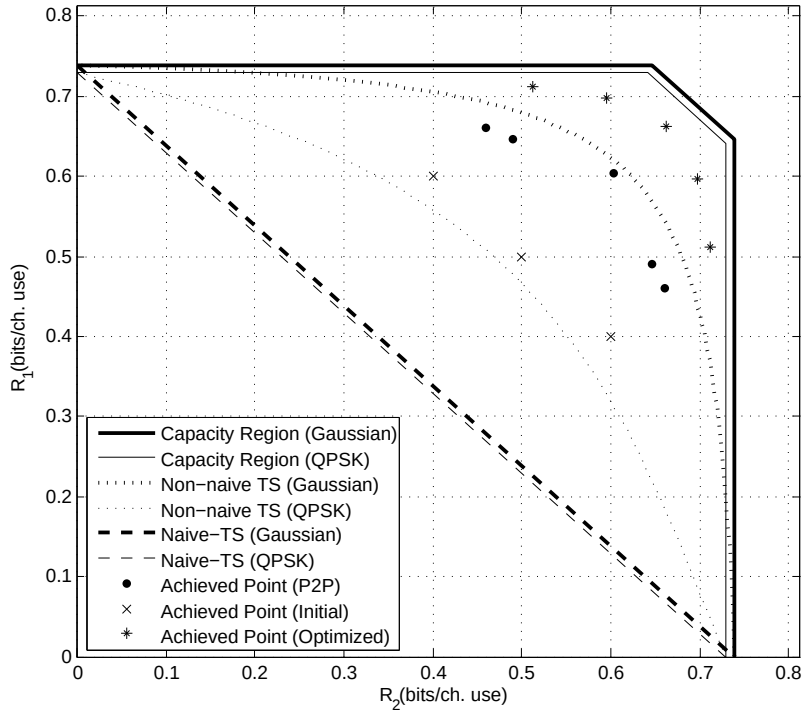

Figure 4.7: Scenario III: Capacity Regions and Achieved Rate Pairs for a Symmetric GIC with Strong Interference $SNR = -1.75$ dB, $INR = -0.25$ dB, $\angle\, h_{11} = \angle\, h_{22} = \frac{\pi}{4}$, $\angle h_{21} = \angle h_{12} = \frac{\pi}{3}$

Scenario IV – Asymmetric GIC with QPSK

For this example, an asymmetric channel is considered, and the corresponding results are depicted in Fig. 4.8. Degree distributions are optimized for both symmetric and

Table 4.3: Degree Distributions for Scenario III

	Msg.	R	d_c	λ_2	λ_3	λ_4	λ_9	λ_{10}	λ_{19}	λ_{20}	λ_{49}	λ_{50}
P2P	$W_{1,2}$	0.302	6	0.2477	0.1277	0.1869	0.1308	0.0093	0.0537	0.0811	0.0633	0.0995
Opt.	$W_{1,2}$	0.331	6	0.2535	0.2346	0.0814	0.0950	0.0555	0.0287	0.0392	0.0152	0.1969
Opt. P2P	W_1	0.245	5	0.2945	0.1266	0.2140	0.0621	0.0478	0.0706	0.0951	0.0497	0.0396
	W_2	0.323	6	0.2467	0.2076	0.0838	0.1042	0.1534	0.0084	0.0480	0.0192	0.1287
Opt. P2P	W_1	0.298	5	0.3413	0.1503	0.2040	0.0167	0.0473	0.0206	0.0376	0.0383	0.1439
	W_2	0.349	6	0.2758	0.1717	0.1256	0.1056	0.1292	0.0116	0.0184	0.0889	0.0732
Opt. P2P	W_1	0.23	5	0.2816	0.1623	0.1576	0.1525	0.0045	0.0816	0.0164	0.1408	0.0027
	W_2	0.33	6	0.2148	0.3127	0.0166	0.1485	0.0877	0.0936	0.0077	0.0828	0.0356
Opt. P2P	W_1	0.256	5	0.2134	0.4389	0.0045	0.0357	0.0315	0.0399	0.0179	0.1086	0.1096
	W_2	0.356	6	0.2643	0.2181	0.0876	0.0881	0.1242	0.1050	0.0620	0.0120	0.0387

asymmetric rate pairs. Parallel to our previous findings, the optimized codes perform better than the P2P codes both of which operating outside the non-naive TS rate region. Specifically, all of the optimized codes and one instance of the P2P codes outperform the single user codes with Gaussian signaling with non-naive TS.

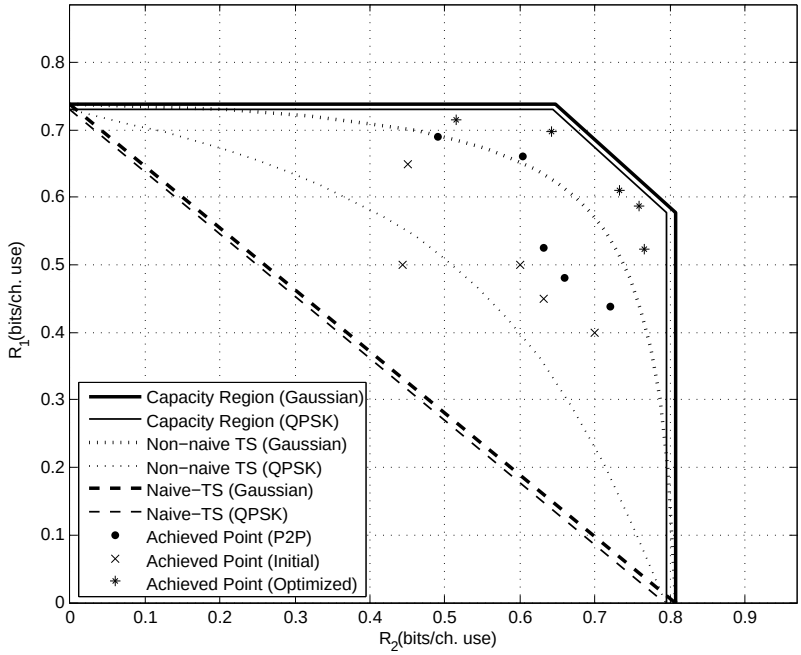

Figure 4.8: Scenario IV: Capacity Regions and Achieved Rate Pairs for an Asymmetric GIC with Strong Interference $SNR_1 = -1.75$ dB, $INR_1 = -0.25$ dB, $SNR_2 = -1.25$ dB, $INR_2 = 0.25$ dB, $\angle h_{11} = \frac{\pi}{4}$, $\angle h_{21} = \frac{\pi}{3}$, $\angle h_{12} = \angle h_{22} = 0$

4.5.2 GIC with Weak Interference

Under weak interference, the interfering signal cannot be decoded in its entirety, and hence sending all the messages as public may not be optimal. As a result, unlike the

Table 4.4: Degree Distributions for Scenario IV

	Msg.	R	d_c	λ_2	λ_3	λ_4	λ_9	λ_{10}	λ_{19}	λ_{20}	λ_{49}	λ_{50}
Opt. P2P Opt. P2P Opt. P2P Opt. P2P Opt. P2P	W_1	0.345	6	0.2510	0.2298	0.0660	0.2137	0.0370	0.0624	0.0768	0.0076	0.0557
	W_2	0.245	5	0.2945	0.1266	0.2140	0.0621	0.0478	0.0706	0.0951	0.0497	0.0396
	W_1	0.357	6	0.2605	0.2418	0.0513	0.1876	0.0752	0.0902	0.0107	0.0812	0.0015
	W_2	0.257	5	0.3307	0.1128	0.1725	0.0477	0.0847	0.0977	0.0304	0.0608	0.0627
	W_1	0.33	6	0.2148	0.3127	0.0166	0.1485	0.0877	0.0936	0.0077	0.0828	0.0356
	W_2	0.302	6	0.2477	0.1277	0.1869	0.1308	0.0093	0.0537	0.0811	0.0633	0.0995
	W_1	0.349	6	0.2607	0.2043	0.1043	0.1252	0.1039	0.0325	0.0685	0.0712	0.0294
	W_2	0.321	6	0.2852	0.1184	0.1285	0.1856	0.0190	0.0723	0.0367	0.0997	0.0546
	W_1	0.263	5	0.2940	0.1676	0.1669	0.1030	0.0940	0.0463	0.0290	0.0679	0.0313
	W_2	0.316	6	0.2345	0.1804	0.1545	0.0309	0.1644	0.0002	0.1018	0.0522	0.0811
	W_1	0.305	5	0.3028	0.3261	0.0418	0.0147	0.0533	0.0808	0.0787	0.0984	0.0034
	W_2	0.366	6	0.2840	0.2279	0.0762	0.1058	0.0500	0.0616	0.0660	0.0675	0.0610
	W_1	0.24	5	0.2701	0.2186	0.1115	0.0852	0.1123	0.0178	0.0665	0.0638	0.0542
	W_2	0.33	6	0.2148	0.3127	0.0166	0.1485	0.0877	0.0936	0.0077	0.0828	0.0356
	W_1	0.294	5	0.3339	0.2518	0.0404	0.0393	0.0601	0.0852	0.1227	0.0434	0.0232
	W_2	0.379	6	0.2797	0.3078	0.0062	0.0965	0.0588	0.0649	0.0219	0.0247	0.1395
	W_1	0.219	5	0.2575	0.2490	0.0619	0.1320	0.0768	0.0586	0.0037	0.0494	0.1111
	W_2	0.36	6	0.2511	0.2213	0.1185	0.1178	0.0940	0.0334	0.1323	0.0118	0.0198
	W_1	0.262	5	0.3020	0.2271	0.1038	0.0633	0.0208	0.0755	0.0317	0.0433	0.1325
	W_2	0.383	6	0.2851	0.1801	0.1842	0.0370	0.1036	0.0256	0.0660	0.0990	0.0194

case of strong interference, power allocation should be addressed prior to the code optimization. To simplify the process, an optimization problem is solved to achieve the largest rate region formulated as

$$\begin{aligned} &\max_{\alpha_1,\alpha_2} R_{u_1} + R_{w_1} + R_{u_2} + R_{w_2} \\ &\text{subject to} \Big\{ R_{u_1}(\alpha_1), R_{w_1}(\alpha_1), R_{u_2}(\alpha_2), R_{w_2}(\alpha_2) \Big\} \in \mathcal{R}_1 \\ &\qquad 0 \leq \alpha_i \leq 1, \quad i = 1, 2, \\ &\qquad R_{u_1} + R_{w_1} = R_{u_2} + R_{w_2} + \Delta R, \end{aligned} \tag{4.30}$$

where R_{u_i} and R_{w_i} denote the rates of the messages U_i and W_i at the transmitter i, respectively. All the rates in (4.30) should be contained in the HK sub-region $\mathcal{R}_1$ characterized through (4.2) computed for the employed constellations (BPSK or QPSK with Gray coding), for which no TS is utilized and the private message and the public message of each transmitter is combined through addition. The last constraint in (4.30) is added to simplify the optimization process where ΔR is an arbitrary value also employed and kept fixed during the code optimization.

Scenario V – Symmetric GIC with BPSK

In this example, a symmetric GIC is considered with channel parameters given in Fig. 4.9. The HK ARR is characterized for BPSK and Gaussian signaling. The obtained ARRs are outerbounded utilizing the results of [34] as shown in the figure. The power allocation is performed for $\Delta R = 0$, $\Delta R = \pm 0.05$, and $\Delta R = \pm 0.15$. For the rate increments during the code optimization, we adopt $\frac{R_{u_i}}{R_{w_i}}, i = 1, 2$, obtained from the power allocation optimization results. Fig. 4.9 clearly shows that for both symmetric and asymmetric rate pairs the optimized codes are superior to the P2P optimal codes. In addition both P2P and optimized codes beat the naive TS scheme, however, they do not exceed the boundary of the non-naive TS region.

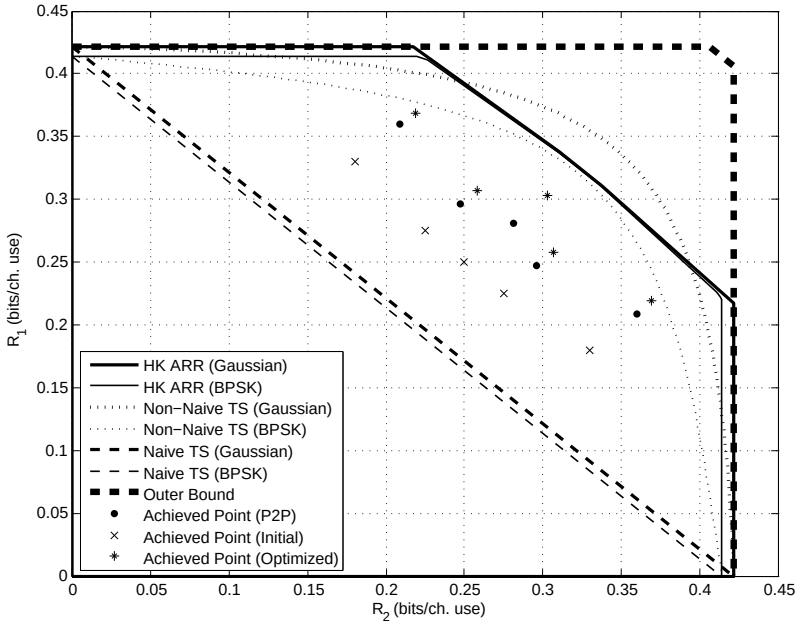

Figure 4.9: Scenario V: Rate Regions and Achieved Rate Pairs for a Symmetric GIC with Weak Interference $SNR = -4.01$ dB, $INR = -5.01$ dB

Table 4.5: Degree Distributions for Scenario V

	α_1, α_2	Msg.	R	d_c	λ_2	λ_3	λ_4	λ_9	λ_{10}	λ_{19}	λ_{20}	λ_{49}	λ_{50}
Opt. P2P	$\alpha_1 = 0.36$	$U_{1,2}$	0.132	4	0.3315	0.2088	0.1273	0.0790	0.0590	0.0235	0.0508	0.0099	0.1102
	$\alpha_2 = 0.36$	$W_{1,2}$	0.149	4	0.3613	0.0793	0.2874	0.0251	0.0504	0.0388	0.0596	0.0580	0.0401
Opt. P2P	$\alpha_1 = 0.36$	$U_{1,2}$	0.142	4	0.3634	0.1674	0.1106	0.0972	0.1013	0.0531	0.0075	0.0628	0.0367
	$\alpha_2 = 0.36$	$W_{1,2}$	0.161	4	0.3609	0.2671	0.0031	0.0721	0.1386	0.0504	0.0317	0.0325	0.0436
P2P	$\alpha_1 = 0.5$	U_1	0.224	5	0.2659	0.2455	0.0512	0.1661	0.0542	0.0203	0.0415	0.0546	0.1007
	$\alpha_2 = 0$	W_1	0.136	4	0.3488	0.1237	0.2267	0.0161	0.0912	0.0299	0.0422	0.0971	0.0243
		W_2	0.209	5	0.2386	0.2859	0.0504	0.0920	0.0892	0.0326	0.0176	0.1183	0.0754
Opt.	$\alpha_1 = 0.5$	U_1	0.229	5	0.2881	0.1978	0.0867	0.1136	0.0835	0.0679	0.0021	0.0953	0.0650
	$\alpha_2 = 0$	W_1	0.14	4	0.3535	0.2281	0.0474	0.1203	0.0706	0.0037	0.0628	0.0283	0.0853
		W_2	0.217	4	0.3835	0.2263	0.1377	0.0308	0.0711	0.0898	0.0365	0.0097	0.0146
P2P	$\alpha_1 = 0.48$	U_1	0.172	4	0.3494	0.2303	0.1019	0.1463	0.0380	0.0642	0.0043	0.0482	0.0174
	$\alpha_2 = 0.35$	W_1	0.124	4	0.3386	0.1606	0.1633	0.1308	0.0293	0.0175	0.0040	0.1143	0.0416
		U_2	0.112	4	0.3300	0.1874	0.1410	0.0020	0.1268	0.0288	0.0234	0.0481	0.1125
		W_2	0.135	4	0.3400	0.2117	0.1038	0.0594	0.0962	0.0443	0.0348	0.0932	0.0166
Opt.	$\alpha_1 = 0.48$	U_1	0.178	4	0.3814	0.1620	0.1543	0.0896	0.0321	0.0261	0.1088	0.0220	0.0237
	$\alpha_2 = 0.35$	W_1	0.129	4	0.3396	0.2320	0.0639	0.0584	0.1261	0.0294	0.0065	0.0539	0.0902
		U_2	0.117	4	0.3525	0.1999	0.0801	0.0610	0.0203	0.1622	0.0145	0.0085	0.1010
		W_2	0.141	4	0.3359	0.2870	0.0113	0.1037	0.0633	0.0624	0.0216	0.0790	0.0358

Scenario VI – Symmetric GIC with QPSK

In this example, we consider a symmetric GIC with channel parameters given in Fig. 4.10. The power allocation optimization is performed for $\Delta R = 0$, $\Delta R = \pm 0.3$, and $\Delta R = \pm 0.4$. It can be observed that, similar to the previous example, the optimized codes beat the P2P codes, both of which outperforming the naive TS rate region. Furthermore, for the asymmetric rate pairs, all the optimized codes and some of P2P codes outperform the non-naive TS rate region.

Table 4.6: Degree Distributions for Scenario VI

	α_1, α_2	Msg.	R	d_c	λ_2	λ_3	λ_4	λ_9	λ_{10}	λ_{19}	λ_{20}	λ_{49}	λ_{50}
Opt. P2P	$\alpha_1 = 0.15$	$U_{1,2}$	0.119	4	0.3270	0.2106	0.1170	0.0227	0.1339	0.0104	0.0259	0.0126	0.1399
	$\alpha_2 = 0.15$	$W_{1,2}$	0.316	6	0.2345	0.1804	0.1545	0.0309	0.1644	0.0002	0.1018	0.0522	0.0811
Opt. P2P	$\alpha_1 = 0.15$	$U_{1,2}$	0.143	4	0.3682	0.1303	0.1657	0.0517	0.1055	0.0868	0.0021	0.0358	0.0539
	$\alpha_2 = 0.15$	$W_{1,2}$	0.377	6	0.3253	0.2005	0.0835	0.0414	0.0536	0.0125	0.0273	0.1647	0.0912
P2P	$\alpha_1 = 0.51$	U_1	0.439	7	0.2110	0.3124	0.0295	0.2368	0.0272	0.1213	0.0336	0.0126	0.0156
	$\alpha_2 = 0$	W_1	0.196	4	0.3650	0.2180	0.1211	0.0224	0.2121	0.0154	0.0020	0.0404	0.0036
		W_2	0.335	6	0.2310	0.2712	0.0518	0.0337	0.2035	0.0197	0.0942	0.0732	0.0217
Opt.	$\alpha_1 = 0.51$	U_1	0.475	7	0.2552	0.2896	0.0379	0.0662	0.2739	0.0364	0.0263	0.0020	0.0125
	$\alpha_2 = 0$	W_1	0.212	4	0.3893	0.2269	0.1236	0.0603	0.0323	0.0486	0.0397	0.0316	0.0477
		W_2	0.387	6	0.3448	0.0318	0.2799	0.0122	0.0958	0.0023	0.1080	0.0455	0.0797
P2P	$\alpha_1 = 0.5$	U_1	0.448	8	0.2019	0.2004	0.1019	0.0789	0.1366	0.1071	0.0559	0.0703	0.0470
	$\alpha_2 = 0$	W_1	0.252	5	0.2799	0.2054	0.1315	0.0421	0.1286	0.1237	0.0078	0.0733	0.0077
		W_2	0.300	6	0.2365	0.2023	0.0902	0.1781	0.0009	0.0784	0.0506	0.1516	0.0114
Opt.	$\alpha_1 = 0.5$	U_1	0.459	7	0.1867	0.3871	0.0485	0.0959	0.1084	0.1263	0.0127	0.0038	0.0306
	$\alpha_2 = 0$	W_1	0.258	5	0.2609	0.3292	0.0059	0.0491	0.1482	0.0740	0.0356	0.0490	0.0481
		W_2	0.317	5	0.3436	0.1022	0.2821	0.0281	0.0774	0.0531	0.0183	0.0113	0.0839

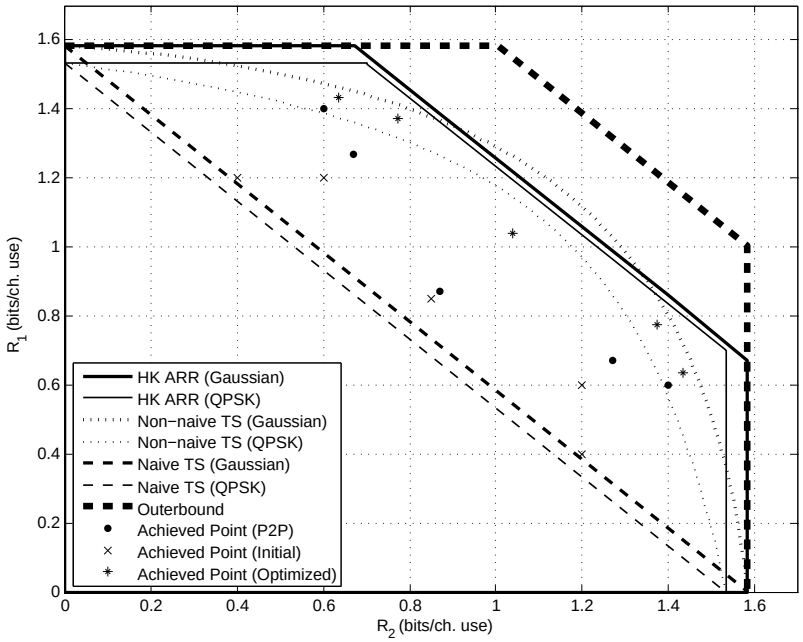

Figure 4.10: Scenario VI : Rate Regions and Achieved Rate Pairs for a GIC with Weak Interference $SNR = 3$ dB, $INR = 2.5$ dB, $\angle h_{11} = \angle h_{22} = \frac{\pi}{4}, \angle h_{21} = \angle h_{12} = \frac{\pi}{3}$

4.5.3 Summary of Results

We now summarize the results obtained in the above examples for GICs with strong and weak interference levels. Under strong interference, we see that the optimized codes and the P2P codes outperform both naive TS and non-naive TS schemes. Moreover, the optimized codes consistently improve upon the P2P codes. For all instances with QPSK, the optimized codes also beat non-naive TS scheme for Gaussian signaling, which is not achieved with BPSK. Under weak interference, similar to the case of strong interference, all the optimized codes offer significantly better performance compared to the off-the-shelf P2P codes. In addition, the optimized codes and the P2P codes beat the naive TS schemes for QPSK and Gaussian inputs. Furthermore, the performance of some of the optimized codes is shown to be superior to the non-naive TS results.

We also comment on the results of a recent paper [65] which designs LDPC codes for a symmetric GIC example with weak interference. Considering the method employed, the following distinctions are observed compared with our approach in this chapter. First, [65] adopts no superposition at the transmitters, i.e., messages of users are not split into distinct parts. Second, it exploits soft interference cancellation (SIC) wherein the adopted decoder *aims* to decode the interfering signal as well as the desired signal to reduce the effect of interference. Third, it employs density evolution on the factor graphs assuming the *no-interleaver-hypothesis* [1]. This assumption is only valid when identical degree distributions are utilized for both codes, and not applicable to the general case where degree distributions of messages are distinct.

4.6 Finite Block Length Code Simulations

4.6.1 Random Constructions

In this section, we evaluate the performance of the optimized degree distributions through finite block length code simulations. Parity check matrices are obtained with tools in [87] where most of the length-4 cycles are removed. For the symmetric scenarios, where identical degree distributions are employed at both transmitters, different realizations are utilized in the simulation. The code block lengths are picked as 50k and the maximum number of decoding iterations is set to 500. Fig. 4.11 shows the decoding results at receiver 1, where for clarity of the presentation we only show the results of the public message or the private message with the worst error rates (i.e., the bottleneck), instead of giving the results for all the messages. Considering a BER of 10^{-5} as reliable transmission, it can be observed that the decoding results for BPSK and QPSK scenarios are within 0.33 dB and 0.92 dB of the decoding thresholds computed earlier.

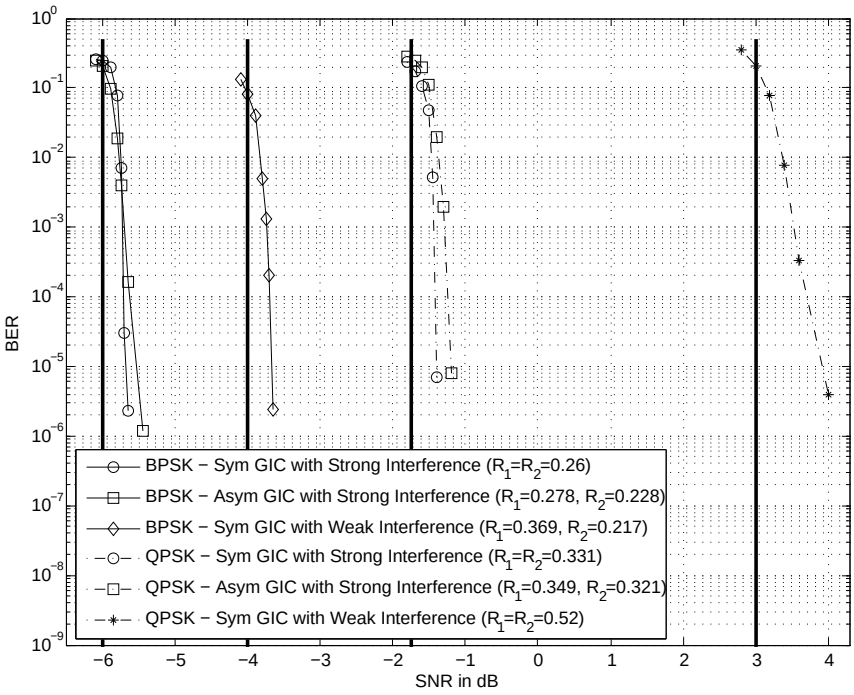

Figure 4.11: Finite Block Length Decoding Results for Specific LDPC Codes with Random Constructions

4.6.2 Algebraic Constructions

We observe that for random constructions the decoding behavior is close to the asymptotic results for large block lengths. However, in practice, LDPC codes with moderate block lengths ($\approx$ 1k) may also be adopted. In this case, a drawback of random designs is the presence of short cycles in the graph which may degrade the decoding performance and may lead to error floors for high SNRs. To remedy this problem, variants of structured LDPC codes have been proposed and studied in the literature [88], [89], where codes are optimized for different parameters, e.g., girth, stopping set, trapping set, minimum distance. Protograph LDPC codes are shown to perform well compared to the other approaches for P2P channels. As the name suggests, the design of these codes is based on a lifted graph from a so-called *base graph*. In [90], proto-

graph LDPC codes are optimized via algebraic designs utilizing *voltage graphs* and *non-abelian groups*, and superior performance is observed compared to the previous designs. In the following, we consider a GIC with strong interference and optimize the degree distributions using moderate code block lengths, by employing the systematic approach of [90].

For code optimization, we consider an asymmetric GIC with $SNR_1 = -1$ dB, $INR_1 = -0.25$ dB, $SNR_2 = -1.5$ dB, and $INR_2 = -0.75$ utilizing BPSK with real channel gains. We employ a base matrix with fixed dimensions of 3×5 for both messages. At each iteration, the degree distributions are perturbed by drawing the elements of the base matrix randomly from the set $\{0, 1\}$. Unlike the previous examples, since the dimension of the base matrix does not change throughout the optimization process, we opt for decreasing SNR_i and INR_i at each iteration keeping the signal to interference ratio fixed. The resulting optimized degree distributions $\lambda(x) = 0.3077x + 0.6923x^2$ and $\rho(x) = 0.6154x^3 + 0.3846x^4$ are admissible for the asymmetric GIC with channel parameters $SNR_1 = -2.15$ dB, $INR_1 = -1.4$ dB, $SNR_2 = -2.65$ dB, and $INR_2 = -1.9$ dB. We design the structured codes for block lengths $N = 1015$ and $N = 1525$ utilizing non-abelian groups. A non-abelian group of order $m = pq$ is characterized by (p, q, s) where q and p are prime numbers, q divides $p - 1$, and $s^q \equiv 1 \pmod{p}$. The non-abelian groups chosen for $N = 1015$ and $N = 1525$ are (29,7,7) and (61,5,9), respectively. Fig. 4.12 shows the decoding results for the resulting random and structured constructions. It is observed that for $N = 1015$, error floors occur at 10^{-4} and 4×10^{-5} for random constructions with girths 4 and 6, respectively. On the other hand, an error floor occurs around 10^{-6} for the structured code with girth 8. For $N = 1525$, error floors occur at around 2×10^{-6} for random constructions with girths 4 and 6, however, no error floor is observed for the structured code with girth 12 all the way down to 10^{-9} BER. We also considered the

performance of the employed structured codes as a function of the SNRs and INRs at BER 10^{-5} (considered as reliable transmission) and observed that the achieved rate pairs outperform the naive and non-naive TS region for $N = 1015$ and $N = 1525$, respectively.

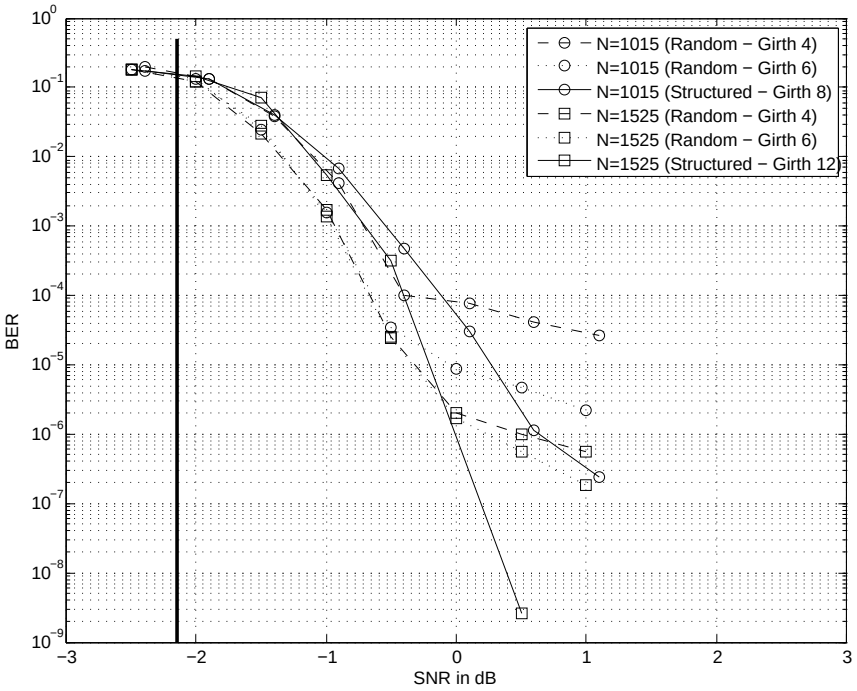

Figure 4.12: Decoding Results of Structured vs. Random Constructions

4.7 Chapter Summary

In this chapter, the Han-Kobayashi coding strategy was implemented for two-user Gaussian interference channels. Fixed channel gains were considered and finite constellations were employed for transmission. In order to analyze the behavior of the decoder, a symmetry property was proved for the exchanged LLRs under JD and the stability condition was derived for the degree distribution profiles of the private and public messages under strong and weak interference levels. A robust method was proposed for code optimization utilizing a random perturbation technique. Performance of the explicit and implementable LDPC codes (as opposed to information theoretic

random codes) were examined through numerous examples, and promising results were obtained for various scenarios, e.g., for cases of strong and weak interference, symmetric and asymmetric rates. Under strong interference, the capacity approaching codes were designed which beat even the non-naive TS rate region with Gaussian signaling. Under weak interference, it was observed that the optimized codes beat the naive TS region (with Gaussian signaling) and operate close to the non-naive TS region boundary. We also note that the designed codes improve consistently on the codes optimized for the P2P channels (used with the same encoding/decoding procedure). Furthermore, simulation results were provided using large block length codes picked from the designed LDPC code ensembles and code optimization was performed for moderate block lengths comparing the performance of structured versus randomized designs wherein the structured codes were shown to be superior to random designs at high SNRs.

Chapter 5

CODE DESIGN FOR FINITE INPUT FINITE OUTPUT INTERFERENCE CHANNELS

In this chapter, we explore the code design problem for the two-user discrete memoryless interference channel (DMIC), i.e., when the inputs and outputs of the channel are finite. Specifically, we consider Z interference channels (ZICs) for which one of the receivers is interference free. We employ irregular LDPC codes concatenated with non-linear trellis codes (NLTCs). Here the NLTCs are utilized to introduce a desired distribution of 0's and 1's in the transmitted codewords dictated by the information theoretic results. At the receiver sides, MAP decoders are employed for the NLTCs providing symbol-by-symbol LLRs to the iterative LDPC decoders. LDPC code optimization is performed for an example of a binary-input binary-output (BIBO) ZIC where the transmitted and the received signals are binary. Through some specific examples, it is observed that the optimized codes outperform single user codes used with TS. In attempt to validate the accuracy of the results, decoding performance of the specific codes picked from the optimized degree distributions are also computed for finite code block lengths.

The chapter is organized as follows. In Section 5.1, we briefly review some existing results for DMICs and describe the proposed framework for code optimization. In Section 5.2, the system model is described in detail. In Section 5.3, we detail the adopted encoding and decoding schemes. In Section 5.4, the HK inner bound for DMICs is revisited and simplified for the case of ZICs. In addition, a sum-capacity result developed in the recent literature is discussed. In Section 5.5, we elaborate on the code optimization procedure. Section 5.6 studies specific examples and reports

Part of this work was presented at IEEE ISIT 2015 [91].

on the achieved rate pairs obtained via the optimized degree distributions as well as finite code block length simulation results. Finally, we provide a summary of the chapter in Section 5.7.

5.1 Introduction

In Chapter 4, we examined LDPC code design principals for the two-user GIC wherein inputs and outputs of the channel can take complex values in general and Gaussian noise samples are added at the receiver sides. In this chapter, we focus on the two-user DMIC first explored in [27]. To highlight some important results on these channels, the capacity region of the DMIC is characterized when the interference is strong enough to be decoded at the receivers [92]. The capacity region is also computed for a class of deterministic ICs [93]. Authors in [94] utilize existing results for the degraded IC [95] and derive a sum capacity for the ZIC with one-sided weak interference satisfying a certain Markov chain condition. It is shown that the sum-capacity is achieved by only decoding the desired messages while treating the interference as noise.

In this chapter, we investigate the problem of practical code design for the two-user BIBO DMIC utilizing the HK strategy. In particular, we consider an example of two-user ZIC wherein the messages of the transmitters are sent as private. Motivated by their excellent performance, we employ irregular LDPC codes to encode the messages of each user. Since LDPC codes belong to a class of linear block codes, the distribution of the encoded bits is uniform which may not be the optimal distribution for use over ICs as the information theoretic results suggest. To address this issue, the output bits of each LDPC encoder are input to an NLTC encoder to introduce a desired distribution in the transmitted signal. At the receiver side, we implement a BCJR algorithm based decoder providing soft information for each of

the LDPC encoded symbols, computed in terms of LLRs. The obtained LLRs are fed to an LDPC decoder whose outputs are fed back to the BCJR decoder to improve the decoding performance.

The code optimization performed in this chapter consists of two steps. First, the NLTCs are designed to satisfy the required (optimal) distribution on the channel inputs. Then, the LDPC codes are optimized keeping the designed NLTCs unchanged. Optimization is carried out explicitly for an example of ZIC where the designed codes are shown to outperform the single user codes used with TS. In addition, it is demonstrated that some of the achieved rate pairs are not attainable by means of only LDPC codes indicating the advantage of adopting NLTCs. We also perform simulations with finite block length codes picked from the ensemble of optimized codes and demonstrate that the resulting BER estimates confirm the computed decoding thresholds.

5.2 System Model

Fig. 5.1 depicts the two-user DMIC comprising of two sender-receiver pairs communicating through a shared medium. The channel is characterized by input sets $(\mathcal{X}_1 \times \mathcal{X}_2)$, output sets $(\mathcal{Y}_1 \times \mathcal{Y}_2)$, which are finite, and the channel transition probability written as

$$p(y_1^n y_2^n | x_1^n x_2^n) = \prod_{i=1}^{n} p(y_{1_i} y_{2_i} | x_{1_i} x_{2_i}), \tag{5.1}$$

for n channel uses. A DMIC is under very strong interference if

$$\begin{aligned} I(X_1; Y_1|X_2) \leq & I(X_1; Y_2), \\ I(X_2; Y_2|X_1) \leq & I(X_2; Y_1), \end{aligned} \tag{5.2}$$

for all product distributions of the form $p_{X_1}(x_1)p_{X_2}(x_2)$ [4]. Similarly, a DMIC is said to have strong interference if

$$\begin{aligned} I(X_1;Y_1|X_2) \leq & I(X_1;Y_2|X_2), \\ I(X_2;Y_2|X_1) \leq & I(X_2;Y_1|X_1), \end{aligned} \tag{5.3}$$

for all product distributions of the form $p(x_1)p(x_2)$ [4]. From an information theoretic

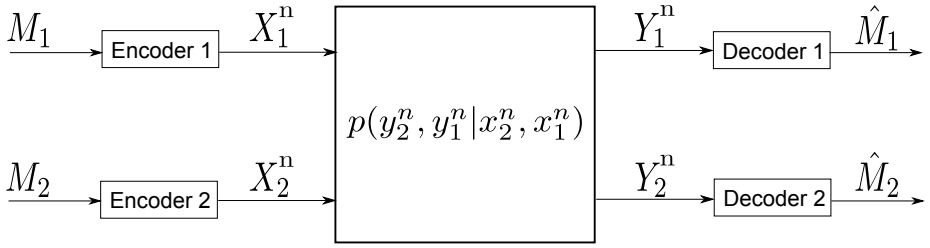

Figure 5.1: Block Diagram of the Two-User DMIC

point of view, an $\left(n, M_1, M_2, P_{e1}^{(n)}, P_{e2}^{(n)}\right)$ code for a DMIC comprises of two message sets $\mathcal{M}_1 = \{1, 2, \ldots, 2^{nR_1}\}$ and $\mathcal{M}_2 = \{1, 2, \ldots, 2^{nR_2}\}$ for transmitters 1 and 2, respectively, with encoding functions $f_1 : \mathcal{M}_1 \to \mathcal{X}_1^n, \quad f_2 : \mathcal{M}_2 \to \mathcal{X}_2^n$ and decoding functions $g_1 : \mathcal{Y}_1^n \to \mathcal{M}_1, \quad g_2 : \mathcal{Y}_2^n \to \mathcal{M}_2$. The average probabilities of error are defined as

$$\begin{aligned} P_{e_1}^{(n)} &= \frac{1}{|\mathcal{M}_1||\mathcal{M}_2|} \sum_{m_1=1}^{2^{nR_1}} \sum_{m_2=1}^{2^{nR_2}} Pr\{g_1(Y_1^n) \neq m_1 | M_1 = m_1, M_2 = m_2\}, \\ P_{e_2}^{(n)} &= \frac{1}{|\mathcal{M}_1||\mathcal{M}_2|} \sum_{m_1=1}^{2^{nR_1}} \sum_{m_2=1}^{2^{nR_2}} Pr\{g_2(Y_2^n) \neq m_2 | M_1 = m_1, M_2 = m_2\}, \end{aligned} \tag{5.4}$$

where $P_{e_1}^{(n)}$ and $P_{e_2}^{(n)}$ are the average error probabilities at receiver 1 and 2, respectively. A rate pair (R_1, R_2) is said to be achievable if $P_{e1}^{(n)}, \ P_{e2}^{(n)} \ \to \ 0$ as $n \to \infty$. The capacity region is the closure of the all achievable rate pairs.

5.3 Proposed Encoding and Decoding Schemes

We consider the simple scheme of transmitting the messages as private where each receiver decodes only its own desired message. Later in the chapter, we discuss

the information theoretic bounds for the considered scheme. Block diagram of the transmitter i is depicted in Fig. 5.2, $i = 1, 2$. At transmitter i each set of k information bits, denoted by U_i^k, are encoded with an irregular LDPC code with rate $\frac{k}{m}$. The encoded bits, represented as C_i^m, are then input to an NLTC (Fig. 5.3) with code rate $\frac{m}{n}$ to introduce the desired distribution of 0's and 1's in the transmitted codeword X_i^n. As a result, the effective code rate of the proposed transmission scheme is $R = \frac{k}{n}$.

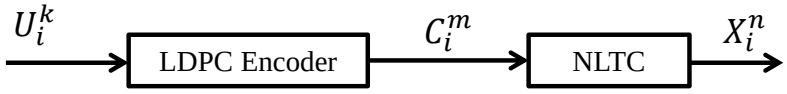

Figure 5.2: Block Diagram of the Transmitter i Implementing HK Strategy

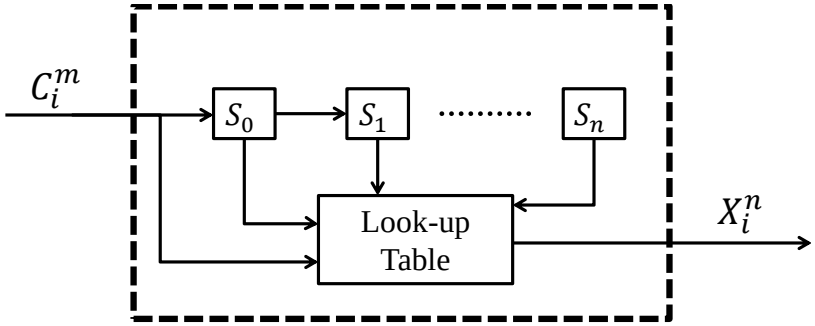

Figure 5.3: Structure of an NLTC

At the receiver sides, the received binary digits are passed through a BCJR algorithm based decoder followed by an LDPC (single user) decoder. The BCJR decoder at receiver i computes the LLRs of the encoded LDPC codes of message i. Having implemented the log-APP algorithm [96], the LLR of the jth LDPC encoded

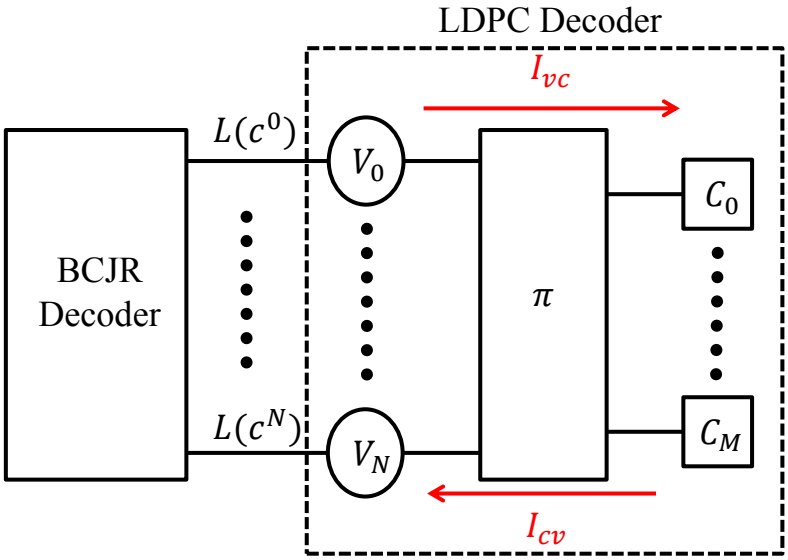

(a) Illustration of the Interaction Between the BCJR Decoder and the LDPC Decoder

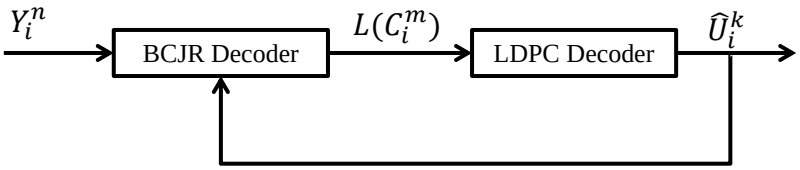

(b) Feedback from the BCJR Decoder to the LDPC Decoder.

Figure 5.4: Block Diagram of the Receiver i

bit of user i is computed as

$$L(c_i^j) = \ln\left(\sum_{(\sigma_{j-1},\sigma_j)\in S_0} \exp\left(\tilde{\alpha}_{j-1}(\sigma_{j-1}) + \tilde{\gamma}_i(\sigma_{j-1},\sigma_j) + \tilde{\beta}_j(\sigma_j)\right)\right) - \ln\left(\sum_{(\sigma_{j-1},\sigma_j)\in S_1} \exp\left(\tilde{\alpha}_{j-1}(\sigma_{j-1}) + \tilde{\gamma}_j(\sigma_{j-1},\sigma_j) + \tilde{\beta}_j(\sigma_j)\right)\right), \tag{5.5}$$

where

$$\tilde{\gamma}_j(\sigma_{j-1},\sigma_j) = \ln\left(p(c_i^j)p(y_i^j|c_i^j)\right), \tag{5.6}$$

and σ_l denotes the state of the trellis diagram at stage l for the NLTC adopted for user i. S_k represents the subset of transitions in the trellis diagram corresponding to $c_i^j = k$. The backward recursion $\left(\tilde{\beta}_j(\sigma_j)\right)$ and forward recursion $\left(\tilde{\alpha}_j(\sigma_j)\right)$ variables

are calculated as

$$\tilde{\alpha}_j(\sigma_j) = \ln\left(\sum_{\sigma_{j-1}\in\sum} \exp\left(\tilde{\alpha}_{j-1}(\sigma_{j-1}) + \tilde{\gamma_j}(\sigma_{j-1},\sigma_j)\right)\right),$$
$$\tilde{\beta}_{j-1}(\sigma_{j-1}) = \ln\left(\sum_{\sigma_j\in\sum} \exp\left(\tilde{\beta}_j(\sigma_j) + \tilde{\gamma_j}(\sigma_{j-1},\sigma_j)\right)\right), \tag{5.7}$$

where

$$\tilde{\alpha}_0(\sigma_0) = \begin{cases} 0 & \sigma_0 = 0 \\ -\infty & \sigma_0 \neq 0 \end{cases}, \quad \tilde{\beta}_N(\sigma_N) = \begin{cases} 0 & \sigma_N = 0 \\ -\infty & \sigma_N \neq 0 \end{cases}, \tag{5.8}$$

with $\sum$ and N denoting the set of all states and the last stage of the trellis diagram, respectively. The computed LLRs are provided to the LDPC single user decoder (Fig. 5.4 (a)). The soft output of the LDPC decoder can be converted to the probability domain through $P\big(c_i^j = l\big) = \frac{\exp\left((-1)^l L\right)}{1+\exp\left((-1)^l L\right)}$ which can be exploited to update the gamma function in (5.6) for further improvement of the decoding. As a consequence, we opt for utilizing the output of the LDPC decoder as an input to the BCJR decoder in an iterative fashion improving the overall performance (Fig. 5.4 (b)).

5.4 Review of Some Relevant Information Theoretic Results

5.4.1 The HK Inner Bound

Capacity region of the DMIC is unknown in general, and it is only characterized for a few special cases; for instance, when the interference is very strong [27], strong [4] and when the channel is degraded [97]. The best achievable rate region to date is due to Han and Kobayashi [30] characterized by

$$R_1 < I(X_1; Y_1|W_2, Q)$$
$$R_2 < I(X_2; Y_2|W_1, Q)$$
$$R_1 + R_2 < I(X_1, W_2; Y_1|Q) + I(X_2; Y_2|W_1, W_2, Q)$$

$$
\begin{aligned}
R_1 + R_2 &< I(X_2, W_1; Y_2|Q) + I(X_1; Y_1|W_1, W_2, Q) \\
R_1 + R_2 &< I(X_1, W_2; Y_1|W_1, Q) + I(X_2, W_1; Y_2|W_2, Q) \\
2R_1 + R_2 &< I(X_1, W_2; Y_1|Q) + I(X_1; Y_1|W_1, W_2, Q) + I(X_2, W_1; Y_2|W_2, Q) \\
R_1 + 2R_2 &< I(X_2, W_1; Y_2|Q) + I(X_2; Y_2|W_1, W_2, Q) + I(X_1, W_2; Y_1|W_1, Q) \qquad (5.9)
\end{aligned}
$$

for some PMF $p(q)p(w_1, x_1|q)p(w_2, x_2|q)$, where $|\mathcal{W}_1| \leq |\mathcal{X}_1| + 4$, $|\mathcal{W}_2| \leq |\mathcal{X}_2| + 4$, and $|Q| \leq 6$. In these expressions, W_i carries the public message information of user i, however, it does not represent any of the channel variables. The complete characterization of the bound requires extensive computations primarily due to the cardinality of the involved variables. Therefore, later in the chapter we attempt to compute a sub-region of the HK inner bound (HK-IB).

5.4.2 The DMIC with One-Sided Interference

Authors in [94] define DMIC with one-sided interference as a DMIC satisfying

$$p(y_2|x_1x_2) = p(y_2|x_2), \qquad (5.10)$$

for all input distribution $p(x_1)p(x_2)$. The considered channel is also referred to as a DM-ZIC. Fig. 5.5 illustrates an example of a two-user DM-ZIC wherein the receiver 2 does not experience interference from user 1, hence (5.10) is satisfied. Considering the HK strategy, transmitter 1's signal does not affect the received signal at receiver 2, hence, its message can be sent as private. This is equivalent to setting $W_1 = \emptyset$ simplifying the HK-IB to

$$
\begin{aligned}
R_1 &< I(X_1; Y_1|W_2, Q) \\
R_2 &< I(X_2; Y_2|Q) \\
R_1 + R_2 &< I(X_1, W_2; Y_1|Q) + I(X_2; Y_2|W_2, Q). \qquad (5.11)
\end{aligned}
$$

for some PMF $p(q)p(x_1|q)p(w_2, x_2|q)$, where $|\mathcal{W}_2| \leq |\mathcal{X}_2| + 3$, and $|Q| \leq 5$.

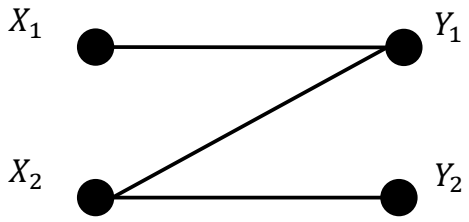

Figure 5.5: A Two-User DM-ZIC

5.4.3 Sum-Capacity of a DM-ZIC with Weak Interference

Authors in [94] declare a two-user DM-ZIC to have a weak interference if the Markov chain $X_2 - X_1Y_2 - Y_1$ holds. They compute the sum-capacity of such a channel as

$$C_{sum} = \max_{p(x_1)p(x_2)} \big\{ I(X_1;Y_1) + I(X_2;Y_2) \big\}, \tag{5.12}$$

which is achieved by treating the interfering signal as noise. This translates into sending the messages of both users as private, or equivalently $W_1 = W_2 = \emptyset$. It is still unknown if the introduced Markov chain is a necessary condition for (5.12) to hold. Parallel to the strong interference condition (5.3), another metric is introduced in [94] for the weak interference as

$$I(X_2;Y_1|X_1) \leq I(X_2;Y_2), \tag{5.13}$$

for all product input distribution on $p(x_1)p(x_2)$.

5.5 LDPC and NLTC Optimization for DM-ZIC

The code optimization is comprised of designing NLTCs and optimizing the LDPC degree distributions. To design an NLTC, the n output bits assigned to trellis branches are chosen to maximize the Hamming distance between the branches. The assignment should also satisfy the distribution of the 0's and 1's obtained through maximizing the achievable sum-rate performed via an exhaustive search over different distribution of 0's and 1's for the transmitted codewords of both users. Fig. 5.6 illustrates an example

of NLTC design for the given probability of $P_X(1) = 0.1875$, where $P_X(1)$ denotes the probability of X being 1.

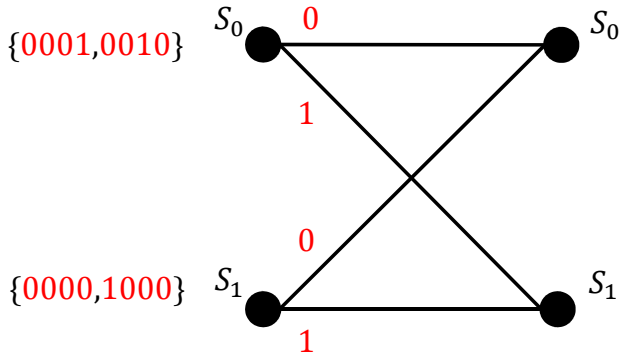

Figure 5.6: An Example of NLTC

LDPC code optimization follows similar steps as in the previous chapters. That is, at each iteration, degree distributions are perturbed and checked if they are admissible verified by tracking the evolution of the mutual information associated with the exchanged LLRs. Considering the all-zero codeword transmission assumption [41], the computation of the mutual information can be performed as [82]

$$\begin{aligned} I(C;L) &\overset{(a)}{=} 1 - E\Big\{ \log_2\left(1+e^{-L}\right)\Big\} \\ &\overset{(b)}{\approx} 1 - \frac{1}{N}\sum_{i=1}^{N} \log_2\left(1+e^{-L_n}\right), \end{aligned} \tag{5.14}$$

where N is the number of encoded bits and L_n denotes the LLR corresponding to the nth coded bit of the all-zero codeword. In (5.14), (a) follows from the all-zero codeword transmission assumption and the symmetry property of the LLRs, and (b) is obtained by invoking the ergodicity of the LLRs. In order to exploit (5.14) for our setup, we adopt channel adapters [80] to enforce the channel symmetry, which is required for the all-zero codeword transmission assumption. Since it is difficult to validate the symmetry property of the LLRs delivered by the BCJR decoder, we treat (5.14) as approximation.

We declare the perturbed degree distribution admissible if the mutual information exceeds 0.995. Note that the LDPC code optimization is performed after we design the NLTC, therefore, the designed NLTCs are kept unchanged throughout the LDPC code optimization.

5.6 Code Design Example

As a specific example, we consider a BIBO ZIC defined as[1]

$$\begin{aligned} Y_1 &= (X_1 \otimes X_2) \oplus Z_1, \\ Y_2 &= X_2 \oplus Z_2, \end{aligned} \tag{5.15}$$

where $\oplus$ and $\otimes$ represent the "XOR" function and the "OR" function. Z_1 and Z_2 are noise samples at receiver 1 and 2 drawn from the Bernoulli distribution with parameters ϵ_1 and ϵ_2. To simplify the computation of the HK inner bound characterized via (5.11), we consider $W_2 = \emptyset$, and assume that no TS (Q) is utilized. This leads to a sub-region of the complete HK-IB of the IC. Fig. 5.7 illustrates the TS line along with the sub-region of the HK-IB computed for the parameters $\epsilon_1 = 0.21$ and $\epsilon_1 = 0.25$.

Details of the designed codes are shown in Table 5.1 wherein each row shows the output bits correspond to the input bit u for the current state S. For each input of the NLTC, y_1, y_2, and y_3 represent the output of the NLTCs for $P_{X_1}(1) = 0.5$ and the transmitter 2 for $P_{X_2}(1) = 0.1875$ and $P_{X_2}(1) = 0.25$, respectively. The constraint length and the number of output bits are 1 and 4, respectively, that is, at each stage of the trellis diagram a 1 bit input determines 4 bit outputs. Fig. 5.6 illustrates one of the designed codes. The degree distribution of the optimized LDPC codes are shown in Table 5.2.

[1]The considered example neither satisfy the Markov chain X_2 – X_1Y_2 – Y_1 nor the condition (5.13) for all product distribution of inputs; therefore, it is not an instance of a weak interference channel. Unfortunately, the example is declared a weak interference channel in [91] by considering a sub-region of all possible values of $p_{X_1} \cdot p_{X_2}$.

Table 5.1: Details of the Employed NLTCs

S	u	y_1	y_2	y_3
0	0	1010	0001	1000
0	1	0101	0010	0100
1	0	0011	0000	0010
1	1	1100	1000	0001

Table 5.2: Degree Distributions of the Optimized Codes

$p_{X_1}(1)$, $p_{X_2}(1)$		R	d_c	λ_2	λ_3	λ_4	λ_9	λ_{10}	λ_{19}	λ_{20}	λ_{49}	λ_{50}
$0.5, 0.1875$	U_1	0.547	9	0.2364	0.2810	0.0281	0.0947	0.0452	0.1118	0.0433	0.1342	0.0253
	U_2	0.379	6	0.2989	0.2294	0.0661	0.0521	0.1094	0.1161	0.0195	0.0759	0.0326
$0.5, 0.25$	U_1	0.481	7	0.3245	0.1942	0.0883	0.0896	0.0860	0.0127	0.0894	0.1032	0.0121
	U_2	0.476	7	0.3077	0.1735	0.1522	0.0926	0.0417	0.0556	0.0673	0.0347	0.0747
$0.5, 0.5$	U_1	0.058	3	0.4852	0.2330	0.0733	0.0167	0.0785	0.0685	0.0335	0.0092	0.0019
	U_2	0.161	4	0.3537	0.2239	0.0891	0.0578	0.1118	0.0330	0.0761	0.0395	0.0151

Fig. 5.7 demonstrates the achieved rate pairs employing the designed NLTCs and LDPC codes[2]. To achieve the two middle rate pairs, we utilize NLTCs because the distribution of X_2 is not uniform. For the other two points, however, the distribution of the 0's and the 1's for the transmitted codewords are uniform, therefore, we only employ LDPC codes. Note that for $P_{X_2}(1) = 0$, transmitter 2 does not practically participate in the transmission and the channel is essentially a P2P channel. It is also worth mentioning that the two achieved middle points are located outside the rate region achieved via uniform distribution. This implies that one cannot achieve these points by means of only LDPC codes highlighting the advantage of proposed approach for code design.

We also estimate the performance of the specific codes with finite block length picked from optimized degree distributions via simulations. To measure the decoding performance, we introduce α as $\frac{0.21}{\epsilon_1}$ where $\frac{\epsilon_1}{\epsilon_2}$ is kept fixed for different values of ϵ_1. Fig. 5.8 shows the decoding results for the code block length 10k. Considering a BER of 10^4 as reliable transmission, the decoding thresholds of the optimized codes

[2]The outer-bound (10) provided in [91] is unfortunately incorrect. In fact, the considered example in the paper does not conform the Markov chain property, hence, the sum-capacity result, used as the third inequality in the outer-bound, does not necessarily hold.

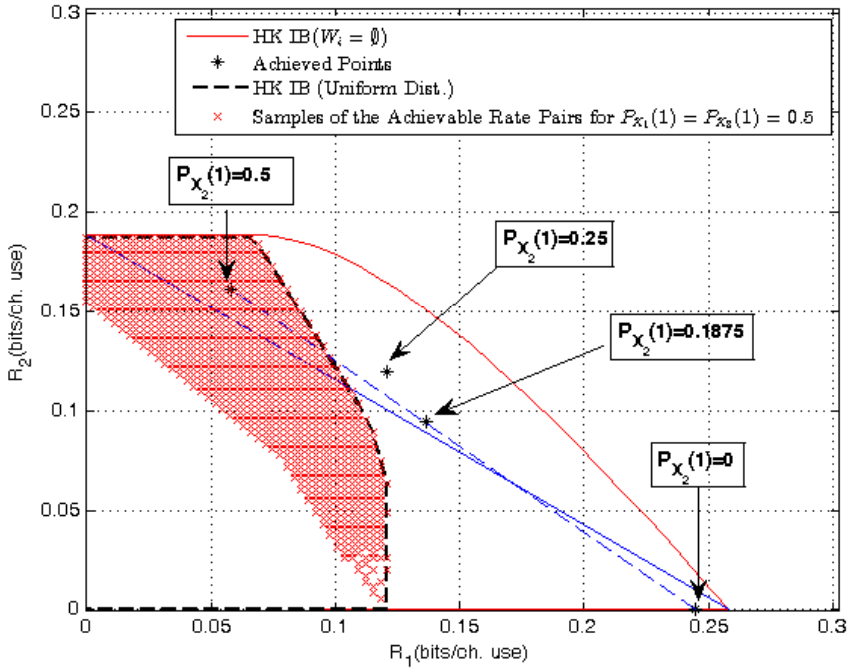

Figure 5.7: Achievable Rate Regions and Achievable Points for the Considered Example

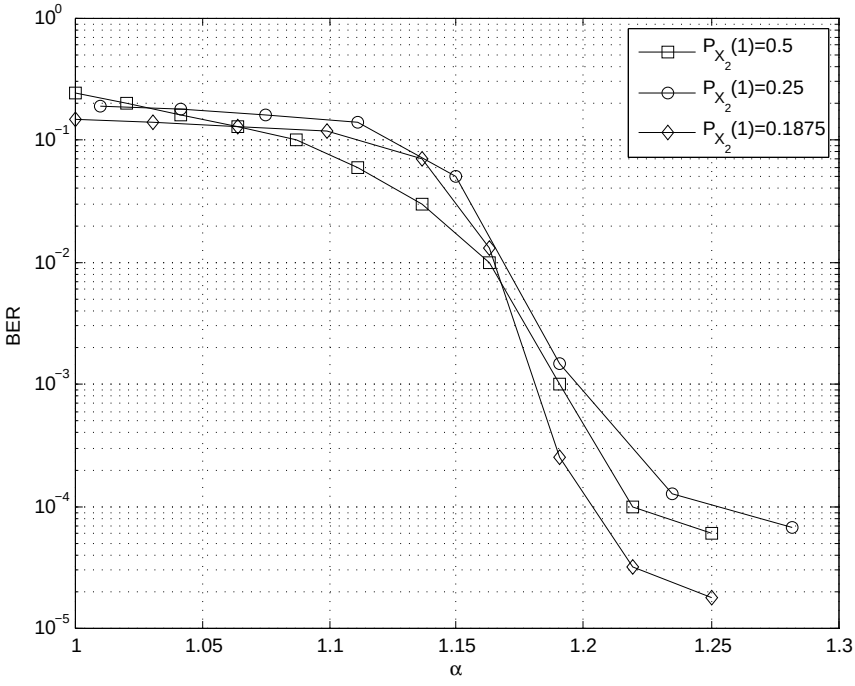

Figure 5.8: Decoding Results for the Optimized Degree Distributions

corresponding to $P_{X_2}(1) = 0.1875$, $P_{X_2}(1) = 0.25$, $P_{X_2}(1) = 0.5$ are observed at $\alpha = 1.2$, $\alpha = 1.25$, and $\alpha = 1.22$, respectively, for the considered code block length.

5.7 Chapter Summary

In this chapter, we focused on code design for the two-user DMIC. In particular, irregular LDPC codes concatenated with NLTCs are employed for transmission, and a BCJR algorithm based decoder interacting with an LDPC single user decoder is used at the receiver sides. Specifically, we considered the two-user BIBO ZIC, where one receiver is interference free. We designed NLTCs based on the optimal distribution obtained by maximizing the sum-rate computed for the HK sub-region. It is observed that optimized codes achieve rate pairs exceeding the TS line implying that the optimize codes offer better performance than the single user codes. In addition, it is shown that some of achieved points in the rate region cannot be obtained by means of employing only LDPC codes highlighting the benefits of employing NLTCs along with irregular LDPC codes in this interference channel scenario.

Chapter 6

DESIGN OF SHORT BLOCK LENGTH CODES FOR INTERFERENCE CHANNELS

In the previous chapters, we have studied LDPC code design for different multi-user channel models with specific emphasis on ICs. We explored different methods of code optimization; however, the main underlying assumption of these methods was the independence of the exchanged LLRs within the decoder which is only valid for a code with a cycle-free bipartite graph corresponding to an infinite block length code. The cycle-free assumption is justified by focusing on codes with large block lengths for which the behavior of the code concentrates around the asymptotic thresholds. However, codes with large block lengths impose extensive delays in the transmission, hence, they are not suitable for delay constrained communications. With this motivation, we now turn our attention to short block length codes for use over ICs in this chapter.

Recently, short block length codes have been designed for two-user GMACs employing trellis-based approaches [98]. Trellis-based codes have been successfully employed for P2P channels and they can achieve superior performance in space-time coding scenarios particularly for quasi-static fading channels. It is also possible to implement optimal decoders for such codes even in certain multi-user setups, and compute performance bounds in an efficient manner. Here, we consider two-user GICs employing trellis-based codes and derive error-rate bounds in order to design optimal codes with short block lengths and study their performance via some examples.

The chapter is organized as follows. In Section 6.1, we revisit the system model for a two-user GIC. In Section 6.2, we review existing performance bounds developed for two-user GMACs and two-user GBCs. In Section 6.3, we utilize the bounds

derived for GMACs from the exisiting literature towards developing a framework for designing trellis-based codes for two-user GICs under strong interference, and present specific design examples. In Section 6.4, we turn our attention to the case of weak interference levels and exploit the bounds developed for two-user GBCs to design codes for this scenario. In Section 6.5, we extend our findings to the case of mixed interference and provide several code design examples. Finally, in Section 6.6, we summarize our contributions and conclude the chapter.

6.1 System Model

Fig. 6.1 illustrates the block diagram of a two-user GIC. Considering receiver i, the n-length received signal vectors can be written as

$$\mathbf{y}_i = \alpha_i \mathbf{c} + \mathbf{z}_i, \quad i = 1, 2, \tag{6.1}$$

where $\mathbf{c}$ denotes the BPSK modulated transmitted codeword matrix as follows

$$\begin{bmatrix} \mathbf{c}^1 \\ \mathbf{c}^2 \end{bmatrix} = \begin{bmatrix} c_1^1 \; c_2^1 \; \dots \; c_n^1 \\ c_1^2 \; c_2^2 \; \dots \; c_n^2 \end{bmatrix}, \tag{6.2}$$

with $\mathbf{c}^1$ and $\mathbf{c}^2$ representing the codewords employed at transmitter 1 and transmitter 2, respectively. The channel gains from the transmitters to the receiver i are denoted as $\alpha_i = [\alpha_{1i} \; \alpha_{2i}]$, where α_{ji} is a real number denoting the gain of the channel from the transmitter j to the receiver i. Note that for a more realistic channel model α_{ji} can be taken as complex but we consider real values for the simplicity of the analysis. The i.i.d. zero mean Gaussian noise samples with variance $\frac{N_0}{2}$ at receiver i are represented by the vector $\mathbf{z}_i$ of length n. As in Chapter 4, the SNR and INR at receiver i are defined as

$$SNR_i = \frac{\alpha_{ii}^2 P_i}{N_0}, \quad INR_i = \frac{\alpha_{ji}^2 P_j}{N_0}, \tag{6.3}$$

where $i, j = 1, 2$, and P_i is the average power of the transmitted codeword bits at the transmitter i. Based on the interference and signal levels, the interference can

be categorized as strong (if $INR_i > SNR_j$), weak (if $SNR_i > INR_j$), or mixed (if $INR_i > SNR_j,\ INR_j < SNR_i$) with $i \neq j$.

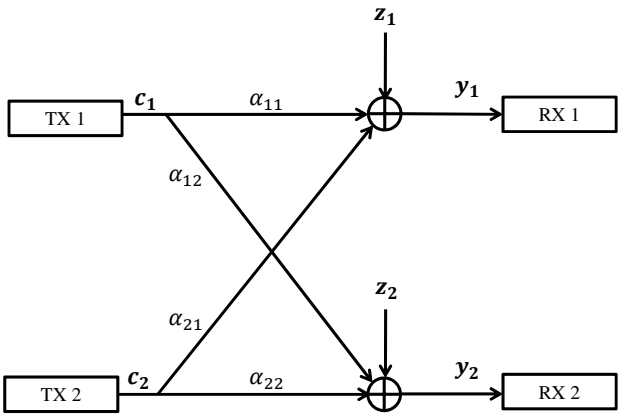

Figure 6.1: Block Diagram of a Two-User GIC

6.2 Error-Rate Bounds for GMACs and GBCs

Authors in [98] studied short block length trellis-based code designs for two-user Gaussian MACs where they derive error rate bounds computed approximately used in the optimization process. Authors in [99] considered two-user GBCs and developed an upper bound on the performance of the successive interference cancellation employed at the better receiver to decode the messages in two stages. In the following we review these two bounds. These techniques will then be utilized to derive performance bounds for the two-user GIC for our short block length code design problem.

6.2.1 Error-Rate Bounds for Two-User GMACs

A two-user GMAC is formed by considering one receiver and two transmitters where the transmitters separately encode their messages. The n-length received signal vector is expressed as

$$\mathbf{y} = \alpha\mathbf{c} + \mathbf{z}, \tag{6.4}$$

following the definitions in the previous section. To compute the performance bound, pairwise error probability can be utilized, which is defined as the two-codeword error

probability, i.e., probability that the received signal is closer to $\hat{\mathbf{c}}$ given that $\mathbf{c}$ is transmitted. A maximum likelihood decoder at the receiver sides decides according to the Euclidean distance between codewords, therefore, the pairwise error probability is computed as

$$P\Big(\mathbf{c} \to \hat{\mathbf{c}} \big| \mathbf{c} \text{ is transmitted}\Big) = Q\left(\sqrt{\frac{Ed^2(\mathbf{c}, \hat{\mathbf{c}})}{2N_0}}\right), \tag{6.5}$$

where Q-function is the tail probability of the standard normal distribution defined as

$$Q(x) = \frac{1}{\sqrt{2\pi}} \int_x^\infty \exp\left(-\frac{t^2}{2}\right) dt, \tag{6.6}$$

and $Ed^2(.,.)$ is the squared Euclidean distance computed as

$$Ed^2(\mathbf{c}, \hat{\mathbf{c}}) = \alpha \mathbf{D}_{\mathbf{c},\hat{\mathbf{c}}} \alpha^\dagger, \tag{6.7}$$

where $\dagger$ denotes the transpose and $\mathbf{D}_{\mathbf{c},\hat{\mathbf{c}}}$ represents the codeword difference matrix, given by

$$\mathbf{D}_{\mathbf{c},\hat{\mathbf{c}}} = (\mathbf{c} - \hat{\mathbf{c}})(\mathbf{c} - \hat{\mathbf{c}})^\dagger. \tag{6.8}$$

Considering the union bound, the frame error probability is upper-bounded as

$$P_f \leq \frac{1}{|\mathcal{C}|} \sum_{\mathbf{c}} \sum_{\hat{\mathbf{c}} \neq \mathbf{c}} P\Big(\mathbf{c} \to \hat{\mathbf{c}} \big| \mathbf{c} \text{ is transmitted}\Big). \tag{6.9}$$

One main difficulty in computing (6.9) is the complexity of enumeration of the multiplicities of the codeword difference matrix $\mathbf{D}_{\mathbf{c},\hat{\mathbf{c}}}$ for all possible correct-erroneous codeword pairs. On the other hand, for certain cases such as convolutional codes this matrix can be computed efficiently and in a systematic manner. In the following, we describe the approach developed in [98] to count the multiplicities of different $\mathbf{D}_{\mathbf{c},\hat{\mathbf{c}}}$ for use in the bound computations.

Consider a two-user joint trellis diagram with states labeled as (s_1, s_2) with s_i representing the state of the trellis for the code of ith user. The joint trellis has $n_{s_1} \times$

n_{s_2} states with n_{s_i} denoting the number of states for the ith user's code. To track all possible codeword pairs $(\mathbf{c}, \hat{\mathbf{c}})$, a product state trellis diagram with states $(s_1, s_2, \hat{s}_1, \hat{s}_2)$ is formed wherein s_i and $\hat{s}_i$ represent the states of the trellises corresponding to the codes $\mathbf{c}^i$ and $\hat{\mathbf{c}}^i$, respectively. To count the multiplicities, a state transition matrix $S_{1,2}$ is assigned to the product state trellis whose element in the kth row and the lth column is expressed as

$$[S_{1,2}]_{k,l} = D_{11}^{q_{11}^{k,l}} \times D_{12}^{q_{12}^{k,l}} \times D_{22}^{q_{22}^{k,l}} \tag{6.10}$$

where D_{11}, D_{12}, D_{22} are dummy variables used to list the multiplicities of the different types of errors between two pairs of codewords [100]. The exponent $q_{i,j}^{k,l}$ is used to compute the contribution of the transition from state k to state l to the ith row and jth column entry of the $\mathbf{D}_{\mathbf{c},\hat{\mathbf{c}}}$. Note that $[\mathbf{D}_{\mathbf{c},\hat{\mathbf{c}}}]_{1,2} = [\mathbf{D}_{\mathbf{c},\hat{\mathbf{c}}}]_{2,1}^{\dagger}$, therefore the codeword difference matrix can be characterized by keeping track of the multiplicities $q_{1,1}^{k,l}$, $q_{1,2}^{k,l}$, and $q_{2,2}^{k,l}$ of dummy variables D_{11}, D_{12}, and D_{22}, respectively.

The union bound can be tightened by considering only simple error events defined as errors associated with the paths that merge only once with the correct path in the trellis diagram. To efficiently count the simple error events, an expurgation technique (given in [100]) is adopted. The technique is nothing but introducing an error state in the product state trellis. The transition to the error state occurs only from states corresponding to the paths for which $\mathbf{c} \neq \hat{\mathbf{c}}$. Also, the only possible transition from this state is to itself. Considering L stages of the joint trellis state transition[1], the complete list of possible $\mathbf{D}_{\mathbf{c},\hat{\mathbf{c}}}$ for the transmitted codewords is obtained via calculating the Lth power of $S_{1,2}$. Taking the trellis termination into account, the final stages of state transition matrix considered in the computation is modified accordingly.

[1]This corresponds to $m.L$ number of input bits for m bits assigned to each branch of a stage in the joint trellis state transition.

Despite the simplicity of the approach, the exact calculation of the bound through this method has high computational cost therefore it is not directly suitable for code design. Authors in [98] simplify the code design process by considering a shorter frame length than the intended design length. This is motivated by the fact that the decoding performance of the convolutional codes does not change significantly by considering a traceback length of four to five times of the constraint length of the code [101, Ch. 4]. In other words, even though the computed bounds would differ for different codeword lengths, the performance of the codes can be ordered based on their performance computed for a sufficiently large (but relatively small) length code which is manageable.

Another simplification is performed in an attempt to cope with the memory limitation where the number of terms for each entry of $S_{1,2}$ is restricted to those components (q_{ij}) with magnitudes less than a specific threshold. Although this greatly helps with the computation, the final computations based on this truncation approach should be considered as approximations rather than being true upper-bounds.

6.2.2 Error-Rate Bound for Two-User GBCs

A two-user GBC is formed by one transmitter and two receivers. The transmitted signal can be obtained by superimposing the messages intended for each receiver, which can be performed through a simple addition (assuming that superposition coding is used). That is, with $\mathbf{c}^i$ denoting the encoded message intended for receiver i, $i = 1, 2$, the n-length symbols received at receiver 1 can be written as

$$\mathbf{y}_1 = \sqrt{P_1}\mathbf{c}^1 + \sqrt{P_2}\mathbf{c}^2 + \mathbf{z}, \tag{6.11}$$

where P_i represents the average power of the received signals of message i.

The two-user GBC is a degraded BC, hence the better receiver can decode both messages. Without loss of generality, we assume that receiver 1 is the better

receiver utilizing a successive interference cancellation. To simplify the analysis the minimum-distance criterion is employed to decode the messages in [99], that is,

$$\hat{\mathbf{c}}^1 = \arg\min_{\tilde{\mathbf{c}}^1} \left\| \mathbf{y}_1 - \sqrt{P_1}\tilde{\mathbf{c}}^1 \right\|^2, \tag{6.12}$$

where $\tilde{\mathbf{c}}^1$ is the decoded codeword. Note that the employed decoding is not an instance of ML decoding which is used for the GMAC. In fact, we obtain a similar bound to the case of GMAC if the ML decoding is utilized, however, we adopt the minimum-distance criterion to simplify the analysis providing an upper bound on the performance of the ML decoding. The performance of the employed decoder becomes close to that of the ML decoder as the difference between the powers of the transmitted codewords increases.

For the transmitted codeword pair $\mathbf{c}$, the pairwise error probability at receiver 1 is defined as the probability that the received signal is closer to a different codeword $\hat{\mathbf{c}}^1$ than the transmitted codeword $\mathbf{c}^1$. Therefore, the frame error probability for the first stage of the decoding can be upper-bounded as

$$P_f \leq \frac{1}{|\mathcal{C}|} \sum_{\mathbf{c}} \sum_{\hat{\mathbf{c}}^1 \neq \mathbf{c}^1} P\big(\mathbf{c}^1 \to \hat{\mathbf{c}}^1 \big| \mathbf{c} \text{ is transmitted}\big), \tag{6.13}$$

Considering (6.11), the pairwise error probability $P\big(\mathbf{c}^1 \to \hat{\mathbf{c}}^1 \big| \mathbf{c} \text{ is transmitted}\big)$ is equivalent to

$$P\left(\left\| \mathbf{y}_1 - \sqrt{P_1}\hat{\mathbf{c}}^1 \right\|^2 \leq \left\| \mathbf{y}_1 - \sqrt{P_1}\mathbf{c}^1 \right\|^2 \middle| \ \mathbf{c} \text{ is transmitted} \right), \tag{6.14}$$

therefore, (6.13) can be simplified to

$$P_f \leq \frac{1}{|\mathcal{C}|} \sum_{\mathbf{c}} \sum_{\hat{\mathbf{c}}^1 \neq \mathbf{c}^1} P\left(\sum_{i=1}^{n} y_{1i}(c_i^1 - \hat{c}_i^1) \leq 0 \middle| \ \mathbf{c} \text{ is transmitted} \right). \tag{6.15}$$

It is shown in [99] that

$$\sum_{i=1}^{n} y_{1i}(c_i^1 - \hat{c}_i^1) = 2\Big(\sqrt{P_1}d_1 + \sqrt{P_2}(d_1 - 2d_2) + G\Big), \tag{6.16}$$

where d_1 is the number of bit errors in $\hat{\mathbf{c}}^1$ and d_2 is the number of positions where $\mathbf{c}^1$ and $\mathbf{c}^2$ differ for the positions where $\mathbf{c}^1 \neq \hat{\mathbf{c}}^1$, and G is a Gaussian random variable with zero mean and variance $\frac{d_1 N_0}{2}$. Therefore, an upper-bound for the error probability in (6.13) can be calculated as

$$P_f \leq \frac{1}{|\mathcal{C}|} \sum_{\mathbf{c}} \sum_{\hat{\mathbf{c}}^1 \neq \mathbf{c}^1} Q\left(\sqrt{\frac{2f\big(d_1, d_2, \sqrt{P_1}, \sqrt{P_2}\big)}{N_0}} \right), \tag{6.17}$$

where f is defined as

$$f\Big(d_1, d_2, \sqrt{P_1}, \sqrt{P_2}\Big) = \frac{\Big(\sqrt{P_1} d_1 + \sqrt{P_2}(d_1 - 2d_2)\Big)^2}{d_1}. \tag{6.18}$$

The major difficulty in computing the bound in (6.17) is that for any possible value of d_1, we are required to compute the distribution of the random variable d_2 but the conditional distribution $P(d_2|d_1)$ depends on the geometry of the employed codes in general. For the case of trellis-based codes, however, the computation of the bound can be efficiently handled by listing the multiplicities of different values of d_2 and d_1 by applying similar technique utilized in [98]. To this end, a product state trellis with states $(\mathbf{s}, \hat{\mathbf{s}})$ is formed where $\mathbf{s} = (\mathbf{s}_1, \mathbf{s}_2)$ and $\hat{\mathbf{s}} = (\hat{\mathbf{s}}_1, \hat{\mathbf{s}}_2)$ denote the states of two codeword pairs. A state transition $S'_{1,2}$ is constructed with the entry in the kth row and lth column expressed as

$$[S'_{1,2}]_{k,l} = D_1^{d_1^{k,l}} \times D_2^{d_2^{k,l}}. \tag{6.19}$$

Similar to the case of GMAC, for the L stage trellis, the multiplicities of the different values of d_1 and d_2 can be obtained by computing the Lth power of $S'_{i,j}$. To address the issue of the memory and complexity requirements, similar techniques as before can be implemented where the number of the terms are limited to those with components (d_1 and d_2) less than a specific threshold.

6.3 Short Block Length Code Design for GIC with Strong Interference

For a GIC with strong interference, it is optimal to decode the interfering signal along with the desired signal from the information theoretic view point. Therefore, we opt for jointly decoding the messages of both users at each receiver. As a consequence, the bounding technique utilized in [98] can be exploited to derive the performance bound for the GIC under strong interference. In the following, we detail the derived upper-bound and the code design framework.

6.3.1 Computation of Error-Rate Bounds

Since at each receiver, both the interfering and the desired signals are decoded, the channel can be considered as two GMACs, therefore, the frame error probability can be upper-bounded as

$$P_f < \frac{1}{|\mathcal{C}|} \sum_{\mathbf{c}} \sum_{\hat{\mathbf{c}} \neq \mathbf{c}} \left(Q\left(\sqrt{\frac{Ed_1^2(\mathbf{c}, \hat{\mathbf{c}})}{2N_0}} \right) + Q\left(\sqrt{\frac{Ed_2^2(\mathbf{c}, \hat{\mathbf{c}})}{2N_0}} \right) \right), \tag{6.20}$$

where $Ed_i^2(.,.)$ is the squared Euclidean distance function computed at receiver i as

$$Ed_i^2(\mathbf{c}, \hat{\mathbf{c}}) = \alpha_i \mathbf{D}_{\mathbf{c},\hat{\mathbf{c}}} \alpha_i^{\dagger}. \tag{6.21}$$

Due to the similarity of the GIC under strong interference with the case of GMAC, the codeword difference matrix $\mathbf{D}_{\mathbf{c},\hat{\mathbf{c}}}$ for all the multiplicities can be efficiently computed following similar steps as in [98]. The code optimization can then be simply performed by searching for pairs of codes (one for each user) minimizing the bound (6.20) computed at a specific SNR.

Similar to [98], we consider shorter length paths through the trellis than the intended code block length for ordering the performance of the codes. Furthermore, to compute the bound, we follow a similar simplification as in [98] and truncate the number of terms kept for each entry of the multiplication matrix. We need to highlight

that this simplification results in an approximate bound because the dismissed terms during the computation may have significant effects to the final value. To be more exact, the computation in (6.21) is a linear combination of $\mathbf{D}_{\mathbf{c},\hat{\mathbf{c}}}$'s components ($q_{ij}$), hence components with large magnitude can still compensate each other leading to a small value with appreciable effect on the computation. As a consequence, the computation provided here should be considered as an approximation to the union bound rather than an actual upper-bound on the error rate.

In the following subsection, we present examples of code design carried out for instances of the GIC with strong interference.

6.3.2 Code Design Examples

We consider code rates of $\frac{1}{2}$ and code block length of $N = 96$. The performance of the optimized trellis-based codes are compared against that of LDPC codes (96.33.964) and (96.33.966) taken from [102]. The constraint length of trellis-based codes is 2, therefore termination for each user's code is achieved via the last two information bits. The trellis-based codes are represented in octal form; i.e., $(m_1, n_1)/(m_2, n_2)$ represents the codes adopted for the GIC where the code (m_i, n_i) represents the convolutional encoder in octal notation for transmitter i. The code optimization is carried out through ordering the codes' performance by computing the approximate bounds. To efficiently handle the matrix multiplications and cope with the memory limitations, the number of terms for each entry of the state transition matrix is truncated to 25.

For the first example, we consider a GIC with $SNR_1 - SNR_2 = 2$ dB, $INR_1 - SNR_2 = 1$ dB, and $INR_2 - SNR_1 = 2$ dB. Code design is performed by minimizing the performance bound (6.20) at $SNR_1 = 8$ dB over the codes with 4 states. The minimum value of the upper-bound is achieved for the code $(2, 5)/(5, 7)$. For comparison purposes, we also consider codes designed for P2P channels. In order

to employ the P2P codes for the two-user setup, an *interleaved* scheme is adopted where the same code with different assignment of generator matrices to the output bits are used for the users. That is, for the first user we employ the code $(5, 7)$, which has the largest minimum distance among the codes with the constraint length 2. For the second user, we adopt the code $(7, 5)$, which obviously is the same code with $(5, 7)$ with a different assignment of coded bits.

Fig. 6.2 illustrates the decoding performance of the trellis-based codes and the LDPC codes employed for the considered GIC. The performance of LDPC codes is computed for both SIC [50] and SUD techniques obtained via simulations. For the former technique, each receiver adopts a joint decoder and aims at *partially* decode the interfering signal helping the overall decoding while for the latter, each receiver treats the interfering signal as noise. It is evident that the SIC scheme provides a better performance than the SUD. It is observed that the optimized trellis-based codes outperform the P2P optimal codes, both offering a better performance than LDPC codes even for the case of SIC.

As another example, code optimization is carried out for a GIC with $SNR_1 - SNR_2 = 1$ dB, $INR_1 - SNR_2 = 2$ dB, and $INR_2 - SNR_1 = 1.5$ dB. Unlike previous example, code design is performed targeting different SNR values, that is, the upper-bound is minimized for codes with 4 states at low and high SNRs separately. For this example, we choose $SNR_1 = 3$ dB and $SNR_1 = 8$ dB for which $(2, 7)/(7, 5)$ and $(6, 7)/(3, 5)$ minimize the upper-bound (6.20), respectively. Fig. 6.3 demonstrates the decoding results for the codes adopted for the considered GIC. The codes optimized at $SNR_1 = 3$ dB have the best performance at low SNRs while $(6, 7)/(3, 5)$ have the best performance at high SNRs. In addition, both optimized codes considerably outperform the P2P optimal codes at high SNRs. Similar to the previous example,

the performance of the LDPC codes computed with SIC is better than that obtained with SUD, however, both are inferior to the performance of trellis-based codes.

This poor performance of LDPC codes can be mainly attributed to the inferiority of the decoding algorithm in multi-user setups for short block lengths. A similar observation is made for the GMAC in [98] where the authors show that the performance of the short block length LDPC codes under joint decoding is inferior to that of the trellis based codes. In fact, the considered BP based JD is sub-optimal primarily due to the fact that for short block lengths, interference cancellation does not work well as the individual decoding results are not very reliable unless one signal is much stronger than the other [98]. Moreover, for the considered code block length the short cycles affect the decoding performance of the BP.

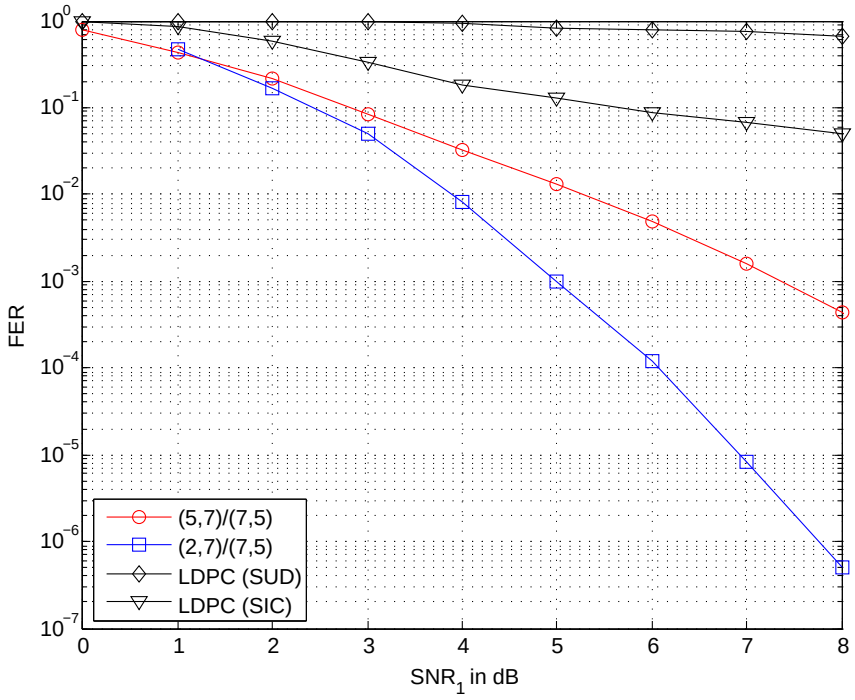

Figure 6.2: Total Frame Error Rate of LDPC Codes and Trellis-Based Codes Employed for a GIC with Strong Interference $SNR_1 - SNR_2 = 2$ dB, $INR_1 - SNR_2 = 1$ dB, and $INR_2 - SNR_1 = 2$ dB

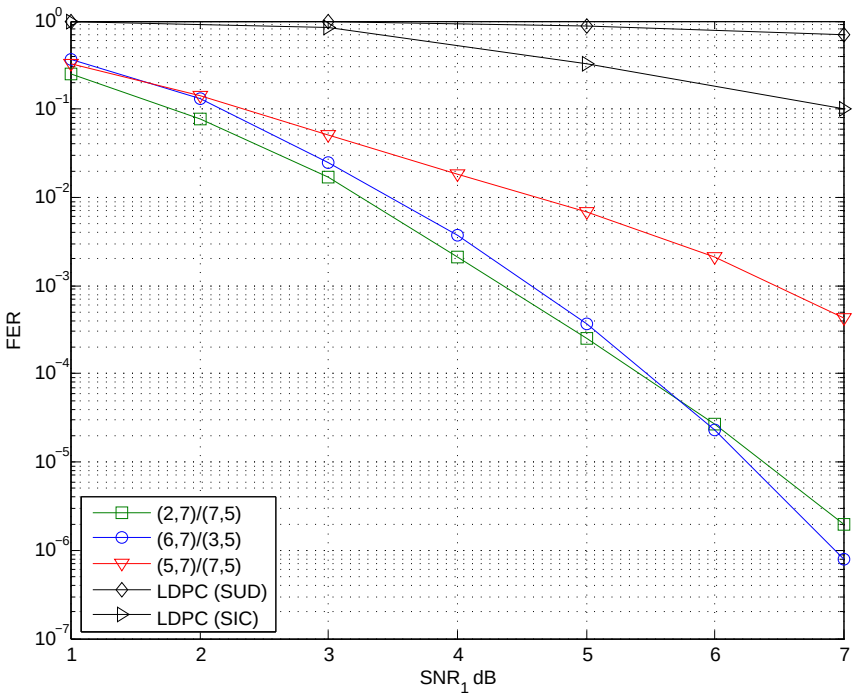

Figure 6.3: Total Frame Error Rate of LDPC Codes and Trellis-Based Codes Employed for a GIC with Strong Interference, $SNR_1 - SNR_2 = 1$ dB, $INR_1 - SNR_2 = 2$ dB, and $INR_2 - SNR_1 = 1.5$ dB

6.4 Short Block Length Code Design for GIC with Weak Interference

Under weak interference, decoding of interfering signals to their entirety is not an optimal strategy from information theoretic point of view. Therefore, for comparison, we investigate the performance of both JD and SUD in the numerical results. To compute the performance bounds, which is exploited to optimize trellis-based codes, we consider SUD which resembles the first stage of the decoding approach taken in [99], hence similar arguments can be followed.

6.4.1 Computation of Error Rate Bound

Considering the upper-bound derived in (6.17), similar strategy can be followed to derive the bound when interference is treated as noise, that is, the total error probability

under weak interference is upper-bounded as

$$P_f \leq \frac{1}{|\mathcal{C}|} \sum_{\mathbf{c}} \sum_{i=1}^{2} \sum_{\hat{\mathbf{c}}^i \neq \mathbf{c}^i} Q\left(\sqrt{\frac{2f(d_{ii}, d_{ji}, \alpha_{ii}, \alpha_{ji})}{N_0}} \right), \quad i,j = 1,2, \quad i \neq j, \tag{6.22}$$

where d_{ii} is the number of bit errors in $\mathbf{c}^i$ and d_{ji} is the number of positions where $\mathbf{c}^j$ and $\mathbf{c}^i$ differ for the positions where $\hat{\mathbf{c}}^i \neq \mathbf{c}^i$. In order to list the multiplicities of different values of d_{ii} and d_{ji}, a product state trellis is constructed to which two state transition matrices $S'_{1,2}$ and $S'_{2,1}$ are associated. The entry in the kth and lth row of $S'_{i,j}$ is computed as

$$[S'_{i,j}]_{k,l} = D_{11}^{d_{ii}^{k,l}} \times D_{12}^{d_{ji}^{k,l}}, \tag{6.23}$$

where $i,j \in \{1,2\}, i \neq j$. Similar to the approach taken in [98], the computed state transition matrices are utilized towards listing the possible values of d_{ij} with their multiplicities characterizing the upper-bound (6.22). Similar simplifications are performed to cope with the memory limitations, therefore the computed values are treated as approximations rather than being actual upper bounds.

The adopted decoding scheme for the weak interference level only aims at decoding the desired signals. As a result, the decoding metrics should be modified accordingly reflecting the fact that the interfering signal is treated as noise. Implementing the minimum distance criterion, we ignore the code constraints of the weaker signal, therefore the decoder i favors the codeword maximizing $P(\mathbf{y}_i|\mathbf{c}^i)$, given by

$$\begin{aligned}
\log P(\mathbf{y}_i|\mathbf{c}^i) =& \sum_{k=0}^{N} \log P(y_{ik}|c_k^i) \\
=& \sum_{k=0}^{N} \log \left(\frac{1}{2\sqrt{\pi N_0}} \left[e^{-\frac{\left(y_{ik} - \alpha_{ii}c_k^i - \alpha_{ji}\right)^2}{N_0}} + e^{-\frac{\left(y_{ik} - \alpha_{ii}c_k^i + \alpha_{ji}\right)^2}{N_0}} \right] \right) \\
=& C + \sum_{k=0}^{N} \log \left(e^{-\frac{(y_{ik} - \alpha_{ii}c_k^i)^2 + \alpha_{ji}^2}{N_0}} \left(e^{\frac{2\alpha_{ji}(y_{ik} - \alpha_{ii}c_k^i)}{N_0}} + e^{-\frac{2\alpha_{ji}(y_{ik} - \alpha_{ii}c_k^i)}{N_0}} \right) \right) \\
=& C' - \sum_{k=0}^{N} \left[(y_{ik} - \alpha_{ii}c_k^i)^2 - \log \left(\cosh \left(\frac{2\alpha_{ji}(y_{ik} - \alpha_{ii}c_k^i)}{N_0} \right) \right) \right],
\end{aligned}$$

where C and C' are constant for all different codewords $\mathbf{c}^i$. The considered decoding algorithm can be efficiently performed by employing a Viterbi decoder at each receiver for which the metric of each branch is computed as

$$\sum_{k=0}^{t}\left[(y_{ik}-\alpha_{ii}c_k^i)^2-\log\left(\cosh\left(\frac{2\alpha_{ji}(y_{ik}-\alpha_{ii}c_k^i)}{N_0}\right)\right)\right], \tag{6.24}$$

where t is the number of output bits for one stage of the trellis section.

It is worth mentioning that, similar to the case of strong interference, joint decoding can also be employed at each receiver resulting in similar performance bounds; however, for simplicity of the computations, we utilize the minimum distance criterion to compute the performance bounds, which is also exploited in the code optimization. In essence, the performance of the employed decoding scheme becomes close to that of joint decoding when the interference levels at the receivers are negligible compared to the desired signals.

The code design is carried out by searching for the codeword pair minimizing the upper-bound (6.22). In the following, we perform code optimization for examples of GICs with weak interference.

6.4.2 Examples of Code Design

Consider a GIC with $SNR_1 - SNR_2 = 0.5$ dB, $INR_1 - SNR_2 = -1$ dB, and $INR_2 - SNR_1 = -1.5$ dB where the SNR and INR constraints satisfy the weak interference condition. The code design is pursued by minimizing (6.22) at $SNR =$ 20 dB over codes with 4 states, which is achieved with $(4,5)/(5,7)$. The performance of the optimized codes is compared against that of the P2P optimal codes and the off-the-shelf LDPC codes. Fig. 6.4 shows the decoding results of the codes employed for the considered GIC. For comparison, the performance of the trellis based codes are obtained for JD and SUD. It is shown that, under SUD where the interfering signal

is treated as noise, the performance of the optimized codes is similar to that of the P2P optimal codes. However, the optimize codes offer better performance than the P2P optimal codes under JD. Moreover, the performance of the LDPC codes with SUD is better than both the optimized codes and the P2P optimal codes, however, they are inferior to the trellis based codes under JD. The poor performance of the considered SUD can be attributed to the level of the interference at the receivers which is comparable to the power of the desired signals.

For the second example, we consider a GIC with $SNR_1 - SNR_2 = 1$ dB, $INR_1 - SNR_2 = -1$ dB, and $INR_2 - SNR_1 = -2$ dB. Code design is carried out at $SNR = 20$ dB, where $(4,5)/(5,7)$ achieves the minimum value of (6.22) among all the codes with 4 states. Fig. 6.5 illustrates the decoding results computed for the different codes. Similar to the previous example, the performance of the optimized codes is superior to that of the P2P optimal codes under JD; however, both perform similarly under SUD. Moreover, LDPC codes beat the employed trellis based codes when SUD is adopted but they are outperformed under JD.

As another example, code optimization is carried out for a GIC with $SNR_1 - SNR_2 = -0.75$ dB, $INR_1 - SNR_2 = -1.5$ dB, and $INR_2 - SNR_1 = -0.5$ dB. For this example P2P optimal codes achieve the minimum of the expression in (6.22) considering all the codes with 4 states where the bounds are computed at $SNR = 20$ dB. For comparison, we also consider the codes ranked second in the minimization which are $(5,7)/(6,7)$. Fig. 6.6 demonstrates the performance of the employed codes for the considered GIC. Under SUD, the P2P optimal codes and the optimized codes have comparable performance both are outperformed by LDPC codes. For the case of JD, however, LDPC codes are inferior to the trellis based codes and the optimized codes provide better performance than the P2P optimal codes.

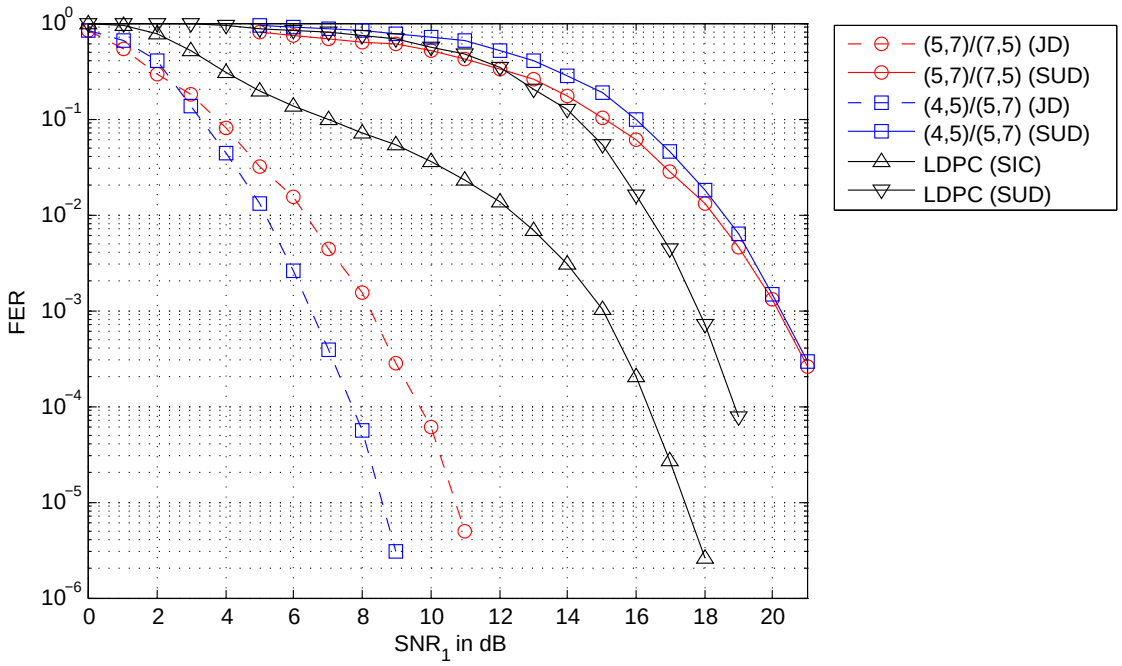

Figure 6.4: Total Frame Error Rate of LDPC Codes and Trellis-Based Codes Employed for a GIC with Weak Interference $SNR_1 - SNR_2 = 0.5$ dB, $INR_1 - SNR_2 = -1$ dB, and $INR_2 - SNR_1 = -1.5$ dB

6.5 Short Block Length GIC with Mixed Interference

For the mixed interference scenario, one receiver experiences strong interference while the other is under weak interference. As a result, to compute the performance bounds, parallel to the case of strong and weak interference regimes, we consider JD and SUD for the receiver under strong interference and the receiver experiencing weak interference, respectively. In the numerical results, we consider both JD and SUD for the receiver under weak interference to assess the performance of the codes. In the following, we elaborate on the computation of the performance bound for this case for use in code design.

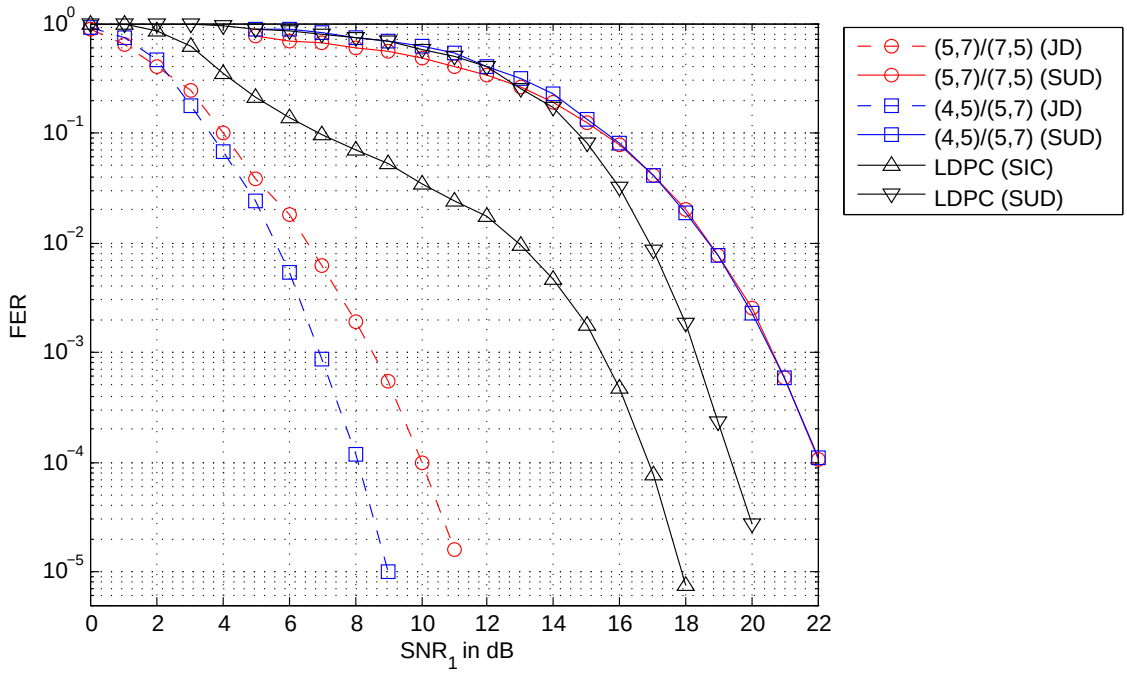

Figure 6.5: Total Frame Error Rate of LDPC Codes and Trellis-Based Codes Employed for a GIC with Weak Interference $SNR_1 - SNR_2 = 1$ dB, $INR_1 - SNR_2 = -1$ dB, and $INR_2 - SNR_1 = -2$ dB

6.5.1 Computation of Error Rate Bound

Without loss of generality, we assume that receiver 1 and receiver 2 experience weak interference and strong interference, respectively. Parallel to the previous scenarios, receiver 1 treats the interfering signal as noise while receiver 2 decodes both messages jointly. Considering the bounds derived for the previous scenarios, the frame error probability, defined as the probability of codewords of either transmitters being decoded to wrong codewords, can be upper bounded as

$$P_f \leq \frac{1}{|\mathcal{C}|} \sum_{\mathbf{c}} \left[\sum_{\hat{\mathbf{c}}^1 \neq \mathbf{c}^1} Q\left(\sqrt{\frac{2f(d_{11}, d_{21}, \alpha_{11}, \alpha_{21})}{N_0}} \right) + \sum_{\hat{\mathbf{c}} \neq \mathbf{c}} Q\left(\sqrt{\frac{E d_2^2(\mathbf{c}, \hat{\mathbf{c}})}{2N_0}} \right) \right]. \quad (6.25)$$

Computation of (6.25) can be efficiently done utilizing the approach explained in previous sections. Note that joint decoding can be also adopted at receiver 1 where similar bounds to the case of strong interference will be obtained.

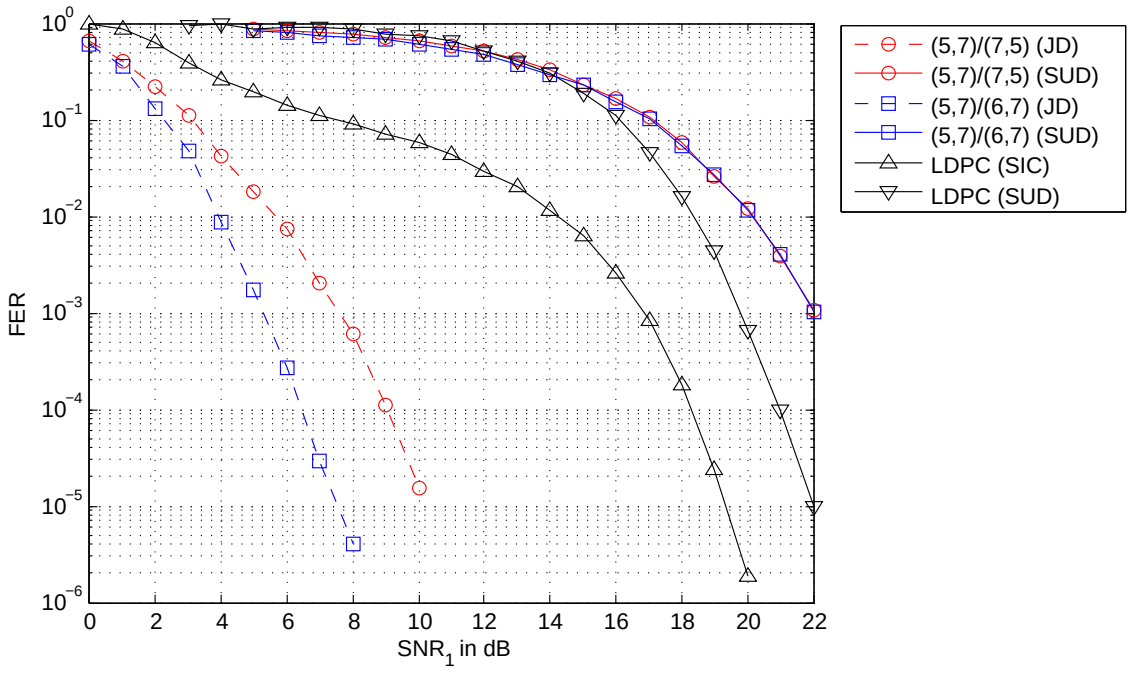

Figure 6.6: Total Frame Error Rate of LDPC Codes and Trellis-Based Codes Employed for a GIC with Weak Interference $SNR_1 - SNR_2 = -0.75$ dB, $INR_1 - SNR_2 = -1.5$ dB, and $INR_2 - SNR_1 = -0.5$ dB

The code design process is nothing but computing the bound for all the codeword pairs and selecting the one corresponding to the best error rate estimate.

6.5.2 Examples of Code Design

For the first example, we consider a GIC with $SNR_1 - SNR_2 = 8$ dB, $INR_1 - SNR_2 = 6$ dB, and $INR_2 - SNR_1 = -6$ dB. The codes are designed through minimizing the (6.25) at $SNR_1 = 15$ dB computed for codes with 4 states. The P2P optimal codes achieve the minimum value, therefore we consider the second best pair of codes $(5,7)/(6,7)$ as well. The performance of the optimized codes is compared against that of the P2P optimal and the LPDC codes. We consider two decoding schemes. In one scheme both messages are decoded at each receiver. For the other scheme, the receiver under weak interference utilize SUD while the other receiver decode the messages jointly.

Fig. 6.7 shows the performance of the adopted codes for the considered GIC. The optimized codes and the P2P optimal codes perform similarly when SUD is adopted for receiver 1; however, the optimized codes outperform the P2P optimal codes when JD is employed. It is worth mentioning that even though the P2P optimal codes achieve the minimum value for the computed performance bound, the second pair of best codes performs better emphasizing that the computed bounds should be treated as only approximations.

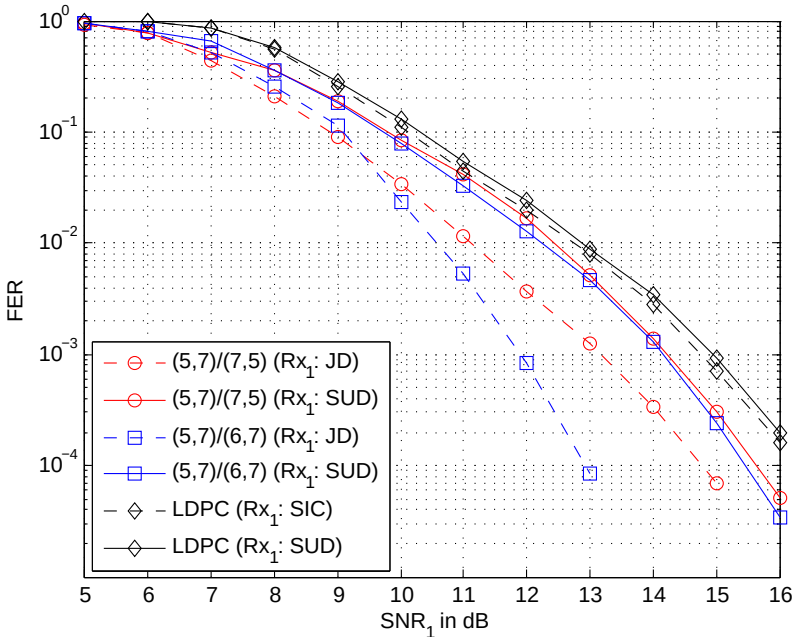

Figure 6.7: Total Frame Error Rates of LDPC Codes and Trellis-Based Codes Employed for a GIC with Mixed Interference $SNR_1 - SNR_2 = 8$ dB, $INR_1 - SNR_2 = 6$ dB, and $INR_2 - SNR_1 = -6$ dB

For the next example, we consider a GIC with $SNR_1 - SNR_2 = 4$ dB, $INR_1 - SNR_2 = 0.5$ dB, and $INR_2 - SNR_1 = -3$ dB. At $SNR_1 = 7$ dB, minimum of the performance bound is achieved by $(5, 7)/(6, 7)$. Fig. 6.8 illustrates the decoding results computed for the codes adopted for the considered GIC. It is shown that the optimized codes beat the P2P optimal codes under both JD and SUD. Moreover, trellis-based codes considerably outperform the LDPC codes regardless of the employed decoding

scheme. As shown, the performances of the LDPC codes are similar for both SUD and SIC. This can be attributed to the fact that the overall frame error rate is controlled by the second receiver which is under strong interference.

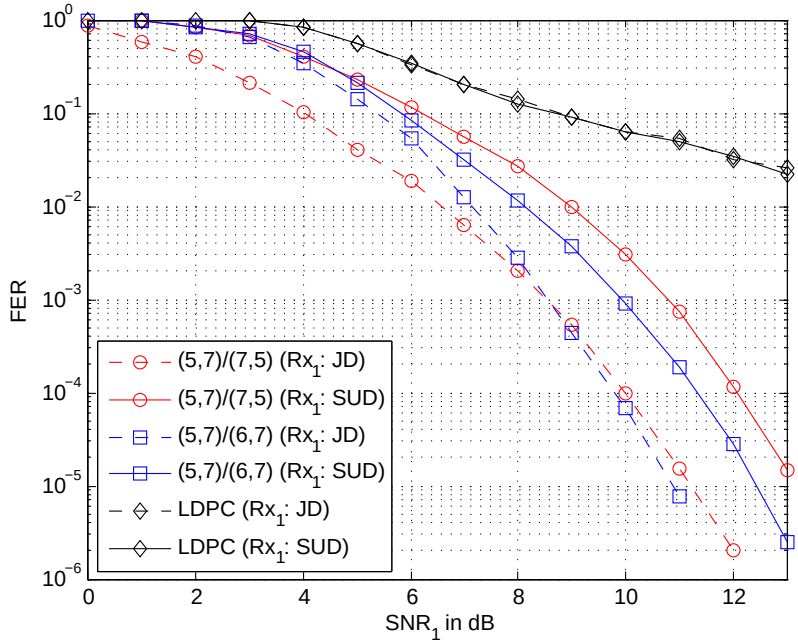

Figure 6.8: Total Frame Error Rates of LDPC Codes and Trellis-Based Codes Employed for a GIC with Mixed Interference $SNR_1 - SNR_2 = 4$ dB, $INR_1 - SNR_2 = 0.5$ dB, and $INR_2 - SNR_1 = -3$ dB

As another example, we take a GIC with mixed interference into consideration where $SNR_1 - SNR_2 = 5$ dB, $INR_1 - SNR_2 = 1$ dB, and $INR_2 - SNR_1 = -4$ dB. We design codes to achieve the minimum of the performance bound at $SNR_1 = 9$ dB. The optimization result is $(5, 7)/(6, 7)$. Fig. 6.9 illustrates the decoding results obtained for the individual and the total frame error rates. It is shown that the optimized codes beat the P2P optimal codes both are superior to the LDPC codes. Moreover, the performances of the trellis based codes are similar under JD and SUD. LDPC codes also have similar performance under SIC and SUD. This is because, as shown in the figure, the total frame error rate is controlled by the receiver 2 experiencing strong interference, therefore decoding both messages at the receiver 1 does not improve the

overall performance.

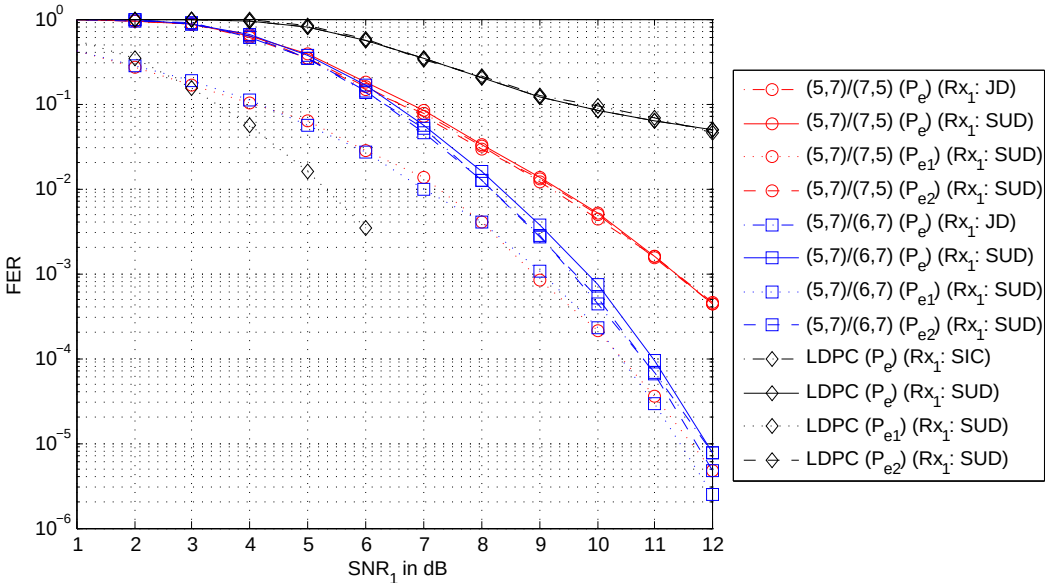

Figure 6.9: Total and Individual Frame Error Rates of LDPC Codes and Trellis-Based Codes Employed for a GIC with Mixed Interference $SNR_1 - SNR_2 = 5$ dB, $INR_1 - SNR_2 = 1$ dB, and $INR_2 - SNR_1 = -4$ dB

To further explore this point, we consider a GIC with $SNR_1 - SNR_2 = 3$ dB, $INR_1 - SNR_2 = 1$ dB, and $INR_2 - SNR_1 = -1$ dB. Code optimization is performed by minimizing the performance bound at $SNR = 14$ dB, which is attained by the P2P optimal codes followed by $(5, 7)/(6, 7)$. Fig. 6.10 demonstrates the individual and the total frame error rate computed for different codes employed over the considered GIC. It is shown that optimized codes and the P2P optimal codes have similar performances under SUD; however, the optimized codes perform better under JD. Moreover, they are superior to the LDPC codes under JD, however, they are outperformed when SUD is employed. Unlike the previous example, we notice that receiver 1, which experiences weak interference, dominates the overall performance for all the employed codes. As a consequence, decoding both messages at receiver 1 results in considerable improvements over SUD.

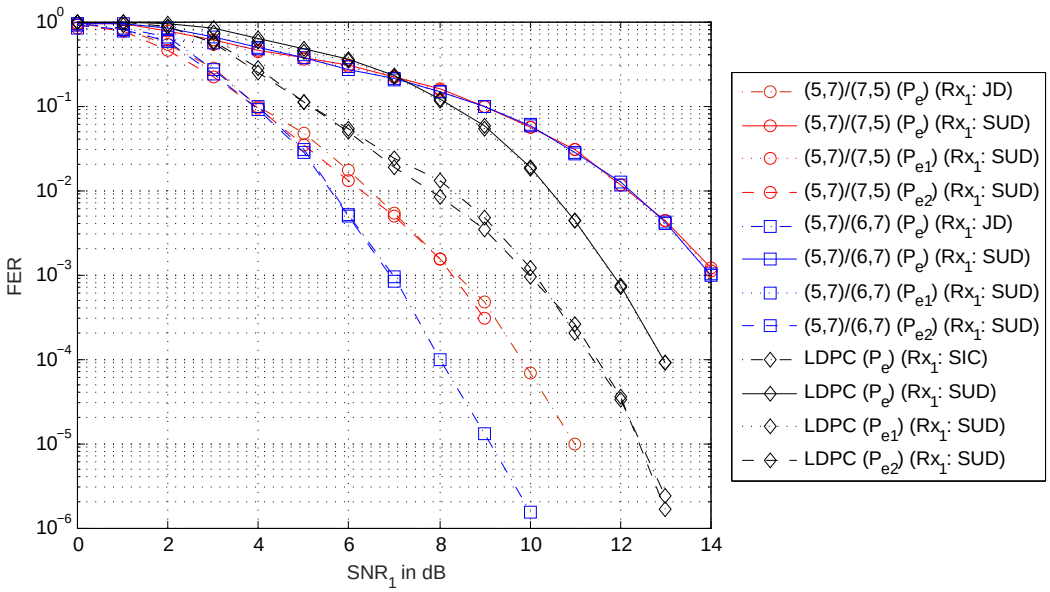

Figure 6.10: Total and Individual Frame Error Rates of LDPC Codes and Trellis-Based Codes Employed for a GIC with Mixed Interference $SNR_1 - SNR_2 = 3$ dB, $INR_1 - SNR_2 = 1$ dB, and $INR_2 - SNR_1 = -1$ dB

6.6 Chapter Summary

In this chapter, we focused on code design for the two-user GIC when code block length is short. In the first part, we reviewed the existing performance bounds developed for the two-user GMAC and the two-user GBC. These results were exploited towards developing performance bounds for the two-user GIC for different interference levels which were then utilized in designing trellis-based codes. It is shown that under strong interference optimized trellis-based codes offer better performance than the P2P optimal codes, both outperforming the LDPC codes. For the case of weak interference, we noticed that optimized codes and the P2P optimal codes have similar performance, and both were inferior to LDPC codes under SUD. However, LDPC codes are outperformed by the trellis-based codes and the optimized codes offer better performance than the P2P optimal codes under JD. For the mixed interference scenario, we observed that under JD the optimized trellis-based codes consistently

outperform the P2P optimal codes and both were superior to the LDPC codes. However, LDPC codes provide better performance than the trellis-based codes when the SUD is employed for the dominant receiver under weak interference.

Chapter 7

SUMMARY AND CONCLUSIONS

In this dissertation, we study the design of LDPC codes and trellis-based codes for different multi-user channels. We review the existing literature on the information theoretic bounds and practical codes optimized for the GMAC, BC, and RCs. For code optimization, we start with the two-user GMAC employing BPSK signaling. We derive the PDF of the LLRs sent from the state nodes to the variable nodes when joint decoding is adopted at the receiver. Through Monte-Carlo simulations, we observe that the PDF of the LLRs sent from the state nodes to the variable nodes can be closely approximated with a GMD. As such, we propose new iterative decoding analysis methods based on the GMD assumption and provide the update rule for the GMD parameters through the decoding iterations. We compare the performance of the proposed GMD analysis to the existing mutual information update rule approximations in the literature and notice that the proposed approach leads to a better estimate of the decoding thresholds. The proposed methods are then incorporated into code optimization performed for two scenarios of channel gains being equal and unequal. For equal channel gains, we compare our optimized codes to the existing designs and show that superior performance is attained. For unequal channel gains, we perform the code optimization incorporating different methods in the literature and show that the codes designed with the proposed methods offer the best performance.

As another investigation, we study the code design for the two-user GMAC for quasi-static Rayleigh fading channels. Common outage capacity is adopted as the performance measure and the corresponding rate region is characterized for BPSK signaling. Code optimization is performed for examples with real and complex chan-

nel gains. The results indicate that the designed codes achieve rate pairs close to the outage region boundaries consistently offering better performance than the P2P codes. Finite code block length simulations of specific codes picked from designed ensembles demonstrate the superior performance of the optimized codes over the P2P alternatives.

We also examine the code design principals for GICs with the fixed channel gains when BPSK and QPSK constellations are adopted for the transmission. HK coding and decoding strategy is employed at the transmitter and receiver sides, where public and private messages are encoded with separate LDPC codes and joint decoding is implemented at the receiver. To simplify the computations of the HK rate region characterization, a sub-region is considered for which public and private messages are combined with standard addition and no TS is utilized. Unlike the two-user GMAC, we exploit a variant of the EXIT chart analysis wherein no Gaussian assumption is considered for mutual information evolution and instead, Monte-Carlo simulation is adopted to compute the true mutual information at each node of the decoder. Having utilized the i.i.d. channel adapters, we prove a symmetry property of the exchanged LLRs under joint decoding of three messages, which plays a key role in computing the mutual information in the EXIT chart analysis. Moreover, stability condition is derived for BPSK and QPSK signaling for strong and weak interference levels, separately. We perform the code optimization for a multitude of scenarios with different interference levels. Under strong interference, the optimized codes beat the non-naive TS rate region with Gaussian signaling. Under weak interference, optimized codes outperform the naive TS region (with Gaussian signaling) and operate close to the non-naive TS region boundary. Furthermore, the designed codes improve consistently upon the codes optimized for the P2P channels. Finite code block length simulations are also performed adopting the designed LDPC code validating the esti-

mated thresholds. Considering practical applications, we also study the code design for short/moderate block lengths utilizing structured LDPC codes, and demonstrate that superior performance is observed over the codes with random constructions at high SNRs.

We also study code design for the two-user DMIC adopting the HK coding/decoding strategy. Particularly, we consider the two-user BIBO ZIC, wherein one receiver is interference free, and characterize the HK rate region. To simplify the characterization, we assume that no TS is utilized and messages are transmitted as private yielding a sub-region of the actual HK rate region. Through exhaustive search, we obtain the optimal distributions for the transmitted codewords leading to the maximum sum-rate computed for the HK sub-region. The proposed coding scheme consists of employing LDPC codes along with NLTCs to introduce the desired distributions into the transmitted bits and exploit BCJR-algorithm based decoders in conjunction with LDPC single user decoders at the receiver sides. The code optimization is nothing but design of NLTCs and the LDPC codes. Optimized codes are shown to operate above the TS line hence offering a better performance than single user codes used with TS. It is also shown that some of the achieved points cannot be obtained through using only LDPC codes (which induce equal density of 0's and 1's) emphasizing the advantage of the NLTCs in our implementation.

In the last part of the thesis, we investigate the code design principals for short block length codes in the context of GICs. Previous methods in the earlier chapters are not suited for short block length codes primarily because the underlying independence assumption exploited for the exchanged LLRs within the iterative decoder is no longer valid. As a consequence, we resort to short block length trellis-based codes which are successfully employed for the two-user GMAC in recent literature. We

utilize the existing bounding techniques originally developed for the two-user GMAC and the two-user GBC, and develop performance bounds for the two-user GIC. The derived performance bounds are then utilized towards designing short block length trellis-based codes for examples with strong, weak and mixed interference levels. Under strong interference, the optimized codes show superior performance to the LDPC codes and the P2P optimal codes. For the weak interference examples, LDPC codes perform the best under SUD and the performances of the P2P optimal codes are close to those of optimized codes. Under JD, however, the optimized codes perform better than the P2P optimal codes and both are superior to the LDPC codes. Similar behavior is observed for the case of mixed interference where the trellis-based codes outperform the LDPC codes when JD is employed for the receiver under weak interference while LDPC codes offer better performance for the case of SUD if the receiver dominating the error rate is under weak interference.

In the rest of the chapter, we point out several promising research directions following the line of research in this dissertation.

In Chapter 3, we utilize the EM method to estimate the parameters of the GM PDFs for the two proposed techniques of modified EXIT chart analysis and the modified DE. Despite the satisfactory performance of the EM method, it imposes a high computational burden rendering the proposed techniques inefficient for the quasi-static fading scenarios. So, a simpler method should be developed for estimating the parameters of the GMDs. One possible solution is to exploit the special characteristic of the PDFs of the exchanged LLRs and applying the existing analytical methods developed in [103] to estimate the GM parameters. Another alternative is to simplify the forms of the PDFs of the outgoing LLRs from the check nodes and the state nodes. For instance, one may use a Taylor expansion and derive the mean and variance of the GM components directly from this approximation.

Another possible extension of the results in this thesis is to consider the LDPC code design for the two-user GIC in the case of fading. New techniques should be developed as the same approach applied to the fixed channel gains scenario may be inefficient and one may resort to approximate methods such as the one adopted in [50]. Also, it is interesting to explore the code design employing nested codes suited for combining the public and private portion of the transmitted message before modulation. Code design for the nested codes requires developing new methods of code optimization as the update rules for decoding should be modified to reflect the encoding scheme used at the transmitters. Parallel to the considered system model, it is also worth exploring the code design for more than two users, possibly also leveraging the interference alignment techniques developed in the current literature.

In the case of the two-user DMIC, we investigate the code design for a simple HK coding strategy, that is, when the messages are sent as private. Better results may be achieved by considering scenarios where the transmitted messages are composed of both public and private parts. In addition, the overall performance of the designed codes can be improved by considering more sophisticated NLTCs through introducing more states and input bits per trellis stage.

Another possible line of research is in the context of short block length code design. For instance, one can allow for both public and private messages to be incorporated in the transmitted signals. This may improve the results especially for the case of weak interference where trellis-based codes fall short under SUD compared to the LDPC codes. Moreover, to further assess the performance of the trellis-based codes, it is interesting to compare the performance of these codes against the LDPC codes optimized for such block length via the existing methods such as PEG [104] or algebraic methods [105].

REFERENCES

[1] A. Roumy and D. Declercq, "Characterization and optimization of LDPC codes for the 2-user Gaussian multiple access channel," *EURASIP Journal on Wireless Communication and Networking*, 2007.

[2] T. Cover, "Broadcast channels," *IEEE Transactions on Information Theory*, vol. 18, no. 1, pp. 2–14, Jan. 1972.

[3] T. Sun, R. Wesel, M. Shane, and K. Jarett, "Superposition turbo TCM for multirate broadcast," *IEEE Transactions on Communications*, vol. 52, no. 3, pp. 368–371, Mar. 2004.

[4] A. E. Gamal and K. Young-Han, *Network Information Theory*. New York: Cambridge University Press, 2011.

[5] T. M. Cover and J. A. Thomas, *Elements of Information Theory*. New York: Wiley, 1991.

[6] G. Kramer, "Topics in multi-user information theory," *Foundations and Trends in Communications and Information Theory*, vol. 4, no. 4-5, pp. 265–444, Mar. 2007.

[7] A. Amraoui, S. Dusad, and R. Urbanke, "Achieving general points in the 2-user Gaussian MAC without time-sharing or rate-splitting by means of iterative coding," in *Proceedings of IEEE International Symposium on Information Theory (ISIT)*, Lausanne, Switzerland, Jun. 2002, p. 334.

[8] P. Bergmans, "A simple converse for broadcast channels with additive white Gaussian noise," *IEEE Transactions on Information Theory*, vol. 20, no. 2, pp. 279–280, Mar. 1974.

[9] K. Marton, "The capacity region of deterministic broadcast channels," in *Proceedings of IEEE International Symposium on Information Theory (ISIT)*, Paris-Cachan, France, 1977.

[10] M. Pinsker, "Capacity of noiseless broadcast channel," *Problem Peredachi Information Transmission*, vol. 14, no. 2, pp. 28–34, Apr. 1978.

[11] K. Marton, "A coding theorem for the discrete memoryless broadcast channel," *IEEE Transactions on Information Theory*, vol. 25, no. 3, pp. 306–311, May 1979.

[12] A. E. Gamal, "The feedback capacity of degraded broadcast channels," *IEEE Transactions on Information Theory*, vol. 24, no. 3, pp. 379–381, May 1978.

[13] G. Dueck, "Partial feedback for two-way and broadcast channels," *Problems of Information and Control*, vol. 46, no. 1, pp. 1–15, July 1980.

[14] L. Ozarow and S. Leung-Yan-Cheong, "An achievable region and outer bound for the Gaussian broadcast channel with feedback," *IEEE Transactions on Information Theory*, vol. 30, no. 4, pp. 667–671, July 1984.

[15] Y. Dong and P. Fan, "On rate regions for broadcast relay channels," in *Proceedings of the IEEE 13th International Conference on Communication Technology (ICCT)*, Jinan, China, Sep. 2011, pp. 966–970.

[16] C. Nair and A. E. Gamal, "An outer bound to the capacity region of the broadcast channel," *IEEE Transactions on Information Theory*, vol. 53, no. 1, pp. 350–355, Jan. 2007.

[17] O. Nagy and L. Hanlen, "Capacity bounds for LTI channels," in *Proceedings of Australian Communications Theory Workshop*, Christchurch, New Zealand, Jan. 2008, pp. 29–32.

[18] G. Caire and S. Shamai, "On the achievable throughput of a multi-antenna Gaussian broadcast channel," *IEEE Transactions on Information Theory*, vol. 49, no. 7, pp. 1691–1706, July 2003.

[19] H. Weingarten, Y. Steinberg, and S. Shamai, "The capacity region of the Gaussian multiple-input multiple-output broadcast channel," *IEEE Transactions on Information Theory*, vol. 52, no. 9, pp. 3936–3964, Sep. 2006.

[20] H. Sato, "An outer bound to the capacity region of broadcast channels," *IEEE Transactions on Information Theory*, vol. 24, no. 3, pp. 374–377, May 1978.

[21] E. V. D. Meulen, "Three-terminal communication channels," *Advances in applied Probability*, vol. 3, pp. 120–154, 1971.

[22] H. Sato, "Information transmission through a channel with relay," The Aloha System, University of Hawaii, Honolulu, 1976.

[23] W. Chang, S.-Y. Chung, and Y. H. Lee, "Gaussian relay channel capacity to within a fixed number of bits," 2010. [Online]. Available: http://arxiv.org/abs/1011.5065

[24] Y.-H. Kim, "Capacity of a class of deterministic relay channels," *IEEE Transactions on Information Theory*, vol. 54, no. 3, pp. 1328–1329, Mar. 2008.

[25] A. S. Avestimehr, S. N. Diggavi, and D. N. C. Tse, "Wireless network information flow: A deterministic approach," *IEEE Transactions on Information Theory*, vol. 57, no. 4, pp. 1872–1905, Apr. 2011.

[26] L. Zhou and W. Yu, "Capacity of the Gaussian relay channel with correlated noises to within a constant gap," *IEEE Communications Letters*, vol. 16, no. 1, pp. 2–5, Jan. 2012.

[27] A. Carleial, "A case where interference does not reduce capacity," *IEEE Transactions on Information Theory*, vol. 21, no. 5, pp. 569–570, Sep. 1975.

[28] H. Sato, "The capacity of the Gaussian interference channel under strong interference," *IEEE Transactions on Information Theory*, vol. 27, no. 6, pp. 786–788, Nov. 1981.

[29] V. S. Annapureddy and V. V. Veeravalli, "Gaussian interference networks: Sum capacity in the low-interference regime and new outer bounds on the capacity region," *IEEE Transactions on Information Theory*, vol. 55, no. 7, pp. 3032–3050, July 2009.

[30] T. Han and K. Kobayashi, "A new achievable rate region for the interference channel," *IEEE Transactions on Information Theory*, vol. 27, no. 1, pp. 49–60, Jan. 1981.

[31] H. Chong, M. Motani, and H. Garg, "On the Han–Kobayashi region for the interference channel," *IEEE Transactions on Information Theory*, vol. 54, no. 7, pp. 3188–3195, July 2008.

[32] H. Sato, "On degraded Gaussian two-user channels," *IEEE Transactions on Information Theory*, vol. 24, no. 5, pp. 638–640, Sep. 1978.

[33] G. Kramer, "Outer bounds on the capacity of Gaussian interference channels," *IEEE Transactions on Information Theory*, vol. 50, no. 3, pp. 581–586, Mar. 2004.

[34] R. Etkin, D. Tse, and H. Wang, "Gaussian interference channel capacity to within one bit," *IEEE Transactions on Information Theory*, vol. 54, no. 12, pp. 5534–5562, Dec. 2008.

[35] A. S. Motahari and A. K. Khandani, "Capacity bounds for the Gaussian interference channel," *IEEE Transactions on Information Theory*, vol. 55, no. 2, pp. 620–643, Feb. 2009.

[36] M. Maddah-Ali, A. Motahari, and A. Khandani, "Signaling over MIMO multi-base systems: Combination of multi-access and broadcast schemes," in *Proceedings of IEEE International Symposium on Information Theory (ISIT)*, July 2006, pp. 2104–2108.

[37] V. Cadambe and S. A. Jafar, "Interference alignment and degrees of freedom of the K-user interference channel," *IEEE Transactions on Information Theory*, vol. 54, no. 8, pp. 3425–3441, Aug. 2008.

[38] Y. Wu, C. Xiao, X. Gao, J. Matyjas, and Z. Ding, "Linear precoder design for MIMO interference channels with finite-alphabet signaling," *IEEE Transactions on Communications*, vol. 61, no. 9, pp. 3766–3780, Sep. 2013.

[39] R. Palanki and A. Khandekar, "Graph-based codes for synchronous multiple access channels," in *Proceedings of the 39th Annual Allerton Conference on Communication, Control, and Computing*, Monticello, Illinois, Oct. 2001, pp. 1263–1271.

[40] N. Chayat and S. Shamai, "Convergence properties of iterative soft onion peeling," in *Proceedings of IEEE Information Theory and Communications Workshop*, Kruger National Park, South Africa, June 1999, pp. 9–11.

[41] T. Richardson, M. Shokrollahi, and R. Urbanke, "Design of capacity-approaching irregular low-density parity-check codes," *IEEE Transactions on Information Theory*, vol. 47, no. 2, pp. 619–637, Feb. 2001.

[42] R. Tanner, "A recursive approach to low complexity codes," *IEEE Transactions on Information Theory*, vol. 27, no. 5, pp. 533–547, Sep. 1981.

[43] A. Sanderovich, M. Peleg, and S. Shamai, "LDPC coded MIMO multiple access with iterative joint decoding," *IEEE Transactions on Information Theory*, vol. 51, no. 4, pp. 1437–1450, Apr. 2005.

[44] S. ten Brink, "Convergence behavior of iteratively decoded parallel concatenated codes," *IEEE Transactions on Communications*, vol. 49, no. 10, pp. 1727–1737, Oct. 2001.

[45] M. Costa, "Writing on dirty paper," *IEEE Transactions on Information Theory*, vol. 29, no. 3, pp. 439–441, May 1983.

[46] Y. Sun, M. Uppal, A. Liveris, S. Cheng, V. Stankovic, and Z. Xiong, "Nested turbo codes for the Costa problem," *IEEE Transactions on Communications*, vol. 56, no. 3, pp. 388–399, Mar. 2008.

[47] Y. Sun, A. Liveris, and V. Stankovic, "Near-capacity dirty-paper code designs based on TCQ and IRA codes," in *Proceedings of IEEE International Symposium on Information Theory (ISIT)*, Adelaide, Australia, Sep. 2005, pp. 184–188.

[48] A. Amraoui, G. Kramer, and S. Shamai, "Coding for the MIMO broadcast channel," in *Proceedings of IEEE International Symposium on Information Theory (ISIT)*, Yokohama, Japan, June 2003, pp. 296–296.

[49] M. Uppal, V. Stankovic, and Z. Xiong, "Code design for MIMO broadcast channels," *IEEE Transactions on Communications*, vol. 57, no. 4, pp. 986–996, Apr. 2009.

[50] P. Berlin and D. Tuninetti, "LDPC codes for fading Gaussian broadcast channels," *IEEE Transactions on Information Theory*, vol. 51, no. 6, pp. 2173–2182, June 2005.

[51] M. Khojastepour, N. Ahmed, and B. Aazhang, "Code design for the relay channel and factor graph decoding," in *Proceedings of the Asilomar Conference on Signals, Systems and Computers*, Pacific Grove, California, Nov. 2004, pp. 2000–2004.

[52] Z. Zheng and T. M. Duman, "Information rates and coding for wireless MIMO relay channels," in *Proceedings of Vehicular Technology Conference (VTC)*, vol. 3, Sep. 2004, pp. 1623–1632.

[53] Z. Zhang and T. M. Duman, "Capacity-approaching turbo coding and iterative decoding for relay channels," *IEEE Transactions on Communications*, vol. 53, no. 11, pp. 1895–1905, Nov. 2005.

[54] Z. Zheng, I. Bahceci, and T. M. Duman, "Capacity approaching codes for relay channels," in *Proceedings of IEEE International Symposium on Information Theory (ISIT)*, Chicago, Illinois, Jun. 2004, p. 2.

[55] Z. Zhang and T. M. Duman, "Capacity approaching turbo coding for half duplex relaying," in *Proceedings of International Symposium on Information Theory (ISIT)*, Adelaide, Australia, Sep. 2005, pp. 1888–1892.

[56] ——, "Capacity-approaching turbo coding for half-duplex relaying," *IEEE Transactions on Communications*, vol. 55, no. 10, pp. 1895–1906, Oct. 2007.

[57] P. Razaghi and W. Yu, "Bilayer low-density parity-check codes for decode-and-forward in relay channels," *IEEE Transactions on Information Theory*, vol. 53, no. 10, pp. 3723–3739, Oct. 2007.

[58] J. Hu and T. M. Duman, "Low density parity check codes over half duplex relay channels," in *Proceedings of IEEE International Symposium on Information Theory (ISIT)*, Seattle, Washington, Jul. 2006, pp. 972–976.

[59] ——, "LDPC codes over ergodic and non-ergodic relay channels," in *Proceedings of the 44th Annual Allerton Conference on Communication, Control and Computing*, Monticello, Illinois, Sep. 2006, pp. 454–461.

[60] ——, "Low density parity check codes over wireless relay channels," *IEEE Transactions on Wireless Communications*, vol. 6, no. 9, pp. 3384–3394, Sep. 2007.

[61] ——, "Frequency selective fading relay channels: Information rates and turbo coding," in *Proceedings of IEEE Global Telecommunications Conference (GLOBECOM)*, Washington, D.C., Nov. 2007, pp. 1653–1657.

[62] ——, "Cooperation over frequency-selective fading relay channels," *IEEE Transactions on Wireless Communications*, vol. 7, no. 12, pp. 5072–5081, Dec. 2008.

[63] A. K. Tanc, T. M. Duman, and C. Tepedelenlioglu, "Design of LDPC codes for two-way relay systems with physical-layer network coding," *IEEE Communications Letters*, vol. 17, no. 12, pp. 2356–2359, Dec. 2013.

[64] S. Papaharalabos, G. Alexandropoulos, and C. Papadias, "A comparative study of interference alignment schemes with LTE-compliant turbo coding," in *Proceedings of IEEE International Conference on Communications Workshops (ICC)*, Budapest, Hungary, June 2013, pp. 159–163.

[65] A. Bennatan, S. Shamai, and A. Calderbank, "Soft-decoding-based strategies for relay and interference channels: Analysis and achievable rates using LDPC codes," *IEEE Transactions on Information Theory*, vol. 60, no. 4, pp. 1977–2009, Apr. 2014.

[66] S. Sharifi, A. K. Tanc, and T. M. Duman, "LDPC code design for the two-user Gaussian multiple access channel," *submitted to IEEE Transactions on Wireless Communications*, Jun. 2015.

[67] Gallager, "Low-density parity check codes," *IRE Transactions on Information Theory*, vol. IT-8, pp. 21–28, Jan. 1962.

[68] D. J. C. MacKay, "Good error-correcting codes based on very sparse matrices," in *Proceedings of International Symposium on Information Theory (ISIT)*, Ulm, Germany, June 1997, p. 113.

[69] A. Yedla, P. Nguyen, H. Pfister, and K. Narayanan, "Universal codes for the Gaussian MAC via spatial coupling," in *Proceedings of the 49th Annual Allerton Conference on Communication, Control and Computing*, Monticello, Illinois, Sep. 2011, pp. 1801–1808.

[70] S. ten Brink, "Convergence behavior of iteratively decoded parallel concatenated codes," *IEEE Transactions on Communications*, vol. 49, no. 10, pp. 1727–1737, 2001.

[71] I. Shahid and P. Yahampath, "Distributed joint source-channel code design for GMAC using irregular LDPC codes," *EURASIP Journal on Wireless Communications and Networking*, Jan. 2014.

[72] T. K. Moon and W. C. Stirling, *Mathematical methods and algorithms for signal processing*. Upper Saddle River, NJ: Prentice-Hall, 2000.

[73] S.-Y. Chung, "On the construction of some capacity-approaching coding schemes," Ph.D. dissertation, Massachusetts Institute of Technology, Cambridge, 2000.

[74] S. ten Brink, G. Kramer, and A. Ashikhmin, "Design of low-density parity-check codes for modulation and detection," *IEEE Transactions on Communications*, vol. 52, no. 4, pp. 670–678, Apr. 2004.

[75] S. Sharifi, A. K. Tanc, and T. M. Duman, "Implementing the Han-Kobayashi scheme using low density parity check codes over Gaussian interference channels," *IEEE Transactions on Communications*, vol. 63, no. 2, pp. 337–350, Feb 2015.

[76] L. Li, N. Jindal, and A. Goldsmith, "Outage capacities and optimal power allocation for fading multiple-access channels," *IEEE Transactions on Information Theory*, vol. 51, no. 4, pp. 1326–1347, Apr. 2005.

[77] R. Narasimhan, "Individual outage rate regions for fading multiple access channels," in *Proceedings of IEEE International Symposium on Information Theory (ISIT)*, Nice, France, June 2007, pp. 1571–1575.

[78] A. Lampe and J. Huber, "On improved multiuser detection with iterated soft decision interference cancellation," in *Proceedings of IEEE Communications Theory Mini-Conference*, Vancouver, BC, Canada, June 1999, pp. 172–176.

[79] P. Patel and J. Holtzman, "Analysis of a simple successive interference cancellation scheme in a DS/CDMA system," *IEEE Journal on Selected Areas in Communications*, vol. 12, no. 5, pp. 796–807, June 1994.

[80] J. Hou, P. Siegel, L. Milstein, and H. Pfister, "Capacity-approaching bandwidth-efficient coded modulation schemes based on low-density parity-check codes," *IEEE Transactions on Information Theory*, vol. 49, no. 9, pp. 2141–2155, Sep. 2003.

[81] X. Han and G. R. Liu, *Computational Inverse Techniques in Nondestructive Evaluation*. London: CRC Press, 2003.

[82] J. Hagenauer, "The EXIT chart–introduction to extrinsic information transfer in iterative processing," in *Proceedings of the 12th European Signal Processing Conference (EUSIPCO)*, Vienna, Austria, Sep. 2004, pp. 1541–1548.

[83] M. Franceschini, G. Ferrari, R. Raheli, and A. Curtoni, "Serial concatenation of LDPC codes and differential modulations," *IEEE Journal on Selected Areas in Communications*, vol. 23, no. 9, pp. 1758–1768, Sep. 2005.

[84] S. Sharifi, A. K. Tanc, and T. M. Duman, "On LDPC codes for Gaussian interference channels," in *Proceedings of IEEE International Symposium on Information Theory (ISIT)*, Honolulu, Hawaii, June 2014, pp. 1992–1996.

[85] R. Storn and K. Price, "Differential evolution–A simple and efficient heuristic for global optimization over continuous spaces," *Journal of Global Optimization*, vol. 11, pp. 341–359, Dec. 1997.

[86] T. Richardson and R. Urbanke, *Modern Coding Theory*. New York: Cambridge University Press, 2008.

[87] [Online]. Available: http://itpp.sourceforge.net/4.3.1/

[88] J. Fan, "Array codes as low-density parity-check codes," in *Proceedings of the 2nd International Symposium on Turbo Codes and Their Applications*, Sep. 2000, pp. 543–546.

[89] S. Song, L. Lan, S. Lin, and K. Abdel-Ghaffar, "Construction of quasi-cyclic LDPC codes based on the primitive elements of finite fields," in *proceedings of 40th Annual Conference on Information Sciences and Systems*, Princeton, New Jersey, Mar. 2006, pp. 835–838.

[90] C. Kelley and J. Kliewer, "Algebraic constructions of graph-based nested codes from protographs," in *Proceedings of IEEE International Symposium on Information Theory (ISIT)*, Austin, Texas, June 2010, pp. 829–833.

[91] S. Sharifi, A. K. Tanc, and T. M. Duman, "LDPC code design for binary-input binary-output Z interference channels," in *Proceedings of IEEE International Symposium on Information Theory (ISIT)*, Hong Kong, China, June 2015, pp. 1084–1088.

[92] H. Sato, "On the capacity region of a discrete two-user channel for strong interference," *IEEE Transactions on Information Theory*, vol. 24, no. 3, pp. 377–379, May 1978.

[93] A. E. Gamal and M. Costa, "The capacity region of a class of deterministic interference channels," *IEEE Transactions on Information Theory*, vol. 28, no. 2, pp. 343–346, Mar. 1982.

[94] F. Zhu and B. Chen, "Capacity bounds and sum rate capacities of a class of discrete memoryless interference channels," *IEEE Transactions on Information Theory*, vol. 60, no. 7, pp. 3763–3772, July 2014.

[95] R. Benzel, "The capacity region of a class of discrete additive degraded interference channels," *IEEE Transactions on Information Theory*, vol. 25, no. 2, pp. 228–231, Mar. 1979.

[96] J. Proakis and M. Salehi, *Digital Communications*, 5th ed. New York: McGraw-Hill, 2008.

[97] N. Liu and S. Ulukus, "The capacity region of a class of discrete degraded interference channels," *IEEE Transactions on Information Theory*, vol. 54, no. 9, pp. 4372–4378, Sep. 2008.

[98] A. Ozcelikkale and T. M. Duman, "Short length trellis-based codes for Gaussian multiple-access channels," *IEEE Signal Processing Letters*, vol. 21, no. 10, pp. 1177–1181, Oct. 2014.

[99] U. Bhat, D. Fertonani, and T. M. Duman, "Approximate performance analysis for linear codes in superposition schemes over Gaussian broadcast channels," *IEEE Transactions on Communications*, vol. 58, no. 8, pp. 2177–2182, Aug. 2010.

[100] A. Stefanov and T. M. Duman, "Performance bounds for space-time trellis codes," *IEEE Transactions on Information Theory*, vol. 49, no. 9, pp. 2134–2140, Sep. 2003.

[101] W. Ryanand and S. Lin, *Channel Codes: Classical and Modern*. Cambridge, U.K.: Cambridge University Press, 2009.

[102] D. MacKay. Encyclopedia of sparse graph codes. [Online]. Available: http://www.inference.phy.cam.ac.uk/mackay/codes/data.html

[103] A. Clifford Cohen, "Estimation in mixtures of two Gaussian distributions," *Technometrics*, vol. 9, no. 1, pp. 15–28, Feb 1967.

[104] X.-Y. Hu, E. Eleftheriou, and D.-M. Arnold, "Progressive edge-growth Tanner graphs," in *Proceedings of IEEE Global Telecommunications Conference (GLOBECOM)*, vol. 2, San Antonio, Texas, Nov 2001, pp. 995–1001.

[105] C. Kelley, "On codes designed via algebraic lifts of graphs," in *Proceedings of the 46th Annual Allerton Conference on Communication, Control, and Computing*, Monticello, Illinois, Sep. 2008, pp. 1254–1261.

APPENDIX A

DERIVATION OF THE MODIFIED J FUNCTION

We compute the defined function $J'(\mu, \sigma)$ in (3.11), given by

$$J'(\mu,\sigma) = 1 - \frac{1}{\sqrt{2\pi\sigma^2}} \int_{-\infty}^{\infty} \exp\Big(- \frac{(z-\mu)^2}{2\sigma^2}\Big) \log_2 \Big(1 + \exp(-z)\Big) dz. \tag{A.1}$$

For the ease of exposition, we write $J'(\mu,\sigma)$ as $J'(\mu,\sigma) = 1 - \frac{I}{\log(2)\sqrt{2\pi\sigma^2}}$. Also, I can be split into two parts I_1 and I_2; that is $I = I_1 + I_2$, where

$$\begin{aligned} I_1 &= \int_{-\infty}^{0} \exp\Big(- \frac{(z-\mu)^2}{2\sigma^2}\Big) \Big(\log\Big(1+\exp(z)\Big) - z\Big) dz, \\ I_2 &= \int_{0}^{\infty} \exp\Big(- \frac{(z-\mu)^2}{2\sigma^2}\Big) \log\Big(1+\exp(-z)\Big) dz. \end{aligned} \tag{A.2}$$

I_1 can be expressed as $I_1 = I_{11} - I_{12}$ where

$$\begin{aligned} I_{12} &= \int_{-\infty}^{0} z \exp\Big(- \frac{(z-\mu)^2}{2\sigma^2}\Big) dz \\ &= \int_{-\infty}^{-\frac{\mu}{\sigma}} (\sigma t + \mu) \exp\Big(- \frac{t^2}{2}\Big) \sigma dt \\ &= \Big(\int_{-\infty}^{-\frac{\mu}{\sigma}} \sigma^2 t \exp\Big(- \frac{t^2}{2}\Big) dt + \mu\sigma \int_{-\infty}^{-\frac{\mu}{\sigma}} \exp\Big(- \frac{t^2}{2}\Big) dt \Big) \\ &= \Big(- \sigma^2 \exp\Big(- \frac{\mu^2}{2\sigma^2}\Big) + \mu\sigma\sqrt{\frac{\pi}{2}} \Big(1 + \operatorname{erf}\Big(- \frac{\mu}{\sqrt{2}\sigma}\Big)\Big)\Big). \end{aligned} \tag{A.3}$$

Expanding $\log\big(1+\exp(z)\big)$ to its Taylor series, I_{11} can be rewritten as

$$\begin{aligned} I_{11} &= \int_{-\infty}^{0} \exp\Big(- \frac{(z-\mu)^2}{2\sigma^2}\Big) \Big(\sum_{m=1}^{\infty} (-1)^{m-1} \frac{\exp(mz)}{m}\Big) dz \\ &= \sum_{m=1}^{\infty} \frac{(-1)^{m-1}}{m} \Big(\int_{-\infty}^{0} \exp\Big(- \frac{(z-\mu)^2}{2\sigma^2}\Big) \exp(mz) dz \Big). \end{aligned} \tag{A.4}$$

The mth term of the summation in (A.4), denoted as A_m, can be computed as

$$\begin{aligned} A_m &= \int_{-\infty}^{0} \exp\Big(- \frac{(z-\mu)^2}{2\sigma^2}\Big) \exp(mz) dz \\ &= \int_{-\infty}^{0} \exp\Big(- \frac{z^2 - 2\mu z + \mu^2 - 2\sigma^2 mz}{2\sigma^2}\Big) dz \\ &= \int_{-\infty}^{0} \exp\Big(- \frac{\big(z - (\mu + \sigma^2 m)\big)^2 - \sigma^4 m^2 - 2\sigma^2 m\mu}{2\sigma^2}\Big) dz \\ &= \exp\Big(\frac{\sigma^2 m^2}{2} + m\mu\Big) \Big(\int_{-\infty}^{0} \exp\Big(- \frac{\big(z - (\mu + \sigma^2 m)\big)^2}{2\sigma^2}\Big) dz \Big). \end{aligned} \tag{A.5}$$

Hence, I_{11} is computed as

$$I_{11} = \left(\sqrt{2\pi\sigma^2}\right)\left[\sum_{m=1}^{\infty} \frac{(-1)^{(m-1)}\left(1 - Q(-\frac{\mu+m\sigma^2}{\sigma})\right)}{m} \exp\left(\frac{\sigma^2 m^2}{2} + m\mu\right)\right], \tag{A.6}$$

where

$$Q(x) = \frac{1}{\sqrt{2\pi}} \int_x^{\infty} \exp\left(-\frac{t^2}{2}\right) dt. \tag{A.7}$$

Similarly, I_2 can be written as

$$\begin{aligned} I_2 &= \int_0^{\infty} \exp\left(-\frac{(z-\mu)^2}{2\sigma^2}\right)\left(\sum_{m=1}^{\infty}(-1)^{m-1}\frac{\exp(-mz)}{m}\right)dz \\ &= \sum_{m=1}^{\infty} \frac{(-1)^{m-1}}{m}\left(\int_0^{\infty} \exp\left(-\frac{(z-\mu)^2}{2\sigma^2}\right)\exp(-mz)dz\right). \end{aligned} \tag{A.8}$$

Considering (A.5), I_2 is simplified to simplified to

$$I_2 = \left(\sqrt{2\pi\sigma^2}\right)\left[\sum_{m=1}^{\infty} \frac{(-1)^{(m-1)}Q\left(-\frac{\mu-m\sigma^2}{\sigma}\right)}{m} \exp\left(\frac{\sigma^2 m^2}{2} - m\mu\right)\right]. \tag{A.9}$$

Note that for $\mu = \frac{\sigma^2}{2}$, the J' reduces to the J function introduced in [74].